

---

Electronic Thesis and Dissertation Repository

---

7-17-2024 5:00 PM

# Development of Four-Dimensional Computed Tomography Based Methods to Measure Shoulder Kinematics in Healthy Individuals and in Patients following Total Shoulder Arthroplasty

James Hunter,

Supervisor: Lalone, Emily A, *The University of Western Ontario*

A thesis submitted in partial fulfillment of the requirements for the Doctor of Philosophy degree in Biomedical Engineering

© James Hunter 2024

Follow this and additional works at: <https://ir.lib.uwo.ca/etd>



Part of the [Biomechanics and Biotransport Commons](#)

---

## Recommended Citation

Hunter, James, "Development of Four-Dimensional Computed Tomography Based Methods to Measure Shoulder Kinematics in Healthy Individuals and in Patients following Total Shoulder Arthroplasty" (2024). *Electronic Thesis and Dissertation Repository*. 10348.  
<https://ir.lib.uwo.ca/etd/10348>

This Dissertation/Thesis is brought to you for free and open access by Scholarship@Western. It has been accepted for inclusion in Electronic Thesis and Dissertation Repository by an authorized administrator of Scholarship@Western. For more information, please contact [wlsadmin@uwo.ca](mailto:wlsadmin@uwo.ca).

## Abstract

Dynamic kinematics of the shoulder, particularly the interplay between the glenohumeral and scapulothoracic joints and the changes associated with aging, remain not fully understood. Current research often focuses on simple motions, neglecting more complex movements common in activities of daily living, such as internal rotation to reach behind the back. Post-total shoulder arthroplasty (TSA) surgery, many patients experience difficulties with internal rotation, affecting tasks like dressing and bathing. This dissertation employs four-dimensional computed tomography (4DCT) to enhance understanding of shoulder biomechanics and TSA outcomes by assessing dynamic shoulder kinematics in a healthy population and a post-implant population.

The first objective was to develop and validate a process for measuring dynamic glenohumeral and scapulothoracic kinematics via 4DCT. This process uses a single vertebra as a reference for scapulothoracic motion and demonstrated satisfactory repeatability. The next objective was to improve its feasibility by automating bone model segmentation from scans. This consisted of creating convolutional neural networks for the humerus and scapula, achieving human-comparable accuracy in a fraction of the time.

The developed techniques were then utilized to quantify healthy shoulder kinematics and the impact of aging. The importance of humeral translation was confirmed, as all participants exhibited some degree of translation. Older participants showed less humeral motion, predominantly humeral translation, although scapulohumeral rhythm remained unchanged relative to the younger participants. The results also revealed age-related alterations in bone positioning, including increased lateral rotation, posterior tilting, and superior translation of the scapula. The altered pose also affected the range of motion of the scapula.

Finally, kinematics between natural and anatomic TSA shoulders were compared, examining the effects of mobility and implant mismatch. The hypothesis that patients with good mobility would exhibit similar kinematics to non-implant participants was unsupported; the good mobility group showed significant differences compared to healthy controls, notably, greater humeral translation. Furthermore, regardless of mobility, all implant patients had limited

humeral internal rotation, compensated by increased humeral extension. No correlation between implant mismatch and range of motion was found, indicating that mismatch does not significantly affect shoulder kinematics.

## Keywords

Computed Tomography, Four-Dimensional Computed Tomography, Shoulder, Glenohumeral, Scapulothoracic, Biomechanics, Kinematics, Total Shoulder Arthroplasty.

## Summary for Lay Audience

Understanding movement in the shoulder, especially the scapula (shoulder blade), is still not fully clear, particularly how it changes as people age. Many studies focus on simple shoulder movements and overlook complex motions needed for daily activities, like reaching behind the back. After receiving a shoulder implant, patients often struggle with this motion, which is essential for tasks like dressing and bathing. This research uses advanced imaging, which can visualize the bones of the shoulder moving, to closely examine shoulder movements in both a healthy population and a post-implant population. The goal of this research is to improve understanding of shoulder function and surgical outcomes.

The first goal was to create a method to measure shoulder movements using this advanced imaging technology, and ensure this method is reliable, which was successfully done. The next goal was to speed up the process of analyzing these images by training a computer program to automatically identify and model the shoulder bones. This program proved to be as accurate as human experts and could complete the task much faster.

The third part of the research aimed to understand how healthy shoulders move, and how aging affects this movement. It was found that older participants had less sliding motion within the shoulder joint. Additionally, the scapula of older individuals was found to be positioned differently than the younger participants, which resulted in differences in how much the scapula had to move to achieve the same end position.

The final study compared the movements of participants with natural shoulders to participants who had received a shoulder implant. It was expected that patients with good motion post-surgery would have shoulder movements similar to those without implants, but this was not the case. Furthermore, all implant participants had restricted rotation of the upper arm, which they compensated for by increasing how much their arm moved backward. Lastly, no link was found between the size of an implant and shoulder motion.

# Co-Authorship Statement

## **Chapter 1:**

Sole authorship: James Hunter  
Manuscript review: Emily Lalone

## **Chapter 2:**

Study design: James Hunter, Emily Lalone  
Data collection: James Hunter, Emily Lalone  
Manuscript preparation: James Hunter  
Manuscript review: George Athwal, Emily Lalone

## **Chapter 3:**

Sole authorship: James Hunter  
Manuscript review: Emily Lalone

## **Chapter 4:**

Study design: James Hunter, Ting-Yim Lee, Emily Lalone  
Data collection: James Hunter, Emily Lalone  
Manuscript preparation: James Hunter  
Manuscript review: George Athwal, Emily Lalone

## **Chapter 5:**

Study design: James Hunter, Ting-Yim Lee, Emily Lalone  
Data collection: James Hunter, Kylie Paliani, Emily Lalone  
Manuscript preparation: James Hunter  
Manuscript review: Emily Lalone

## **Chapter 6:**

Sole authorship: James Hunter  
Manuscript review: Emily Lalone

## Acknowledgments

This thesis would not have been possible without the guidance and support of many people. First, I would like to thank my supervisor Dr. Emily Lalone, without your kindness, mentorship, and confidence in my abilities, I would not be where I am today. I feel extremely fortunate to have been able to work with you these past few years, thank you for seeing my potential. I would also like to thank those on my advisory committee: Dr. George Athwal, Dr. Daniel Langhor, and Dr. James Johnson. Your feedback and encouragement were integral to my success.

I would also like to acknowledge all my colleagues in the Lalone lab: Baraa Daher, Carla DuToit, Elizabeth Norman, Kylie Paliani, Lauren Staatman, Maxwell Campbell, Megan Hutter, and Randa Mudathir. I want to further express my gratitude to Elizabeth, Lauren, and Kylie, I am grateful for your support and friendship throughout.

I would like to extend my deepest gratitude to my partner, Livi. You were always there to support me and never doubted my success, I cannot thank you enough. Finally, I would like to thank my parents, even though you didn't understand the work I was doing, your unconditional love, support, and encouragement means the world to me.

# Table of Contents

Abstract.....	ii
Summary for Lay Audience.....	iv
Co-Authorship Statement.....	v
Acknowledgments.....	vi
Table of Contents.....	vii
List of Tables.....	xi
List of Figures.....	xii
List of Appendices.....	xiv
List of Abbreviations.....	xv
Chapter 1.....	1
1 Introduction.....	1
1.1 Shoulder Anatomy.....	2
1.1.1 Osteology.....	3
1.1.2 Passive Soft Tissues.....	6
1.1.3 Musculature.....	7
1.2 Shoulder Kinematics and Motion.....	10
1.3 Imaging/Measurement Techniques.....	13
1.4 Aging.....	14
1.5 Osteoarthritis.....	15
1.6 Shoulder Arthroplasty.....	17
1.6.1 Design.....	18
1.6.2 Mismatch.....	21
1.6.3 Internal Rotation Deficiency.....	23
1.7 Motivation.....	24

1.8 Objectives and Hypotheses .....	25
1.9 Thesis Overview .....	27
Chapter 2 .....	28
2 Development of the Single-Vertebra Image-Based Technique for Measuring Shoulder Kinematics using Four-Dimensional Computed Tomography .....	28
2.1 Introduction.....	29
2.2 Methods.....	29
2.2.1 Data Acquisition .....	29
2.2.2 Kinematic Analysis (SVIB): .....	32
2.2.3 Data and Statistical Analysis .....	35
2.3 Results.....	36
2.3.1 Vertebra vs Thoracic Comparison .....	36
2.3.2 Repeatability .....	40
2.4 Discussion.....	43
Chapter 3 .....	48
3 Automating Bone Model Creation from Computed Tomography Scans Using Neural Networks .....	48
3.1 Introduction.....	49
3.2 Methods.....	49
3.2.1 Network Architecture.....	49
3.2.2 Training.....	51
3.2.3 Reconstruction .....	53
3.2.4 Validation.....	54
3.3 Results.....	55
3.4 Discussion.....	56
Chapter 4 .....	59
4 Age-Related Differences in Healthy Shoulder Kinematics .....	59



4.1	Introduction.....	60
4.2	Methods.....	60
4.2.1	Participants.....	60
4.2.2	Motions .....	61
4.2.3	Data Acquisition and Analysis.....	62
4.2.4	Statistical Analysis.....	64
4.3	Results.....	64
4.3.1	Participants.....	64
4.3.2	Pathways .....	65
4.3.3	Maximum Range of Motion.....	69
4.3.4	Neutral Positioning .....	72
4.3.5	Scapulohumeral Rhythm.....	74
4.4	Discussion.....	74
	Chapter 5.....	80
5	Kinematic Analysis of Anatomic Total Shoulder Arthroplasty and the Effects of Patient Mobility and Implant Mismatch .....	80
5.1	Introduction.....	81
5.2	Methods.....	82
5.2.1	Participants.....	82
5.2.2	Motions .....	82
5.2.3	Data Acquisition and Analysis.....	82
5.2.4	Statistical Analysis.....	84
5.3	Results.....	84
5.3.1	Participants.....	84
5.3.2	Mobility.....	85
5.3.3	Mismatch.....	89

5.4 Discussion.....	92
Chapter 6.....	96
6 General Discussion and Conclusions.....	96
6.1 Summary and Conclusions.....	97
6.2 Strengths and Limitations.....	99
6.3 Future Directions.....	100
References.....	103
Curriculum Vitae.....	113

## List of Tables

Table 1–1: Scapulohumeral muscles - origin, insertion, and action. An asterisk (*) indicates muscles of the rotator cuff. ....	8
Table 1–2: Humerothoracic muscles - origin, insertion, and action. ....	8
Table 1–3: Scapulothoracic muscles - origin, insertion, and action. ....	9
Table 1–4: Biarticular muscles - origin, insertion, and action. ....	9
Table 1–5: Mismatch chart for AEQUALIS PERFORM+ glenoids with SIMPLICITI heads. Diametrical mismatch is in mm, green cells are in the cleared mismatch range, red cells are non-cleared mismatch values. The cleared range for this combination is 1 to 24.8mm. (Wright Medical Group, 2016) .....	22
Table 3–1: Mean positional differences of neural network generated models relative to manual ground truth models. ....	55
Table 4–1: Participant demographics, categorized by age cohort and motion. The table includes sample sizes, the average age with standard deviation, and the age range for each subgroup.....	65
Table 4–2: P-values for the kinematic pathways categorized by factor and degree of freedom. Bold values indicate significance ( $p \leq 0.05$ ).....	66
Table 4–3: Average neutral positioning with standard deviation of each cohort for each degree of freedom. The p-value is provided for each age-related comparison where bold values indicate significance ( $p \leq 0.05$ ). ....	73
Table 4–4: Average scapulohumeral rhythm with standard deviation of each cohort for each motion. The p-value is provided for each age-related comparison.....	74
Table 5–1: Distribution of participants across mismatch and mobility groups. ....	84

# List of Figures

Figure 1–1: Relevant bones and joints of the shoulder.....	2
Figure 1–2: Anatomy of the humerus. ....	3
Figure 1–3: Anatomy of the scapula. ....	5
Figure 1–4: Scapulohumeral muscles of the shoulder. ....	10
Figure 1–5: Rotations of the humerus.....	12
Figure 1–6: Rotations of the scapula. ....	12
Figure 1–7: Walch-Bercik classification of glenoid erosion. ....	16
Figure 1–8: Total shoulder arthroplasty components. ....	20
Figure 1–9: Axial CT scan of the shoulder illustrating diametric mismatch.....	22
Figure 2–1: Participant positioning in the CT scanner. ....	31
Figure 2–2: Local coordinate systems and associated anatomical landmarks.....	34
Figure 2–3: Comparison of vertebra and thorax coordinate systems. ....	37
Figure 2–4: Kinematics relative to a vertebra and a thorax coordinate system. ....	38
Figure 2–5: Bland-Altman plot comparing vertebra and thorax coordinate systems. ....	39
Figure 2–6: Range of motion relative to a vertebra and a thorax coordinate system. ....	40
Figure 2–7: Repeated kinematic calculations. ....	42
Figure 2–8: Repeated range of motion calculations. ....	43
Figure 3–1: Modified U-Net architecture. ....	50
Figure 3–2: Graphical interface of custom 3DSlicer module. ....	54

Figure 3–3: Example performance of the networks.....	56
Figure 4–1: Static position and examined motions.....	62
Figure 4–2: Forward elevation kinematic pathways.....	67
Figure 4–3: Internal rotation kinematic pathways.....	68
Figure 4–4: Forward elevation range of motion.....	70
Figure 4–5: Internal rotation range of motion.....	71
Figure 4–6: Humeral translation as a percentage of glenoid width.....	72
Figure 4–7: Comparison of neutral scapula pose.....	74
Figure 5–1: Flowchart illustrating the recruitment and inclusion process.....	85
Figure 5–2: Range of motion of the mobility groups.....	87
Figure 5–3: Kinematic pathways of the mobility groups.....	88
Figure 5–4: Range of motion of the mismatch groups.....	90
Figure 5–5: Kinematic pathways of the mismatch groups.....	91
Figure 5–6: Relationship between mismatch and range of motion.....	92

## List of Appendices

Appendix A: The Impact of Voxel Resolution and Scan Orientation on CT-Based Bone Models.....	112
--	-----

## List of Abbreviations

- 3D – Three-dimensional
- 4DCT – Four-dimensional computed tomography
- ANOVA – Analysis of variance
- ASES – American Shoulder and Elbow Surgeons
- aTSA – Anatomic total shoulder arthroplasty
- CT – Computed tomography
- DLP – Dose length product
- DoF – Degree(s) of freedom
- FE – Forward elevation
- GHOA – Glenohumeral osteoarthritis
- IR – Internal rotation
- ISB – International Society of Biomechanics
- JCS – Joint coordinate system
- MAD – Mean absolute deviation
- MRI – Magnetic resonance imaging
- RMSE – Root-mean-square error
- ROM – Range of motion
- rTSA – Reverse total shoulder arthroplasty
- SVIB – Single-vertebra image-based
- T1 – First thoracic vertebra
- TSA – Total shoulder arthroplasty

# Chapter 1

## 1 Introduction

### OVERVIEW

*This introductory chapter provides an overview of the intricate anatomy of the shoulder, detailing the bones, soft tissues, and muscles that constitute this complex joint. Additionally, it explores current techniques and challenges in the field of shoulder biomechanics. This chapter also discusses glenohumeral osteoarthritis, and reviews total shoulder arthroplasty, covering the design and known challenges. It concludes with the motivation, objectives, and hypotheses of this dissertation.*



## 1.1 Shoulder Anatomy

The shoulder has the largest range of motion (ROM) of any other joint complex in the human body (Culham & Peat, 1993). The extensive mobility of the shoulder in conjunction with the elbow allows the hand to be positioned in a wide range of locations and orientations, enabling the intricate movements and precise manipulation used in everyday life. The shoulder is made up of three bones: the humerus, scapula, and clavicle. These bones form four joints: scapulothoracic, glenohumeral, acromioclavicular, and sternoclavicular (Figure 1–1). Each joint is a point of articulation where motion occurs and proper healthy shoulder mobility requires a coordinated contribution from all of these joints (Culham & Peat, 1993).

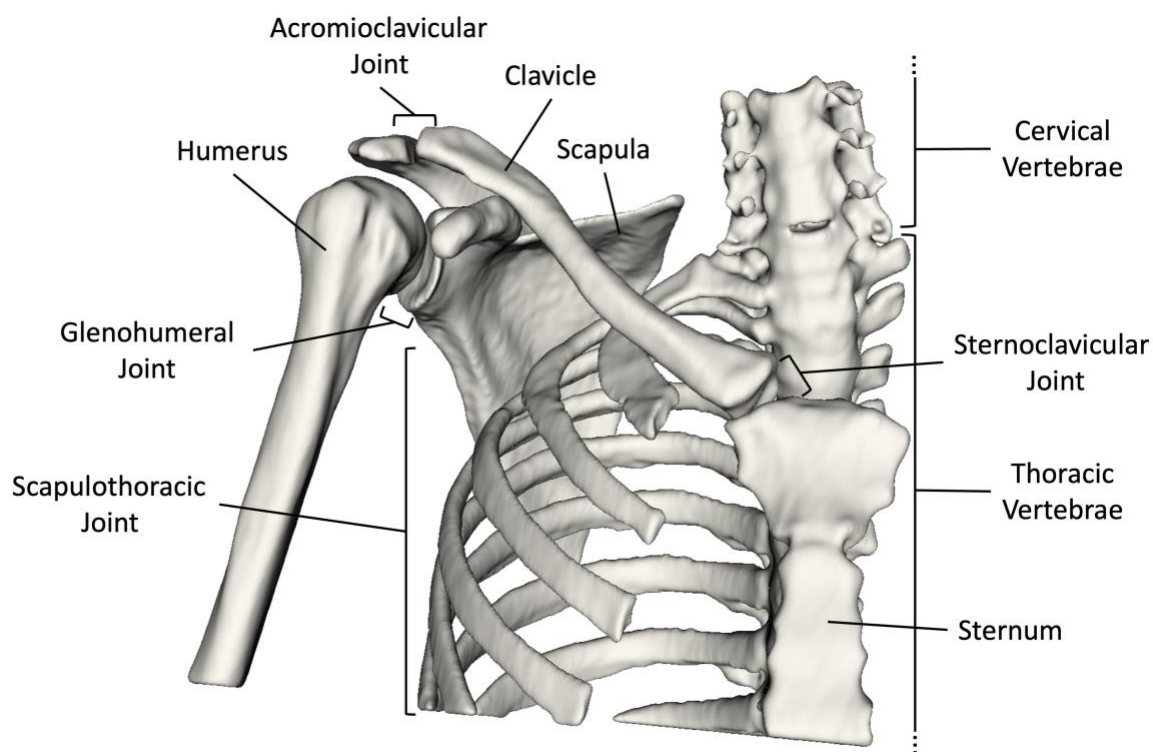


**Figure 1–1: Relevant bones and joints of the shoulder.**

### 1.1.1 Osteology

The humerus (Figure 1–2) is the long bone of the upper arm connecting the shoulder to the elbow. The proximal end features the head which is a spherical articular surface. The anatomical neck transitions the head to the long cylindrical shaft. Important landmarks for muscle attachment include the greater tuberosity, located posterolaterally, and the lesser tuberosity, located anterolaterally, which are separated by the bicipital groove. The deltoid tuberosity is located approximately at the midpoint of the humeral shaft.

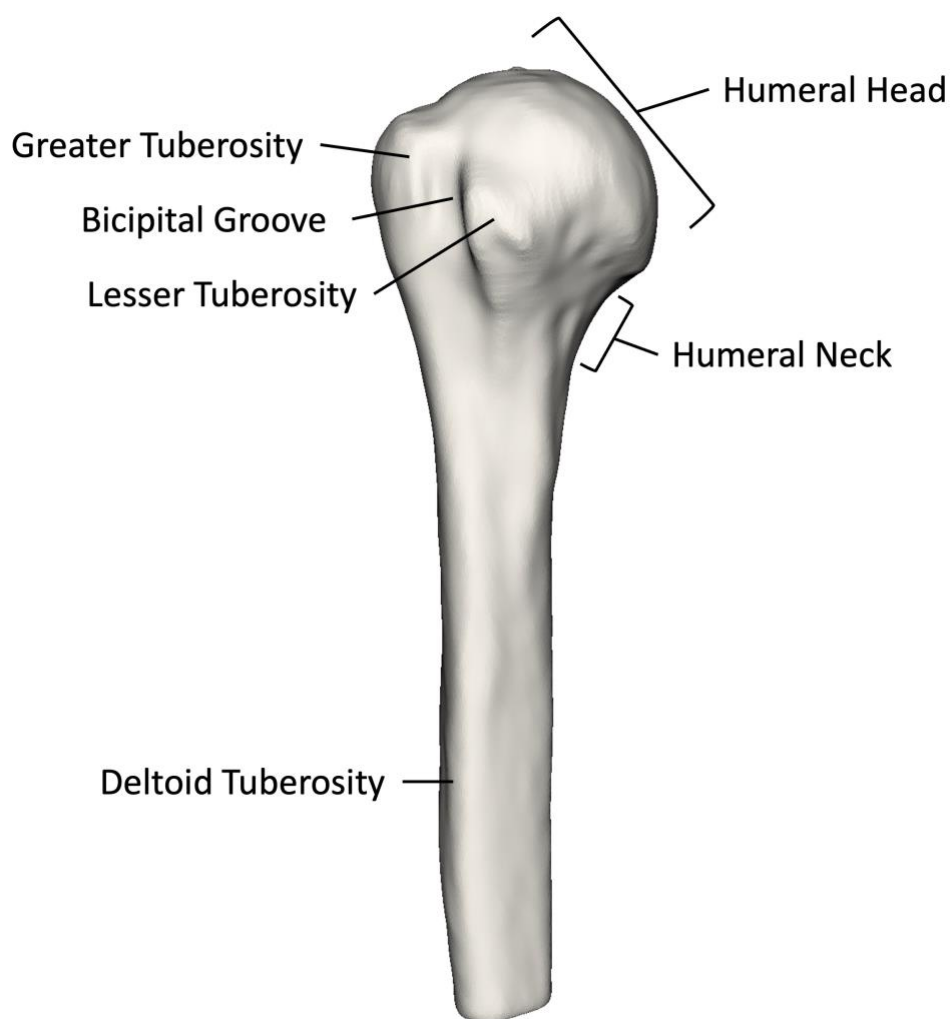


**Figure 1–2: Anatomy of the humerus.**

The scapula (Figure 1–3) is a thin flat triangular shaped bone located on the upper back. Typically, the scapula lies over ribs two to seven, and the superior angle of the scapula is in line with the second thoracic vertebra with the inferior angle in line with the seventh or eighth thoracic vertebra (Culham & Peat, 1993). Despite being the main point of connection between the upper arm and the torso, the scapula has no direct bony articulation or ligamentous attachment to the axial skeleton. However, the relative motion between the scapula and the torso is referred to as the scapulothoracic joint. The scapula features many prominent landmarks that serve as attachment points for muscles; fossae are shallow depressions in the bony surface while processes are structures that protrude from the surface. The scapular spine is a process that divides the posterior face of the scapula into the supraspinous and infraspinous fossae, both slightly convex surfaces. The opposing anterior concave face is termed the subscapular fossa. The glenoid fossa is a shallow pear-shaped cup on the lateral aspect of the bone and is where the humeral head articulates to create the glenohumeral joint. The glenoid has a radius of curvature larger than the humerus which allows for translational motion to occur (J. P. Iannotti et al., 1992). The coracoid process projects anterolaterally from the superior border. The acromion extends laterally from the scapular spine superior to the humeral head and articulates with the clavicle. The clavicle connects the scapula to the torso, articulating with the acromion and the sternum to form the acromioclavicular and sternoclavicular joints, respectively. The clavicle guides rotation of the scapula and resists compression to maintain spacing during muscle loading keeping the scapula unimpeded during motion.

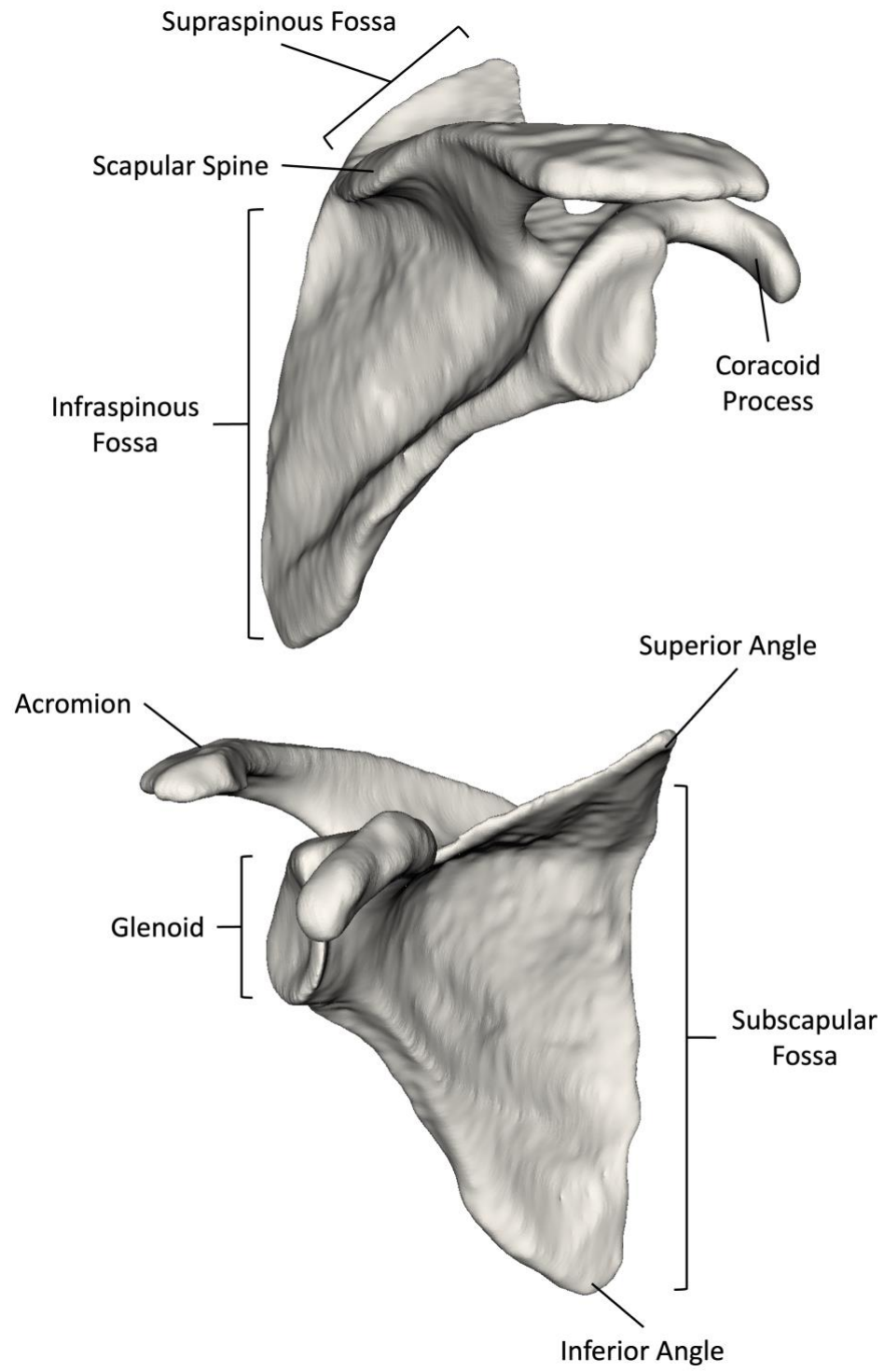


**Figure 1–3: Anatomy of the scapula.**

### 1.1.2 Passive Soft Tissues

The passive soft tissues in the shoulder are crucial for stabilization and enabling proper movement within the joint. Ligaments are strong bands of connective tissue which connect bone to bone, providing stabilization of the shoulder joints while also limiting movement to a safe range. There are three glenohumeral ligaments: superior, middle, and inferior, all of which provide stability specifically to the glenohumeral joint and prevent excessive movement of the humeral head (Culham & Peat, 1993). The superior ligament originates from the superior rim of the glenoid fossa and attaches to the anatomical neck of the humerus, primarily resisting inferior and anterior translation of the humeral head. Spanning from the anterior glenoid to the anterior aspect of the humeral neck, the middle ligament limits lateral rotation of the humerus. The inferior ligament, connected to the labrum's anterior, posterior, and inferior aspects, attaches to the humeral neck, preventing inferior translation and subluxation of the humeral head. The coracohumeral ligament, arising from the coracoid process and attaching onto the humeral tuberosities, limits lateral rotation of the humerus and helps counteract the downward gravitational pull on the humeral head (Culham & Peat, 1993). Additionally, the coracoacromial ligament spans between the coracoid and the acromion to limit superior translation of the humerus. Finally, the coracoclavicular ligament, extending from the coracoid to the clavicle, provides support to the scapula and prevents displacement of the acromioclavicular joint.

The synovial joints of the shoulder (glenohumeral, acromioclavicular, and sternoclavicular) all possess a joint capsule. A joint capsule is a fibrous membrane surrounding a joint, which both produces and contains synovial fluid, an essential lubricant for the joint. To further facilitate smooth movement between the bones of a joint, articular cartilage covers the bones within the joint capsule providing a slippery surface for frictionless movement. Additionally, articular cartilage also functions as a shock absorber, evenly distributing forces across the joint to mitigate bone wear. Within the glenohumeral joint capsule is the glenoid labrum, a ring of fibrous cartilage surrounding the rim of the glenoid. The main function of this structure is to provide stability to the glenohumeral joint by deepening the socket for the humeral head and increasing the congruency between the humeral head and the glenoid (Culham & Peat, 1993). Additionally, the labrum serves as

an attachment site for several ligaments and tendons, further contributing to the structural integrity of the shoulder complex. Furthermore, the labrum acts as a shock absorber, distributing forces across the joint during movement.

Similar in function to joint capsules are bursae, fibrous membranes filled with synovial fluid, that help movement by reducing friction and providing cushioning between various structures that are not joints. Relevant to the shoulder, five bursae exist: the subacromial, situated between the acromion and the rotator cuff tendons; the subscapular, located between the superior and middle glenohumeral ligaments and the scapula; the subcoracoid, positioned between the coracoid and the underlying tendons; the coracoclavicular, located between the coracoid and the clavicle; and the supra-acromial, found between the acromion and the deltoid muscle (Lau & Weerakkody, 2016).

### 1.1.3 Musculature

Muscles are important for both creating motion and stabilizing joints. The shoulder muscles can be divided into four groups based on their locations: scapulohumeral, originating on the scapula and inserting on the humerus (Table 1–1); humerothoracic, originating on the thorax and inserting on the humerus (Table 1–2); scapulothoracic, originating on the thorax and inserting on the scapula (Table 1–3); and biarticular, spanning two joints instead of one (Table 1–4). Additionally, the scapulohumeral muscles can be further grouped into a subset of rotator cuff muscles which specifically surround the glenohumeral joint and further stabilize the joint capsule.

**Table 1–1: Scapulohumeral muscles - origin, insertion, and action. An asterisk (\*) indicates muscles of the rotator cuff.**

<b>Muscle</b>	<b>Origin</b>	<b>Insertion</b>	<b>Action (Humerus)</b>
Supraspinatus*	Supraspinous fossa	Greater tuberosity	Stabilization/ Abduction
Infraspinatus*	Infraspinous fossa	Greater tuberosity	Stabilization/ External rotation
Subscapularis*	Subscapular fossa	Lesser tuberosity	Stabilization/ Internal rotation
Teres minor*	Lateral scapula border (superior)	Greater tuberosity	Stabilization/ Adduction/ External rotation
Teres major	Lateral scapula border (inferior)	Anterior humeral shaft	Stabilization/ Adduction/ Internal rotation
Deltoid	Lateral clavicle, acromion, scapular spine	Deltoid tuberosity	Abduction
Coracobrachialis	Coracoid process	Medial humerus	Adduction/ Flexion

**Table 1–2: Humerothoracic muscles - origin, insertion, and action.**

<b>Muscle</b>	<b>Origin</b>	<b>Insertion</b>	<b>Action (Humerus)</b>
Pectoralis major	Clavicle and sternum	Bicipital groove	Adduction/ Flexion/ Internal rotation
Latissimus dorsi	Lower thoracic and upper lumbar vertebrae, pelvis, inferior angle scapula	Bicipital groove	Adduction/ Extension/ Internal rotation

**Table 1–3: Scapulothoracic muscles - origin, insertion, and action.**

<b>Muscle</b>	<b>Origin</b>	<b>Insertion</b>	<b>Action (Scapula)</b>
Serratus anterior	Anterior Ribs	Anterior medial scapula border	Protraction
Levator scapulae	Cervical vertebrae	Posterior medial scapula border	Elevation/downward rotation
Rhomboids	Upper thoracic Vertebrae	Posterior medial scapula border	Retraction/elevation
Trapezius	Cervical and thoracic vertebrae	Superior scapular spine	Stabilization/posture
Pectoralis minor	Anterior ribs	Anterior coracoid process	Protraction/downward rotation/internal rotation

**Table 1–4: Biarticular muscles - origin, insertion, and action.**

<b>Muscle</b>	<b>Origin</b>	<b>Insertion</b>	<b>Action (Forearm)</b>
Triceps brachii	Infraglenoid tubercle/ humerus	Ulna	Extension
Biceps brachii	Coracoid process/ supraglenoid tubercle	Radius	Flexion/Supination



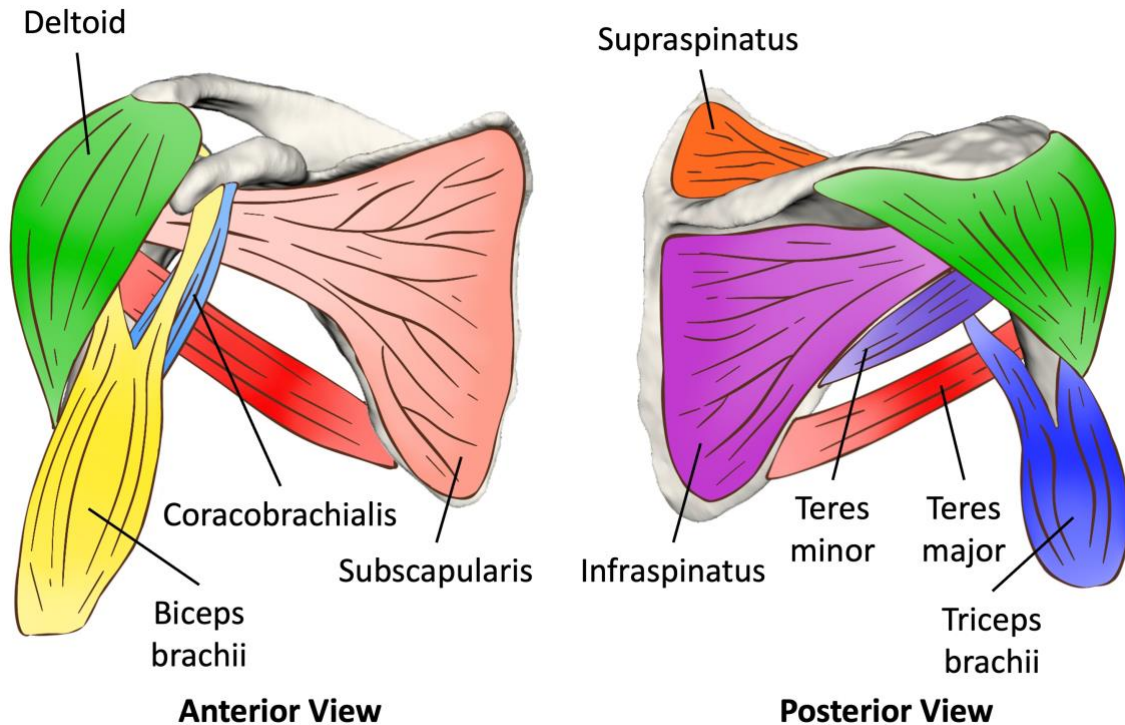


**Figure 1–4: Scapulohumeral muscles of the shoulder.**

## 1.2 Shoulder Kinematics and Motion

Shoulder motion involves a cooperative effort among the four shoulder joints: glenohumeral, scapulothoracic, acromioclavicular, and sternoclavicular. Of these, the glenohumeral and scapulothoracic joints are the most mobile, with the glenohumeral responsible for about two-thirds of motion and the scapulothoracic contributing the remaining third (Scibek, 2012). This ratio is known as scapulohumeral rhythm, which is a metric used to quantify the relative contributions of the scapula and humerus in the overall motion of the shoulder. It is worth noting that only one axis of rotation is typically considered when measuring the angles involved in the calculation of scapulohumeral rhythm, as such, this metric is usually only employed for planar motions such as scapular plane elevation. Unlike elbows or knees, which predominantly flex or extend, both primary shoulder joints are highly versatile in all directions (Charbonnier et al., 2014; Krishnan et al., 2019). Consequently, unlike the lower extremity with a standard gait cycle, there is high variability in upper limb motion which complicates kinematic measurements and

comparisons (Rau et al., 2000). Since natural shoulder movements are typically not cyclic nor comprised of discrete phases, research prefers simple planar motions to simplify analysis (Rau et al., 2000). Correspondingly, research has disproportionately focused on the glenohumeral joint, while scapulothoracic mechanics are mainly explored in select planar motions such as abduction or flexion, according to recent review papers (Daher et al., 2023; Krishnan et al., 2019). To capture the full range of possible motions in three-dimensional (3D) space, movement needs to be described with six degrees-of-freedom (DoF). This includes three translational movements (moving along the x, y, and z axes) and three rotational movements (rotating around the x, y, and z axes). Clinical studies often utilize Euler angles, successive planar rotations about three axes, to describe rotations of the glenohumeral and scapulothoracic joints. Glenohumeral rotations can be described by flexion/extension, abduction/adduction, and internal/external rotation (Figure 1–5). The glenohumeral joint is the most mobile joint in the body with an average ROM of 160° of flexion, 150° of abduction, and 60° of external rotation (Gill et al., 2020). Scapulothoracic rotations can be described by protraction/retraction, lateral/medial rotation, and anterior/posterior tilting (Figure 1–6). Rotational ROM of the scapula varies between studies based on the type of motion, the measurement technique, and other possible factors. Though, an average ROM of the scapula is 25° of retraction, 50° of lateral rotation, and 30° of posterior tilting for scapular plane elevation (McClure et al., 2001).

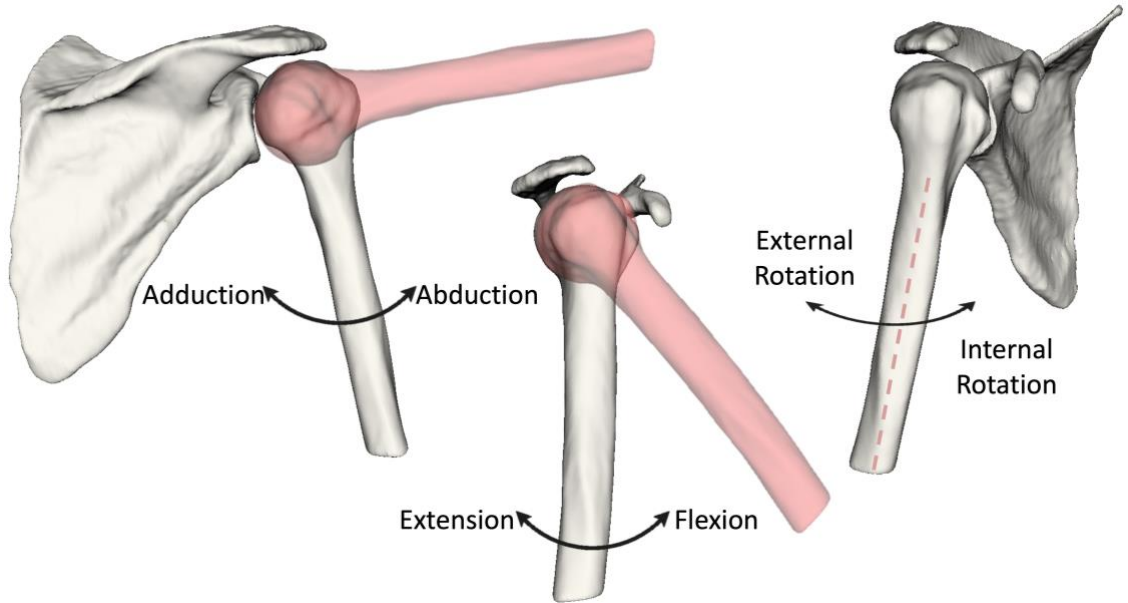


**Figure 1-5: Rotations of the humerus.**

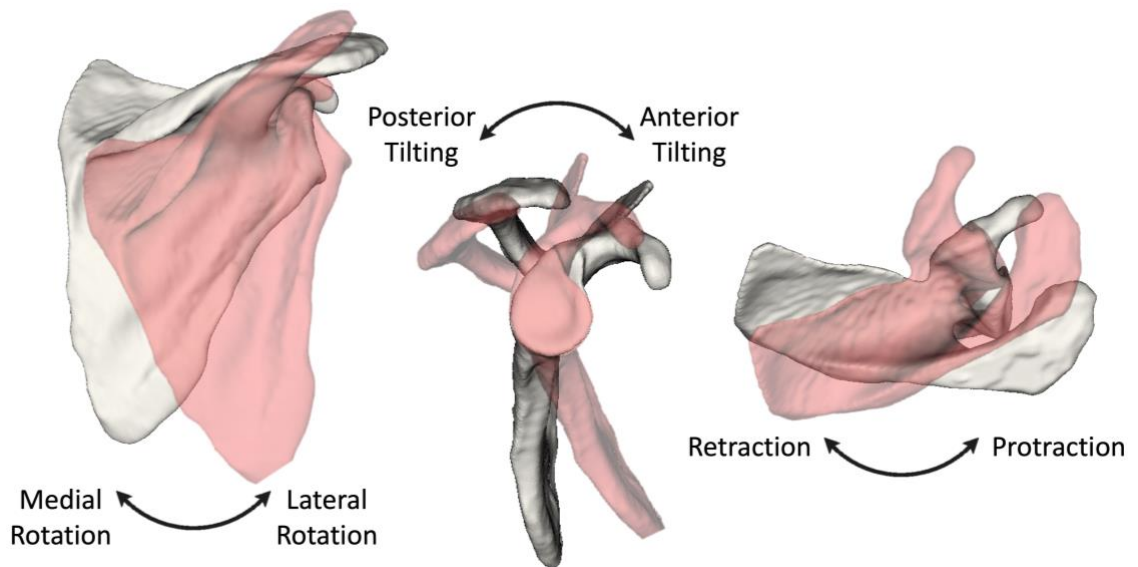


**Figure 1-6: Rotations of the scapula.**

### 1.3 Imaging/Measurement Techniques

There are many challenges researchers face when measuring shoulder kinematics (Charbonnier et al., 2014). In the past, kinematics have been analyzed using x-ray, magnetic resonance imaging (MRI), and computed tomography (CT); however, these static or two-dimensional measurements do not truly represent dynamic 3D motion (Charbonnier et al., 2014). Motion capture, with optical or electromagnetic sensors, is another common technique to track shoulder motion; however, this requires external markers making it difficult to palpate and track subcutaneous landmarks, often leading to soft-tissue artifacts (Bourne et al., 2011; Charbonnier et al., 2014; Jackson et al., 2012; Klotz et al., 2013). Using bone-fixed markers prevents skin-motion artifact (McClure et al., 2001), but its invasiveness is a limiting factor on sample size and the use of local anesthesia may affect the kinematic validity (Hajizadeh et al., 2019). In recent literature, radiographic imaging has been the standard technique using biplane x-ray (Baumer et al., 2016; Bey et al., 2006, 2008), biplane fluoroscopy (Giphart et al., 2013; Kijima et al., 2015; Kolz et al., 2021; Massimini et al., 2012), or single-plane fluoroscopy (Kon et al., 2008; Matsuki et al., 2011; Nishinaka et al., 2008). In this approach, a 3D model, usually obtained through CT, is registered to dynamic radiographic images to determine the bones pose throughout a motion. This technique is dynamic and does not suffer from soft-tissue artifact but the size of the imaging volume is limited (Baumer et al., 2016) which can be problematic with the large ROM in the shoulder (Krishnan et al., 2019). Additionally, a small field of view means common landmarks found on the thorax and spine are not usually available and thus scapulothoracic kinematics are often referenced to an external reference such as the scanner's global coordinate system (Kijima et al., 2015; Kon et al., 2008; Matsuki et al., 2011); this is an obvious disadvantage as any torso motion is erroneously included. To address some of these challenges, recent studies have employed four-dimensional CT (4DCT) as it provides a 3D view of the shoulder complex over time (3DCT + time) and can provide dynamic images of the joint (Alta et al., 2012; Bell et al., 2015; Matsumura et al., 2019). Additionally, the technique is non-invasive and does not suffer from soft-tissue artifact.

Relatively recent advancements in imaging technology have enabled 4DCT to be a viable imaging modality for both clinical and research applications. Improvements in detector technology have gradually allowed for increasingly more CT slices to be captured simultaneously. From 4 detector rows in 1998 to present-day 320-row systems, a practical field of view can now be captured in a single gantry rotation (Hsiao et al., 2010). Coupled with improved gantry rotation speed, which not only reduces radiation exposure but also minimizes motion artifacts, modern scanners can image a 160mm long field of view in 0.3 seconds (Hsiao et al., 2010). For 4DCT, this acquisition process is repeatedly performed to capture the same volume at numerous time points, enabling the generation of dynamic 3D imaging datasets (Wong et al., 2022). Early applications of 4DCT were in radiation oncology, particularly for thoracic and abdominal tumors, where respiration caused movement of lesions and quantifying the motion using 4DCT enabled more precise administration of therapeutic radiation. Additionally, 4DCT can be useful in assessing dynamic anatomical structures such as the heart, capturing its entire cycle to examine flow dynamics and valvular conditions. With evidence regarding the safety and efficacy of 4DCT in these domains, its adoption for other uses is growing among clinicians and researchers. Specifically, imaging a moving joint with 4DCT has applications for musculoskeletal research, providing insight into instability, impingement, and joint mechanics (Wong et al., 2022). However, this technology is still in its infancy and papers characterizing healthy motion of the shoulder using 4DCT are limited.

## 1.4 Aging

Aging is an inevitable biological process characterized by numerous physiological changes, most relevant for this research are the alterations in the musculoskeletal system. The shoulder, being a complex structure of bones, muscles, tendons, and ligaments, is particularly vulnerable to the effects of aging. Body wide, bone density diminishes, reducing the capability to adapt to loading forces (Freemont & Hoyland, 2007). Additionally, the viscoelastic properties of articular cartilage decline, reducing the ability to efficiently absorb mechanical stress; concurrently, ligaments lose elasticity lessening overall flexibility (Freemont & Hoyland, 2007). Furthermore, there is an overall reduction in muscular power, decreasing strength and stabilization (Freemont & Hoyland, 2007).

Studies focused on the shoulder have reported a decline in muscle mass and strength (Murgia et al., 2018; Pike et al., 2022), reduced passive (Barnes et al., 2001; Macedo & Magee, 2009) and active (Barnes et al., 2001; Doriot & Wang, 2006; Pike et al., 2022; Stathokostas et al., 2013) ROM, and changes in joint mechanics (Kolz et al., 2021), all of which influence overall shoulder motion. The risk of joint diseases such as osteoarthritis is also strongly linked to age (Loeser, 2011).

## 1.5 Osteoarthritis

Glenohumeral osteoarthritis (GHOA) is a form of degenerative joint disease where the smooth articular cartilage is gradually worn down. The near-frictionless articulation of the glenohumeral joint deteriorates, the failing articular cartilage abnormally distributes joint forces, subsequently triggering adaptive changes of the subchondral bone. Both the humeral head and glenoid often wear down, resulting in osseous deformity and reduced ROM (Walch et al., 1999). Often, this condition is a result from joint trauma, including chronic dislocations, surgery, inflammatory arthropathy, or rotator cuff tears; however, the disease can also be idiopathic (Chillemi & Franceschini, 2013). Regardless, the resulting symptoms are often pain and loss of function which can make many activities of daily living complicated, negatively impacting quality of life. For patients with manual labour professions, the debilitating symptoms can also have serious impacts on their ability to perform occupational tasks. It is estimated that 5%-17% of patients with shoulder complaints suffer from GHOA (Ibounig et al., 2021). The demographic most affected is the elderly population with a GHOA prevalence of 32% in patients over the age of sixty (Chillemi & Franceschini, 2013).

A primary feature of GHOA is glenoid erosion, although it does not present the same in all patients. The Walch classification system describes the type and magnitude of glenoid erosion patterns to guide surgical intervention (Walch et al., 1999). The original classification has three types and is based on two-dimensional axial plane measurements from CT scans. Type A (59% of patients in original study) is a symmetrical/central erosion without subluxation of the humeral head; A1 is considered minor erosion and A2 is considered severe erosion. Type B (32%) is asymmetrical wear which is accompanied by posterior subluxation of the humeral head; B1 is characterised by little/no glenoid erosion

but with humeral head subluxation, posterior joint space narrowing, and/or osteophytes, whereas B2 has extensive posterior glenoid erosion forming a biconcave glenoid. Type C (9%) is classified as glenoid retroversion greater than  $25^\circ$  regardless of erosion or subluxation although generally the humeral head is well centered or slightly subluxated (Walch et al., 1999). Bercik et al. (2016) proposed an improved classification system which uses 3D reconstruction and adds additional types B3, and D. A type B3 glenoid is monoconcave with posterior erosion and at least  $15^\circ$  of retroversion, or greater than 70% of posterior humeral head subluxation, or both. The additional type D is defined as any level of glenoid anteversion or anterior humeral head subluxation less than 40%. Additionally, the A2 glenoid classification is updated to a more precise definition of when a straight line connecting the anterior and posterior rims of the glenoid transects the humeral head. The Walch-Bercik classification of glenoid erosion is illustrated in Figure 1–7.

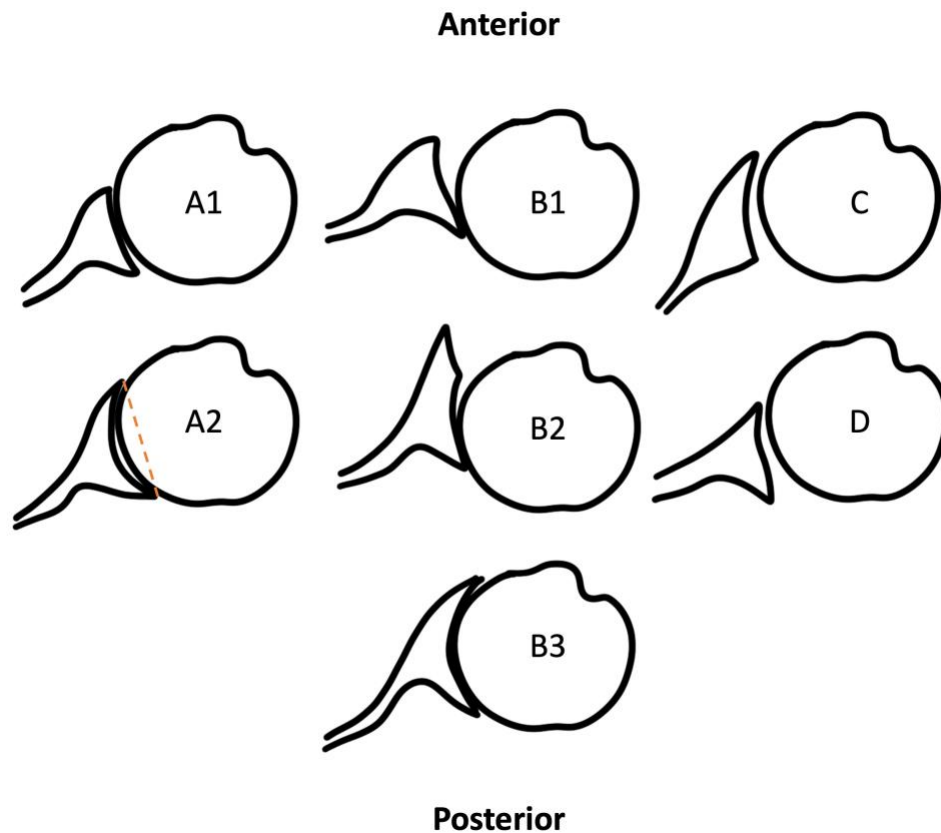


**Figure 1–7: Walch-Bercik classification of glenoid erosion.**

There are a variety of conservative and surgical options to treat GHOA including activity modification, non-steroidal anti-inflammatory drugs, and/or steroid injections, but these options typically only manage the disease by offering pain reduction and potential improvements in ROM. Surgical options include hemiarthroplasty, anatomic shoulder arthroplasty, or reverse shoulder arthroplasty. However, even without complications, surgical recovery includes a prolonged period of immobilization that can result in a delay for return to work and difficulties with activities of daily living.

## 1.6 Shoulder Arthroplasty

Total shoulder arthroplasty (TSA) is a full replacement of the native glenohumeral joint. There are two variations, anatomic (aTSA) which mimics the anatomy of the shoulder joint and reverse (rTSA) which reverses the ball and socket components. This surgical intervention aims to alleviate pain and improve function in patients suffering from a multitude of conditions that lead to deterioration of the glenohumeral joint. The most common diagnoses leading to TSA are GHOA (63%), rheumatoid arthritis (17%), and musculoskeletal trauma (15%) (Singh et al., 2011). Typically, rTSA are used for patients with severe rotator cuff deficiency because a rTSA shifts the center of rotation medially, providing a mechanical advantage to the deltoid muscle, and further stabilizes the joint which is normally done by the rotator cuff muscles (Hansen & Routman, 2019). However, rTSA is also commonly used for severe comminuted fractures of the proximal humerus or as revision to aTSA.

In 2017, over 800,000 people were living with a form of shoulder replacement (aTSA, rTSA, or hemiarthroplasty) in the United States, giving a prevalence of 0.258%, an increase from 0.031% in 1995 and 0.083% in 2005 (Farley et al., 2021). Additionally, there is a higher prevalence in females (0.294%) compared to males (0.221%). This demographic is primarily elderly with over 2% of people over the age of 80 living with a shoulder replacement. Hemiarthroplasty accounted for approximately 25% of shoulder replacements in 2017 but it is decreasing in popularity in favour of anatomic and reverse implants. From 2010 to 2017 the prevalence of hemiarthroplasty decreased from 0.070% to 0.061% while the prevalence of anatomic and reverse increased from 0.062% to 0.197%. The survival rates of TSA are promising, with 94%, 90%, and 81% at 5-, 10-, and 20-years,



respectively (Singh et al., 2011). Patient satisfaction after aTSA is also high at approximately 90%, but still leaves room for improvement (Jacobs et al., 2016). Dissatisfied patients typically exhibit less improvement in ROM following surgery and have lower American Shoulder and Elbow Surgeons (ASES) scores, indicating worse pain and function both preoperatively and postoperatively (Friedman et al., 2019; Jacobs et al., 2016). As research improves the understanding of these issues and the underlying causes are identified, satisfaction rates should improve as implant designs, surgical techniques, and rehabilitation strategies advance.

### 1.6.1 Design

A standard aTSA implant is comprised of two main components: the glenoid component and the humeral component. The glenoid component is typically made of ultra-high molecular weight polyethylene, a tough plastic with high wear resistance. Although some designs feature a metal backing based on the type of fixation used. Fixation techniques vary and include cemented, noncemented, or hybrid approaches (Strauss et al., 2009). Cemented pegged or keeled components are the most prevalent as there is immediate fixation. Noncemented components are initially fixed with screws or press-fitted into the bone, with long-term bone growth providing further stability. Hybrid fixation blends both techniques, using minimal cement alongside bone in-growth (Strauss et al., 2009).

Most modern humeral components are modular systems with multiple parts: the humeral head, the spherical metal surface that articulates with the glenoid, and the humeral implant, affixed into the humerus bone. These systems commonly have heads available in a variety of sizes to suit individual patient anatomy. Typically, a metal stem is inserted into the humeral shaft, although stemless designs are also prevalent. Fixation of a stem can be cemented, although there are difficulties extracting cement from the humeral canal in the case of revision surgery, and a bone plug should be used to limit cement migration (Sanchez-Sotelo, 2011). Cementless designs are preferred and feature textured surfaces that allow for bone in-growth providing long-term fixation (Sanchez-Sotelo, 2011). Stemless designs utilize metaphyseal fixation which has numerous benefits including the preservation of bone, reduced stress shielding, and simplified potential revision surgery (Churchill & Athwal, 2016).

The AEQUALIS PERFORM+ system (Wright Medical Group, Memphis, Tennessee, USA) is a popular series of glenoid components designed specifically for patients with posterior glenoid erosion. It is identical to the AEQUALIS PERFORM (Wright Medical Group, Memphis, Tennessee, USA) but features a posterior wedge to restore humeral positioning while maximizing bone preservation. The glenoid components are offered in four sizes (small, medium, large, extra-large) and with a three augment angles (15°, 25°, and 35°) for the wedge. The SIMPLICITI shoulder system (Wright Medical Group, Memphis, Tennessee, USA) is a widely used stemless humeral implant compatible with the aforementioned glenoid systems (Figure 1–8).

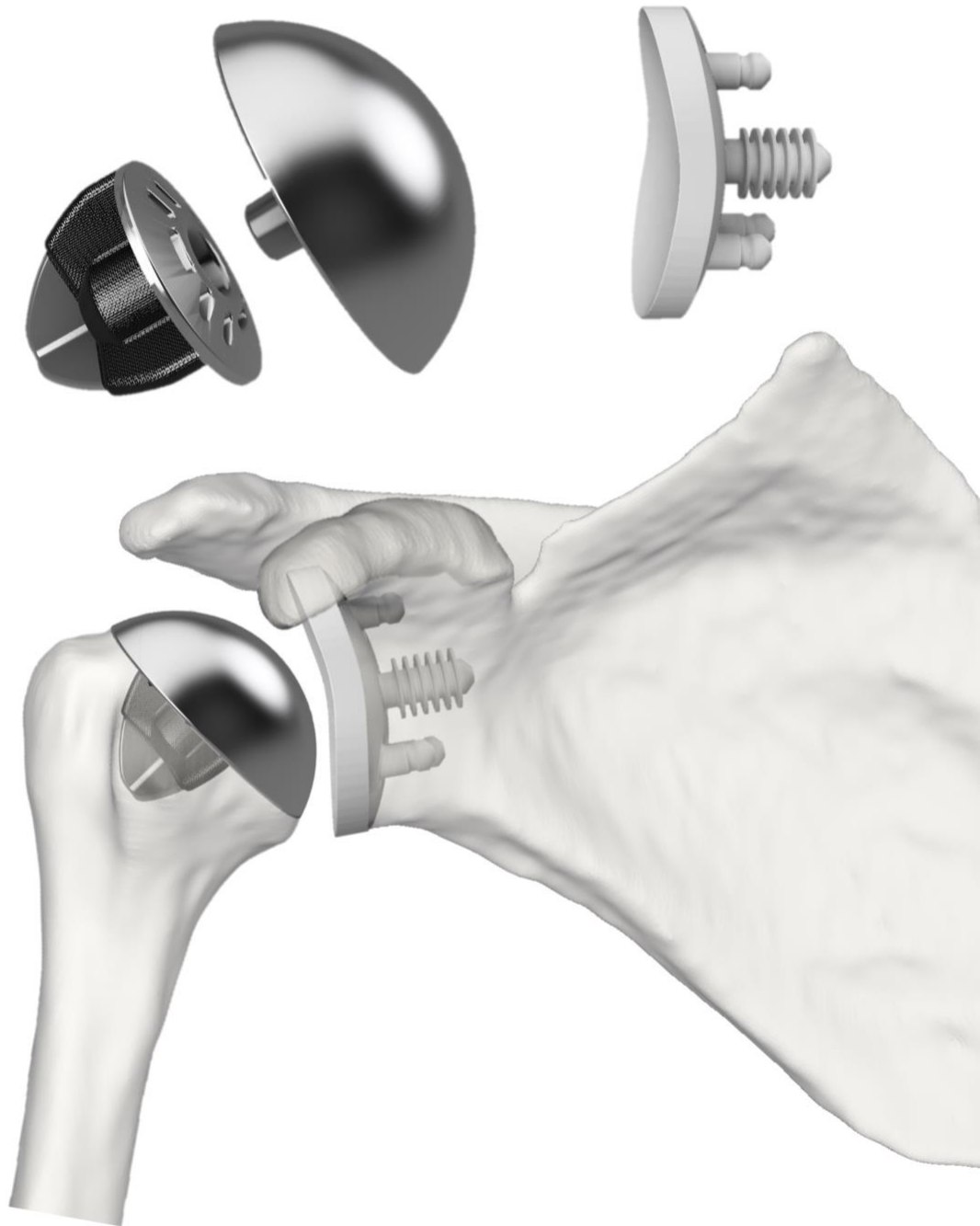


**Figure 1–8: Total shoulder arthroplasty components.**

*The AEQUALIS PERFORM glenoid and the SIMPLICITI humeral components of a total shoulder arthroplasty.*

## 1.6.2 Mismatch

Given the availability of multiple sizes for each component in an aTSA, a wide array of combinations is possible. The glenoid and humeral components each have a distinct curvature, with the difference between them termed as mismatch, typically quantified in terms of diametrical mismatch, i.e., the difference in diameter of curvature (Figure 1–9). For the AEQUALIS PERFORM and PERFORM+ systems, glenoid components are offered in four sizes, spanning from 55mm to 68mm in diameter of curvature. This glenoid is compatible with many humeral head systems, including the SIMPLICITI humeral head which comes in 9 sizes, ranging from 41mm to 54mm in diameter of curvature. Permissible diametrical mismatch combinations according to the manufacturer range from 1mm to 24.8mm, where the glenoid component has a larger curvature than the head (Table 1–5).

There is no consensus on an ideal mismatch between components in an aTSA. It is known that some degree of mismatch is necessary because totally conforming designs limit translation more than a natural joint (Karduna et al., 1997). In cadaveric and isolated component testing, the general trend is that a small mismatch provides stability but increases shear forces on the glenoid; in contrast, a larger mismatch leads to greater translation but with reduced articular contact, consequently increasing pressure on the implant and fixation cement, leading to higher wear and risk of glenoid loosening (Diop et al., 2006; Karduna et al., 1997; Sabesan et al., 2015; Terrier et al., 2006). On the low end of the spectrum, a radial mismatch greater than 4mm is beneficial as it results in reduced translational forces, glenoid strain, and implant displacement (Diop et al., 2006). As an upper limit, a radial mismatch above 10mm should be avoided as contact pressure can exceed the yield strength of polyethylene resulting in permanent damage (Terrier et al., 2006). Additionally, an *in vivo* study on glenoid loosening, using radiolucent lines observed in postoperative radiographic follow-ups, suggests that the ideal radial mismatch is between 6 and 10mm (Walch et al., 2002). However, a more recent study with similar methods found that a mismatch as low as 3.4mm has no significant effect on the risk of glenoid loosening (Schoch et al., 2019). Furthermore, in terms of clinical outcomes, radial mismatch ranging from 3.4 to 7.7mm does not appear to significantly affect ROM, function, pain, complication rate, or revision rate (Schoch et al., 2019).

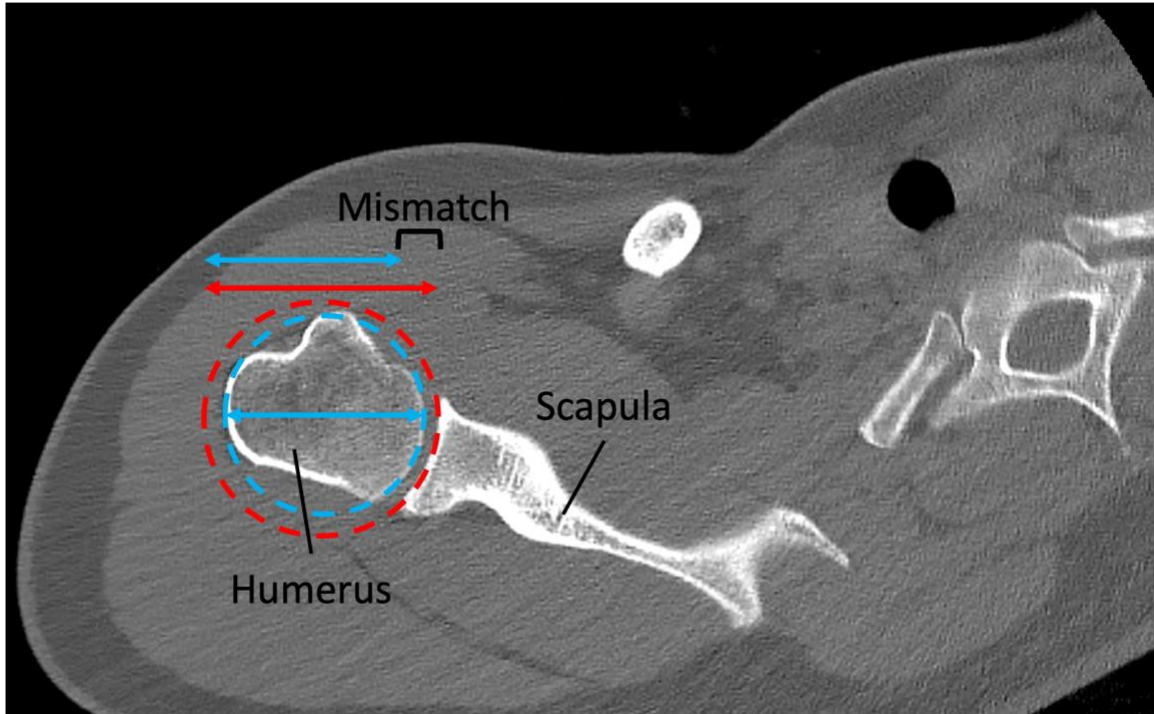


**Figure 1–9: Axial CT scan of the shoulder illustrating diametric mismatch.**

*The red circle matches the curvature of the glenoid of the scapula, the blue circle matches the curvature of the humeral head. Mismatch is defined as the difference in diameter between the circles.*

**Table 1–5: Mismatch chart for AEQUALIS PERFORM+ glenoids with SIMPLICITI heads. Diametrical mismatch is in mm, green cells are in the cleared mismatch range, red cells are non-cleared mismatch values. The cleared range for this combination is 1 to 24.8mm. (Wright Medical Group, 2016)**

Size	Heads	37X13.5	39X14	41X15	43X16	46X17	48X18	50X16	50X19	52X19	52X23	54X23	54X27
Glenoid	Diameter of curvature	39	41.2	43	45	48	50	55	52	54.6	52.4	54.7	54
Small	55.4	16.4	14.2	12.4	10.4	7.4	5.4	0.4	3.4	0.8	3	0.7	1.4
Medium	59.6	20.6	18.4	16.6	14.6	11.6	9.6	4.6	7.6	5	7.2	4.9	5.6
Large	63.6	24.6	22.4	20.6	18.6	15.6	13.6	8.6	11.6	9	11.2	8.9	9.6
XL	67.8	28.8	26.6	24.8	22.8	19.8	17.8	12.8	15.8	13.2	15.4	13.1	13.8

### 1.6.3 Internal Rotation Deficiency

After undergoing implant surgery, patients may lose the ability to reach behind their back, also known as internal rotation (Miller et al., 2003; Rojas et al., 2020; Triplet et al., 2015, 2018). This deficiency is most prevalent for those with a rTSA but also occurs following an aTSA, affecting as many as 68% of patients in some capacity (Miller et al., 2003). A deficiency in this motion is problematic for patients' functional ROM during activities of daily living, including dressing, bathing, and toileting (Langer et al., 2012; Rojas et al., 2020; Triplet et al., 2015). During assessments of shoulder function such as the ASES, internal rotation is commonly measured by one's ability to reach the small and middle of their back to perform the tasks of tucking in a shirt and washing their back or unhooking a bra (Richards et al., 1994). During implant surgery using the standard deltopectoral approach, the subscapularis, an important rotator cuff muscle responsible for internal rotation, is tenotomized and repaired. Issues leading to subscapularis deficiency after aTSA include muscle tears, poor-quality tissue, inadequate physical therapy, excess tension caused by oversized components, or denervation (Miller et al., 2003). Consequently, the recovery of internal rotation is strongly linked to the restoration of the subscapularis (Liem et al., 2012; Miller et al., 2003). Furthermore, multiple studies have shown a strong correlation between preoperative and postoperative ROM (Friedman et al., 2019; Jacobs et al., 2016; Levy et al., 2016). Long wait times for surgery coupled with a lack of preoperative physical therapy may result in prolonged disuse of the shoulder, leading to muscle atrophy, reduced flexibility, increased stiffness, and/or the formation of adhesions, all of which would further limit preoperative and consequently postoperative motion. Inadequate post-surgery rehabilitation can also impede recovery and limit ROM. Since there is no single standardized physical therapy protocol following TSA, approaches can differ significantly (Mulieri et al., 2010; Schick et al., 2023). If physical therapy is too conservative, it may lead to stiffness whereas overly aggressive physical therapy could compromise the integrity of the subscapularis repair and/or the implant, reducing stability and function (Mulieri et al., 2010). Furthermore, patient compliance and adherence to their rehabilitation program can vary, impacting the effectiveness and overall outcomes. The implant itself is another crucial factor, the components must be sized and placed appropriately with some degree of mismatch to allow for glenohumeral translation while

still maintaining stability of the joint. Finally, variations in surgical approaches and reconstruction techniques can impact the restoration of internal rotation. The various factors influencing postoperative outcomes after TSA emphasizes the importance of a comprehensive approach to preoperative preparation, surgical technique, and postoperative rehabilitation. Addressing issues related to subscapularis deficiency, optimizing preoperative ROM, implementing optimal physical therapy programs, and ensuring appropriate sizing and placement of implants are all essential for maximizing patient outcomes and restoring functional motion following surgery.

## 1.7 Motivation

Dynamic kinematics of the shoulder are not yet fully understood in the field of biomechanics. While numerous studies have investigated glenohumeral kinematics, scapulothoracic kinematics are less understood, despite the crucial contributions of both joints in shoulder function. Additionally, it is unknown how the intricate glenohumeral-scapulothoracic relationship changes with age. Moreover, existing research tends to focus on simplistic motions such as abduction or flexion, overlooking the complexities of multi-planar movements involved in everyday activities such as internal rotation, an important yet under-studied movement.

After TSA surgery, many patients experience a loss of internal rotation, which is crucial for daily activities like dressing and bathing when reaching behind the back is required. The recovery of internal rotation may depend on a variety of factors including restoration of the subscapularis muscle, proper preoperative and postoperative rehabilitation, appropriately sizing components, and variations in surgical technique. Nonetheless, the exact causes and subsequent effects on shoulder kinematics are unknown. Furthermore, in satisfied TSA patients with a good ROM, it is unknown if their kinematics are comparable to natural shoulders or if compensatory motion is present.

One factor contributing to these gaps in knowledge is technological availability. Many methodologies rely on imaging techniques that only capture static or quasi-static measurements, failing to encapsulate the true dynamic nature of shoulder motion. Although motion capture systems can record dynamic movements, their accuracy is significantly

compromised by skin motion artifacts, limiting precise measurement. Consequently, dynamic bone imaging-based kinematics emerges as the gold standard, as the absence of motion artifacts provides a more accurate representation of shoulder motion while remaining non-invasive. Utilizing 4DCT for studying shoulder kinematics is valuable because it enables dynamic motion assessment, even for intricate motions such as internal rotation behind the back, capturing movements in real-time. Since 4DCT visualizes bones directly, it eliminates the inaccuracies caused by skin motion artifacts, resulting in highly accurate data. This technology allows for the precise measurement of both scapulothoracic and glenohumeral motions, providing a comprehensive understanding of shoulder kinematics. Moreover, 4DCT can be further utilized for tracking implants post-surgery, revealing how kinematics may change with the presence of an implant. Similarly, 4DCT can provide precise dynamic assessments to better understand and address TSA deficiencies, leading to improved patient outcomes and functional recovery.

## 1.8 Objectives and Hypotheses

The overall goal of this dissertation was to develop a method for measuring shoulder kinematics via 4DCT imaging, and then apply this process to quantify healthy glenohumeral and scapulothoracic kinematics, and investigate how these kinematics may change with age and with an implant.

The objectives of this thesis are as follows:

- 1) To develop a process of measuring glenohumeral and scapulothoracic kinematics through bone motion obtained via 4DCT, and to assess the repeatability of this process.
- 2) To improve the feasibility of using 4DCT by automating the most time-consuming step, segmenting the scans to create bone models.
- 3) To quantify healthy shoulder kinematics and investigate the influence of age. The specific aims are to:
  - a) Identify the importance of humeral translation.
  - b) Identify how kinematics, ROM, and scapulohumeral rhythm change with age.



- c) Determine if the natural position of the bones changes with age.
- 4) To compare the kinematics between natural and aTSA shoulders, focusing on the impact of mismatch and mobility. The specific aims are to:
  - a) Compare aTSA and non-implant kinematics to identify any compensatory movements.
  - b) Identify any differences in kinematics based on patient mobility.
  - c) Identify any differences in kinematics based on patient mismatch.

The hypotheses for this thesis correlate to each objective, and are as follows:

- 1) The developed process will be repeatable and comparable to existing methods.
- 2) No hypothesis necessary.
- 3)
  - a) Humeral translation is required for proper shoulder motion.
  - b) Older participants will exhibit less humeral motion and unchanged scapular motion, subsequently leading to a lower scapulohumeral rhythm compared to the younger participants.
  - c) The average scapula position will change with age.
- 4)
  - a) Patients with good mobility will have similar kinematics and ROM as non-implant participants.
  - b) Patients with poor mobility will exhibit less humeral translation and humeral internal rotation.
  - c) Greater mismatch will correlate with greater humeral translation.

## 1.9 Thesis Overview

**Chapter 2:** Describes and validates a novel process for measuring shoulder kinematics with the use of 4DCT.

**Chapter 3:** Describes the design and performance of neural networks created for automated CT segmentation.

**Chapter 4:** Investigates six-DoF kinematics of healthy shoulders during forward elevation and internal rotation, and analyses how kinematics change with age.

**Chapter 5:** Investigates six-DoF kinematics of aTSA shoulders during internal rotation and analyses the impact of patient mobility and implant mismatch.

**Chapter 6:** General summary, discussion, and conclusion of the work presented in this thesis.

**Appendix A:** Quantifies the errors in bone modeling due to voxel resolution and scan orientation.

## Chapter 2

### 2 Development of the Single-Vertebra Image-Based Technique for Measuring Shoulder Kinematics using Four-Dimensional Computed Tomography

#### OVERVIEW

*This chapter introduces and validates a new technique for analyzing six degrees-of-freedom shoulder kinematics using four-dimensional computed tomography, which uses a single vertebra to reference thoracic motion. Differences between the vertebra coordinate system and the International Society of Biomechanics torso coordinate system are compared. Finally, the errors associated with repeated analysis are examined.<sup>1</sup>*

<sup>1</sup>A version of this work has been published: Hunter, J., Lee, T. Y., Athwal, G. S., & Lalone, E. A. (2023). Development of a single-vertebra image-based technique to quantify shoulder kinematics using four-dimensional computed tomography. *Computer Methods in Biomechanics and Biomedical Engineering: Imaging & Visualization*, 12(1). <https://doi.org/10.1080/21681163.2023.2282074>

## 2.1 Introduction

Analyzing shoulder girdle kinematics is challenging as the shoulder is comprised of a complex group of highly mobile joints with a large range of motion (ROM) in all three directions (Krishnan et al., 2019). Moreover, to fully describe shoulder motion, all six degrees-of-freedom (DoF) in the joints need to be defined (Charbonnier et al., 2014). These measurements are possible with the advancements of four-dimensional computed tomography (4DCT). However, this technology is still in its infancy and papers characterizing healthy motion of the shoulder using 4DCT are limited.

The International Society of Biomechanics (ISB) has recommendations for various landmarks and coordinate system definitions (Wu et al., 2005). Briefly, the humeral coordinate system employs the epicondyles as landmarks, and the torso coordinate system uses landmarks on the sternum and spine. However, to capture all of these landmarks, a large field of view is required, no less than 28cm across and 26cm axial. Additionally, treating a torso coordinate system as a static reference may be a poor assumption given that the spine is not a rigid body. Moreover, this assumption may be valid when standing but with 4DCT the different motions that are performed require different positioning such as laying on the back or the side.

The primary objective of this chapter was to describe a new technique for analyzing shoulder kinematics which uses 4DCT and associated anatomical landmarks, referred to as the Single-Vertebra Imaged-Based (SVIB) technique. Secondary objectives were to determine whether the vertebra derived local coordinate system is comparable to the ISB thorax derived local coordinate system and to assess repeatability of the proposed SVIB technique.

## 2.2 Methods

### 2.2.1 Data Acquisition

Following approval from Western's Research Ethics Board, participants were recruited with the inclusion criteria of males 18 years of age or over, and no history of dominant shoulder injury. After obtaining informed consent, participants were checked to ensure they

had a healthy ROM in their dominant shoulder (able to reach behind their back up to at least their lower thoracic vertebrae). Additionally, imaging was reviewed post hoc and any participants that did not have the required anatomical landmarks visible were excluded. A total of four participants (average age  $27 \pm 8$ ) were included in this study.

A computed tomography (CT) scanner (Revolution CT Scanner, GE Healthcare, Waukesha, Wisconsin, USA) was used to image the shoulder. First, a localizer scan was used to determine the proper field of view, then a static scan with the participant in a neutral position, then a second localizer scan after repositioning, and lastly a dynamic scan. The static scan followed standard static imaging protocol (120kV, 211mA, 1.0s rotation time, 512x512 matrix, axial) and produced 192 1.25mm thick slices for a volume of size 250x250x240mm<sup>3</sup>. For the static scan, the participant was positioned supine with their head and back supported (with padded foam) to ensure that the scapula was not pressed against the gantry table (Figure 2–1A). The dynamic scan followed a standard dynamic imaging protocol (80kV, 130mA, 0.35s rotation time, 512x512 matrix, axial) producing 64 2.50mm thick slices repeatedly for 21 seconds generating 60 volumes (approximately 2.9 frames per second) of size 450x450x160mm<sup>3</sup>. For the dynamic scan, participants performed internal rotation to the back while lying on their non-dominant side (Figure 2–1B). For this motion, the dominant hand starts on the abdomen and is moved around the torso while keeping the elbow flexed, finishing with the participant reaching their hand as far up their back as possible. The dynamic scan included this motion being performed as usual in addition to the participant returning to the starting position. For the purposes of this study only one direction of the motion was analyzed and as such only the first 25 – 35 frames were analyzed based on the endpoint of motion. To ensure the motion was properly executed, a demonstration was given before the scan and participants were able to practice the motion, additionally, a technologist remained in the scanner room during the scan and counted throughout the scan to ensure the motion was performed at the correct speed such that the motion was fully completed within the scan time. The scan duration (approximately 10 seconds to reach the final position and 10 seconds to return) was selected to prevent any motion blurring by maintaining a deliberately slow speed. However, participants exhibited slight variations in time, as they were instructed to maintain a continuous pace rather than rushing to complete the motion if they felt they were moving too slowly.



**Figure 2–1: Participant positioning in the CT scanner.**

*Participant positioning during the (A) static and (B) dynamic scans.*

Each localizer scan has a dose length product (DLP) of 8 mGy\*cm, the static scan has a DLP of 281 mGy\*cm, and the dynamic scan has a DLP of 428 mGy\*cm. Therefore, using the effective dose conversion factor for a typical chest CT ( $0.014 \text{ mSv} \cdot \text{mGy}^{-1} \cdot \text{cm}^{-1}$ ) (American Association of Physicists in Medicine, 2008), the effective dose of the entire procedure is estimated at 10.1mSv. For context, a typical chest CT scan is 7mSV and annual average background radiation is approximately 1.8mSV in Canada and 2.4mSV worldwide (UNSCEAR, 2008).

### 2.2.2 Kinematic Analysis (SVIB):

Using the scans, reconstructed three-dimensional bone models of the proximal humerus, scapula, and first thoracic (T1) vertebra were created in 3DSlicer ([www.slicer.org](http://www.slicer.org), Version 4.11) using a semi-automated reconstruction technique. This consists of thresholding the bone, followed by manual cleanup, and finally applying a smoothing function. Each of these models were made for the static scan and for every other frame of the dynamic scan. The static models were registered to each dynamic model using an iterative closest point algorithm (Besl & McKay, 1992) performed in 3DSlicer via the CMFregistration extension ([cmf.slicer.org](http://cmf.slicer.org)). The result of the registration was a transformation matrix describing the position of each dynamic model relative to its respective static model.

Anatomical landmarks were then identified on the static scan and used to create coordinate systems. All landmarks are manually selected apart from the humeral origin, which is calculated based on a sphere to humeral head registration. Specifically, multiple points are randomly selected on the articular surface to generate a best fit sphere. The humerus follows a modified ISB coordinate system where the axes are mathematically aligned to the scapula coordinate system, which is shown to have no statistical difference in ROM calculation for an abduction motion (Levasseur et al., 2007). The scapula and vertebra coordinate systems are based on the ISB recommendations (Wu et al., 2002, 2005), although the scapula origin is placed at the glenoid center rather than the acromion. The local coordinate systems, summarized in Figure 2–2, are defined as the following:

**Humerus coordinate system:** The origin is located at the centroid of a sphere fit to the articular surface of the humeral head (GH). The humeral Zh-axis (+lateral), Xh-axis

(+anterior), and Yh-axis (+superior) are defined to be coincident with the respective scapular axes (Levasseur et al., 2007).

**Scapula coordinate system:** The origin is located at the glenoid center (GC), defined as the midpoint along a vector connecting the most inferior and superior points on the glenoid. The vector from the trigonum spinae scapulae (TS) to the acromial angle (AA) is defined as the Zs-axis (+lateral). The vector perpendicular to the plane formed by the inferior angle (AI), TS, and AA is the Xs-axis (+anterior). The Ys-axis (+superior) is the cross product of the Zs- and Xs-axes (Wu et al., 2005).

**Vertebra coordinate system:** The origin is located at the midpoint between the centers of the upper endplate (UE) and the lower endplate (LE). The vector from LE to UE is defined as the Yv-axis (+superior). The vector parallel to a line joining the left pedicle (LP) and right pedicle (RP) is the Zv-axis (+lateral). The Xv-axis (+anterior) is the cross product of the Yv- and Zv-axes (Wu et al., 2002).

These coordinate systems form two joint coordinate systems (JCS), which consist of a reference and a moving coordinate system. The transformation matrix between the reference (<sub>r</sub>) and the moving (<sub>m</sub>) coordinate system for each frame *i* is calculated as follows:

$$T_{r_i}^{m_i} = [T_{r_i}^r * T_r^G]^{-1} * [T_{m_i}^m * T_m^G]$$

, where the matrices  $T_r^G$  and  $T_m^G$  define the transformations between the static models and the global frame (G) for the reference and moving frames, respectively. The matrices  $T_{r_i}^r$  and  $T_{m_i}^m$  are the transformations obtained through registration of the static models to the dynamic models for each frame *i* for the reference and moving frames, respectively. Note that the matrices are pre-multiplied due to the registration transformations being calculated in the global frame.



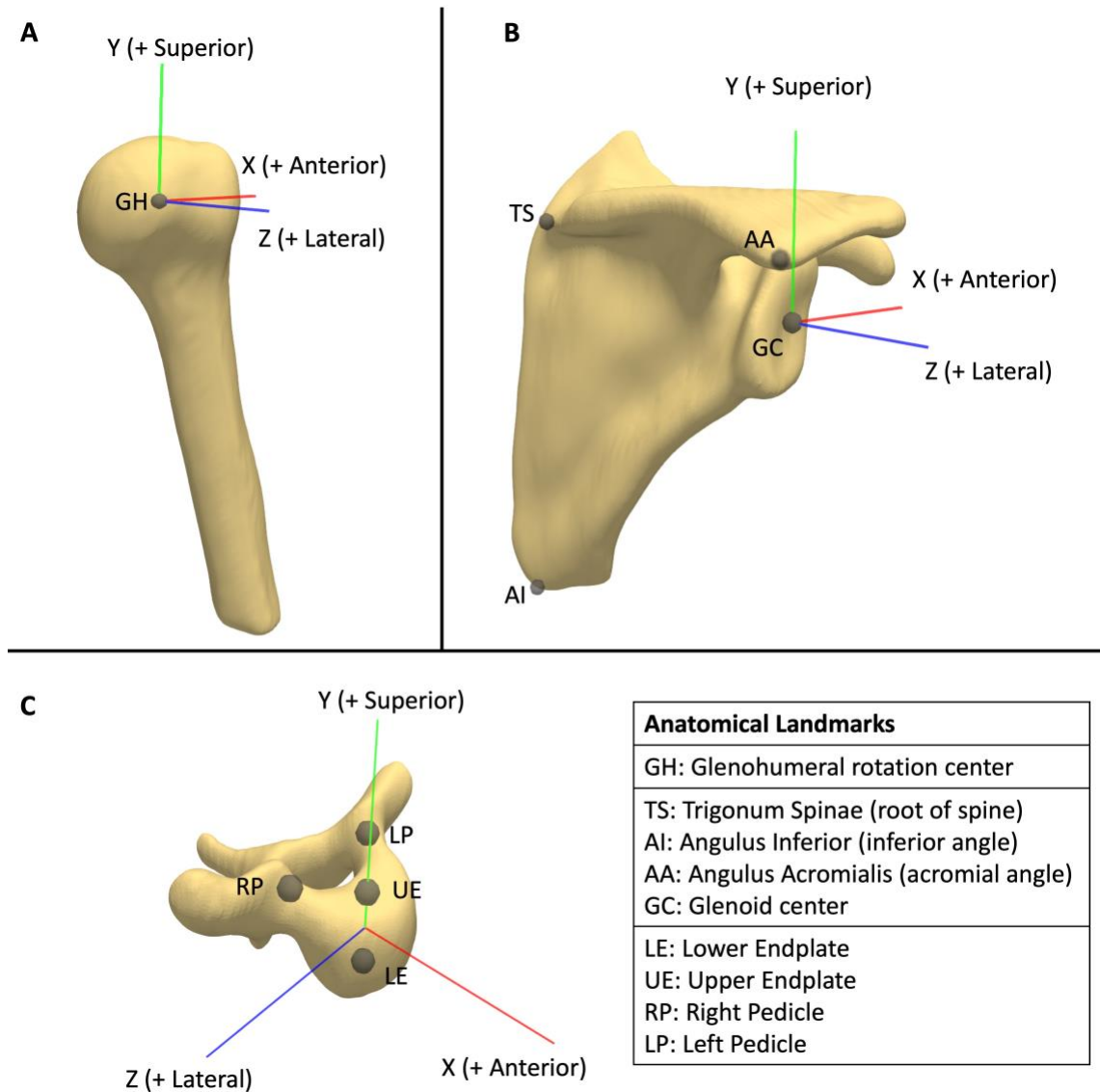


**Figure 2–2: Local coordinate systems and associated anatomical landmarks.**

*Local coordinate systems for the (A) humerus, (B) scapula, and (C) T1 vertebra with the anatomical landmarks used to create each coordinate system.*

The scapulothoracic JCS describes the scapula position relative to the spine, decomposed into translations and a standard Y-X'-Z'' rotation sequence (Wu et al., 2005). Positive rotations about the scapula axes are labeled as protraction (Y), medial rotation (X'), and posterior tilting (Z'') (Figure 1–6). The glenohumeral JCS describes the humerus relative to the scapula, decomposed into translations and a X-Z'-Y'' rotation sequence; note that this

is different than the ISB recommended Y-X'-Y'' sequence as it has been shown to have singularity issues when approaching elevation angles of 0° and 180° (Phadke et al., 2011; Šenk & Chèze, 2006). Positive rotations about the humeral axes are labeled as adduction (X), flexion (Z'), and internal rotation (Y'') (Figure 1–5), all rotations follow the right-hand rule for positive axes. All matrix multiplications and decompositions were performed in MATLAB (MathWorks, Version R2020a).

### 2.2.3 Data and Statistical Analysis

The conventional (ISB) JCS for the scapula uses the thorax as the reference, rather than a single vertebra. However, based on an individual's bodily proportions, the required anatomic landmarks for the thorax are not necessarily in the field of view of all scans, thus it is important to compare the differences between the two references. For the participants of this study, the necessary landmarks were available, therefore coordinate systems were created for both the T1 vertebra (Wu et al., 2002) and the thorax.

The ISB thorax coordinate system is defined as the following: The origin is located at the Incisura Jugularis (IJ) of the sternum, also known as the jugular notch. The vector connecting the midpoint between the xiphoid process (PX) and T8, and the midpoint between IJ and C7 is defined as the Yt axis (+superior). The vector perpendicular to the plane formed by IJ, C7, and the midpoint between PX and T8 is defined as the Zt axis (+lateral). The Xt axis (+anterior) is the cross product of the Yt- and Zt-axes. (Wu et al., 2005).

The transformation between the two coordinate systems was calculated and decomposed into a Y-X'-Z'' rotation sequence. The rotational differences were used to calculate an average root-mean-square error (RMSE). In addition, the kinematics of the scapula over the entire internal rotation to the back motion were analyzed. The relationship between the two kinematic pathways (translations and rotations throughout the motion) was compared with the Pearson correlation coefficient. Additionally, a Bland-Altman plot was generated to evaluate the agreement and bias between the T1 and the thorax coordinate systems. Values for ROM were calculated as the difference between the maximum and minimum values. This was done for all six DoF using both the vertebra and thorax references for

each participant. Average differences in ROM values between the two coordinate systems were calculated. An analysis of variance (ANOVA) test was done to determine if a statistical difference could be found in any ROM calculation between the two coordinate systems. Statistical significance was set as  $p < 0.05$ . All statistical analysis was performed in MATLAB (MathWorks, Version R2020a).

The technique for measuring shoulder kinematics is a complicated multistep process, and each step can introduce error, especially when performed manually; thus, it is important to assess the repeatability of the process. To assess this, the model making, coordinate system creation, and registration steps were repeated thrice by the same investigator for the scans of one participant (age 25) and the results compared. For each DoF in the scapula JCS and humeral JCS, the standard deviation at each individual time point was determined and used to calculate an average standard deviation. Additionally, the differences in ROM were also assessed in terms of mean absolute deviation (MAD). Lastly, the repeatability of landmark selection was assessed by manually selecting the required landmarks for all bones five times for each participant. Landmark repeatability was assessed by looking at the average standard deviations of landmark points and of coordinate system orientation.

## 2.3 Results

### 2.3.1 Vertebra vs Thoracic Comparison

On average, compared to the ISB thoracic coordinate system, the vertebra coordinate system is rotated  $3.4^\circ$  externally (Y-axis),  $7.2^\circ$  medially (X-axis), and  $18.1^\circ$  anteriorly (Z-axis). The average coordinate frame positions are shown in Figure 2–3. These rotational errors correspond to an average RMSE of  $11.6^\circ$ .

As expected, the thorax and vertebra series are not identical, but they have a strong linear correlation, the mean Pearson correlation coefficient was 0.915 with a median value of 0.996. The kinematic pathways follow a similar trend with an apparent offset present (Figure 2–4). The average offset of the vertebra pathway relative to the thorax was -6.4mm, and  $-1.4^\circ$  (Figure 2–4). The Bland-Altman plot further quantifies this offset; the mean bias of the translational DoF were 14.2mm, -1.1mm, and 7.2mm for the respective X, Y, and Z

axes (Figure 2–5). The mean bias of the rotational DoF were  $3.2^\circ$ ,  $1.0^\circ$ , and  $0.1^\circ$  for the respective Y, X, and Z axes (Figure 2–5).

The average signed difference between the spine- and thorax-referenced scapula ROM was 0.3mm and  $0.8^\circ$  while the average absolute difference was 2.7mm and  $2.5^\circ$  (Figure 2–6). Furthermore, no statistical differences were found for any ROM calculation, with p-values ranging from 0.53 to 0.99.

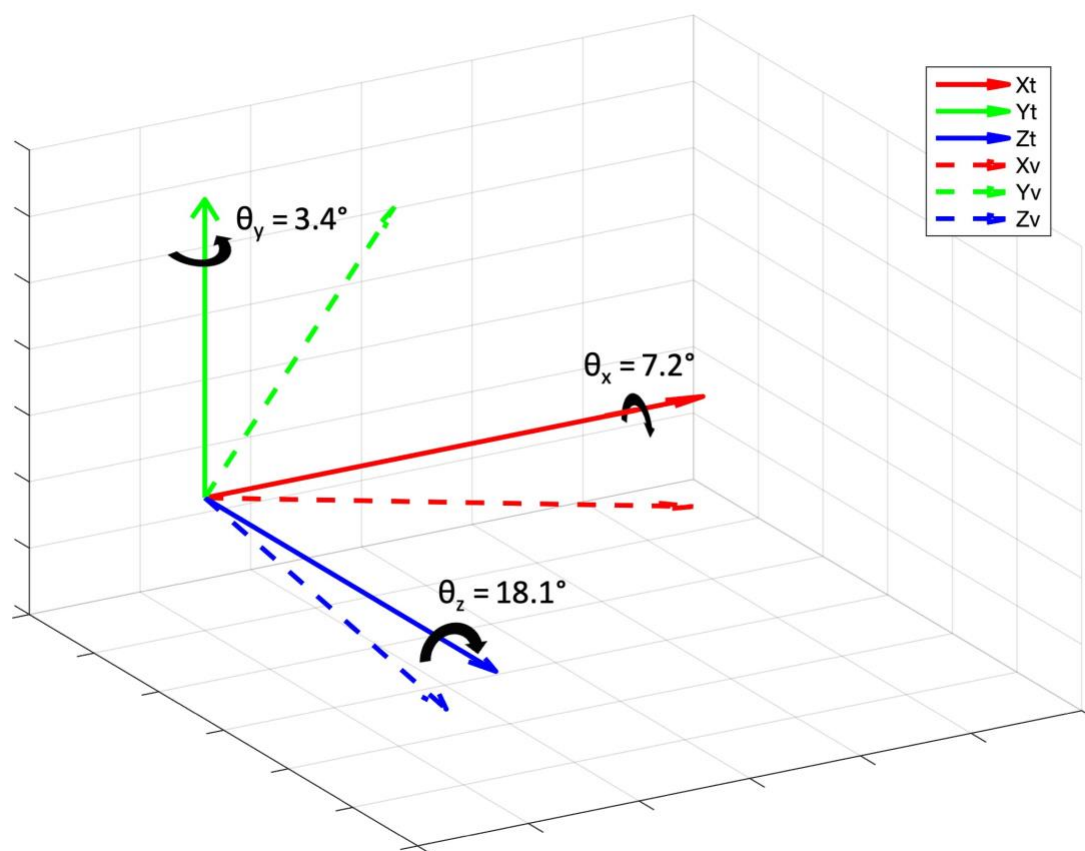


**Figure 2–3: Comparison of vertebra and thorax coordinate systems.**

*Average position of the vertebra coordinate system (– –) relative to the average thorax coordinate system (–) which is rotated  $3.4^\circ$  around the Y-axis,  $7.2^\circ$  around the X-axis, and  $18.1^\circ$  around the Z-axis.*

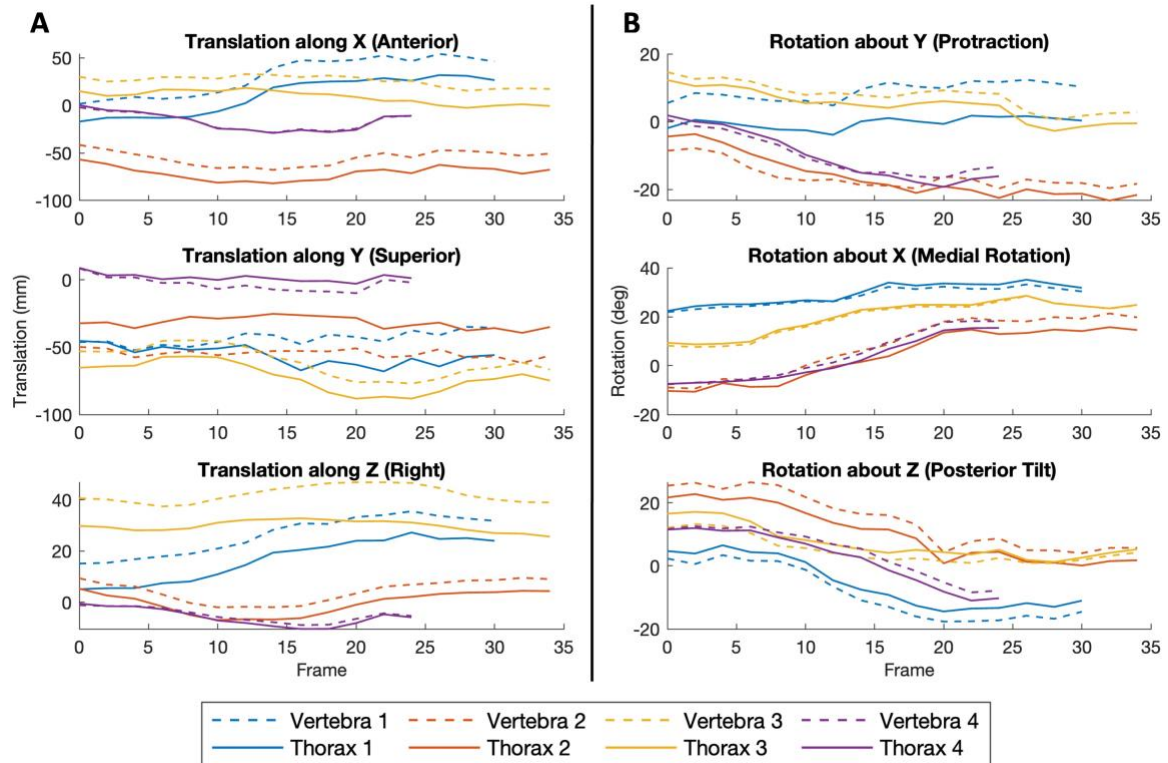


**Figure 2-4: Kinematics relative to a vertebra and a thorax coordinate system.**

*Six degree of freedom kinematics of the scapula for (A) translational and (B) rotational degrees of freedom relative to a vertebra coordinate system (—) and a thorax coordinate system (—) for four participants. Average translational difference was  $-6.4\text{mm}$ , and average rotational difference was  $-1.4^\circ$ .*

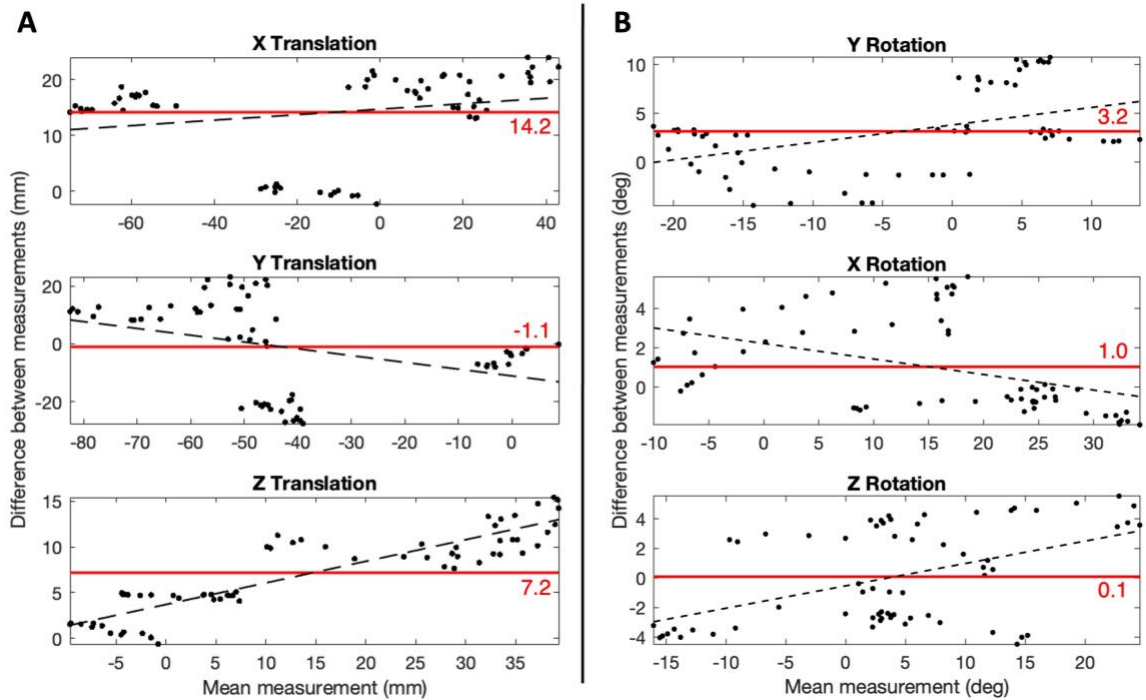


**Figure 2–5: Bland-Altman plot comparing vertebra and thorax coordinate systems.**

*An illustration of the agreement between the vertebra and thorax methods for measuring scapula kinematics for the (A) translational and (B) rotational degrees of freedom. For each plot the horizontal red line shows the mean difference, and the dashed line represents the linear regression line of the data points.*

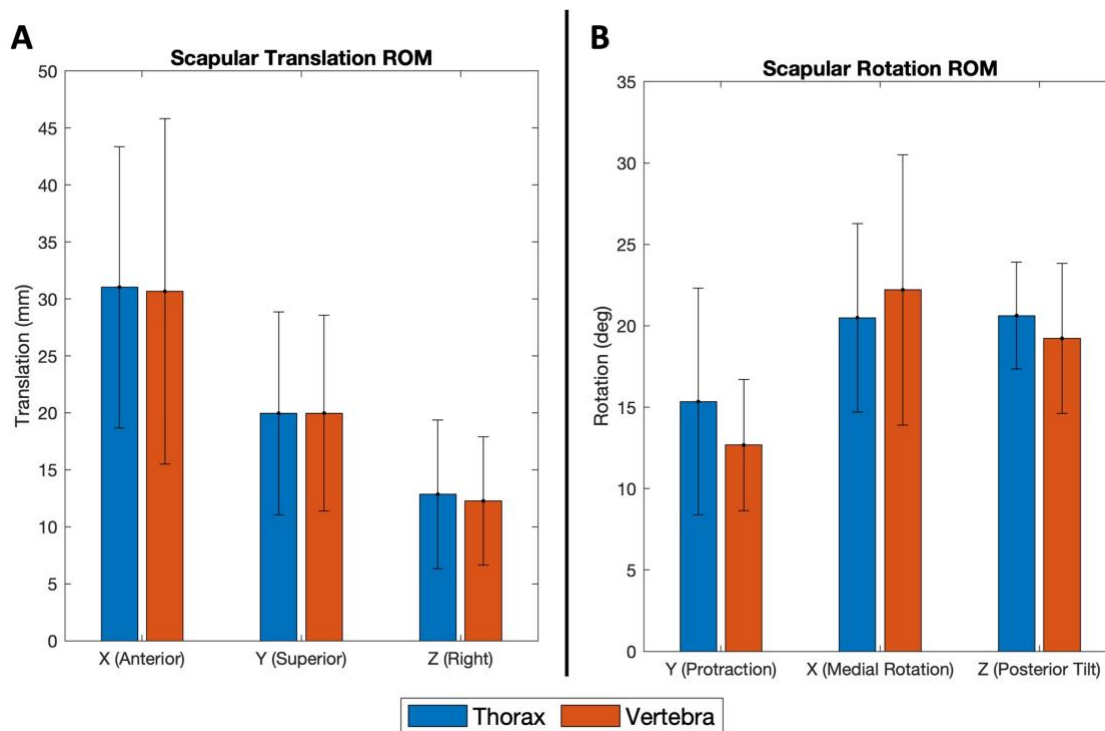


**Figure 2–6: Range of motion relative to a vertebra and a thorax coordinate system.**

*Average range of motion of the scapula for (A) translational and (B) rotational degrees of freedom relative to a thorax coordinate system (blue) and vertebra coordinate system (red) for four participants. Average translational differences were 0.3mm (signed) and 2.7mm (absolute), average rotational differences were 0.8° (signed) and 2.5° (absolute).*

### 2.3.2 Repeatability

Regarding repeatability, for the scapula JCS, the average translational standard deviation was 3.4mm and the average rotational standard deviation was 1.1° (Figure 2–7). For the humeral JCS, the average translational standard deviation was 0.2mm and the average rotational standard deviation was 0.9° (Figure 2–7). For the ROM calculations in the scapula JCS, the translational MAD was 1.1mm and the rotational MAD was 0.5° (Figure 2–8). For the ROM calculations in the humeral JCS, the translational MAD was 0.2mm and the rotational MAD was 1.4° (Figure 2–8). For both JCS, the Y-axis (superior-inferior) had the largest discrepancy in translation and the Z-axis (medial-lateral) had the largest discrepancy in rotation. For landmark selection repeatability, the scapula, humerus, and

vertebra selected points had, on average, a standard deviation of 0.24mm, 0.27mm, and 0.23mm, respectively; the total average standard deviation was 0.25mm. For the scapula the inferior angle landmark had the minimum standard deviation (0.17mm) and the trigonum had the maximum (0.33mm). For the vertebra the upper endplate had the minimum standard deviation (0.17mm) and the lower endplate had the maximum (0.30mm). Regarding differences in the resultant coordinate systems, the scapula, humerus, and vertebra origins had average standard deviations of 0.24mm, 0.27mm, and 0.18mm, respectively. The scapula and humerus had an average standard deviation of  $0.18^\circ$  of rotation about the coordinate systems axes, while the vertebra had a standard deviation of  $0.66^\circ$  on average about the axes.



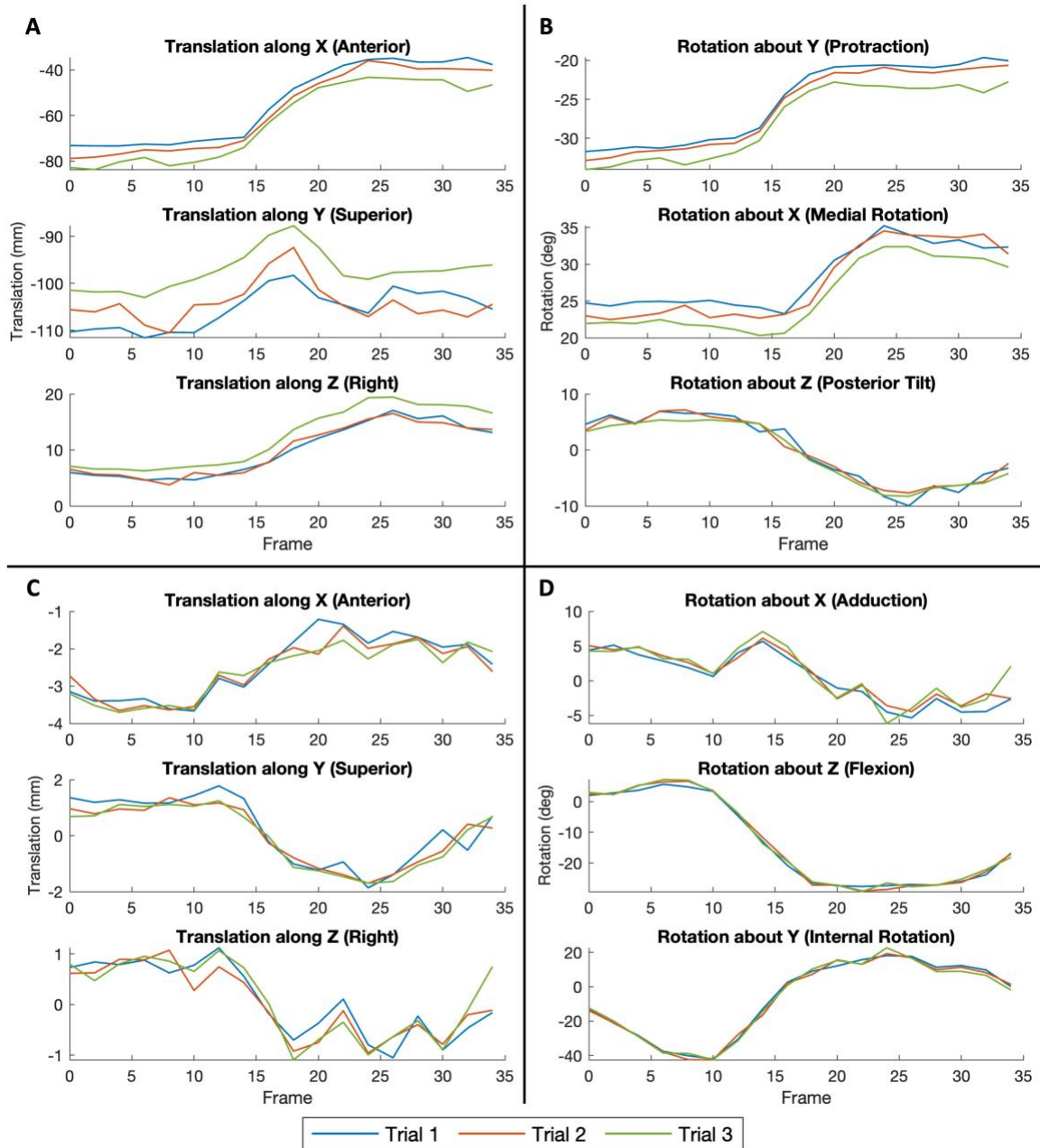


**Figure 2–7: Repeated kinematic calculations.**

*Threefold repeatability (blue, red, and green series each represent one trial) of scapulothoracic (A) translational and (B) rotational kinematics, and glenohumeral (C) translational and (D) rotational kinematics. Average standard deviations were (A) 3.4mm (B) 1.1° (C) 0.2mm (D) 0.9°.*

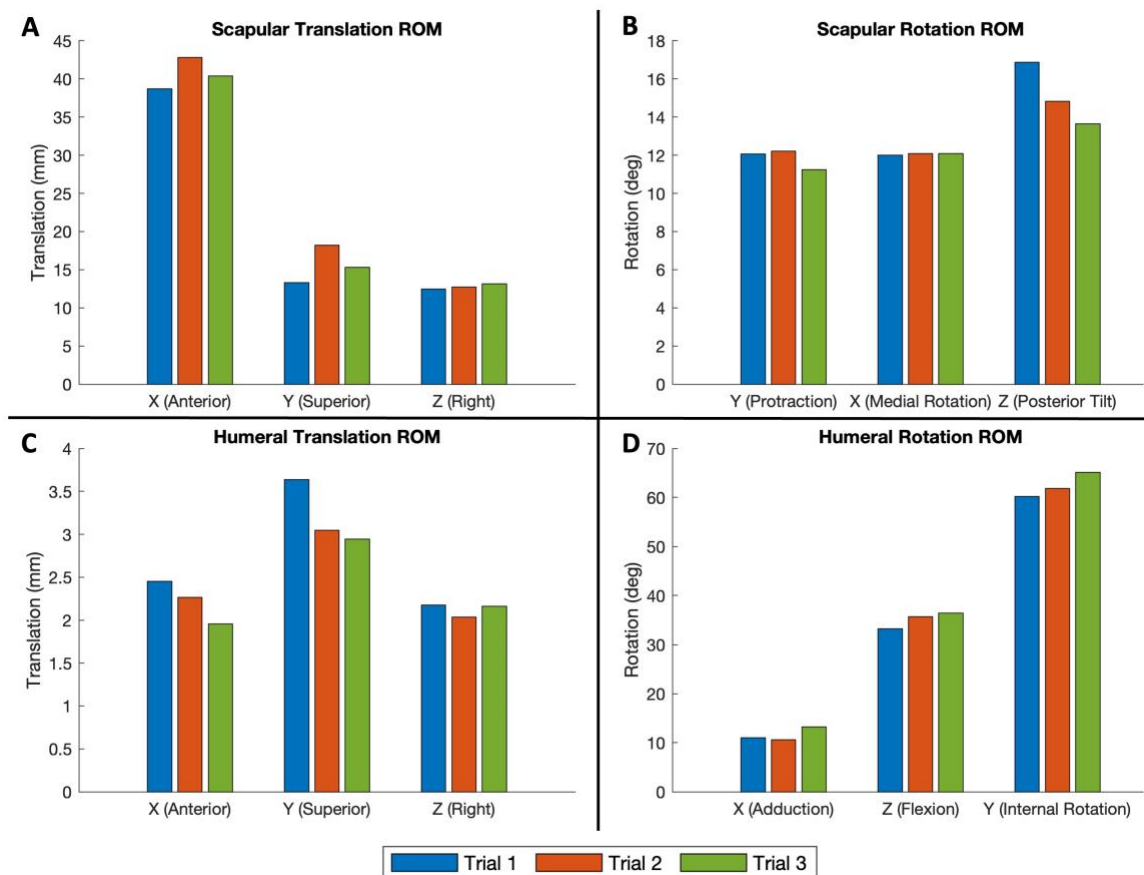


**Figure 2–8: Repeated range of motion calculations.**

Range of motion calculations for three trials (blue, red, and green) for scapulothoracic (A) translations and (B) rotations, and glenohumeral (C) translations and (D) rotations. Mean absolute deviations were (A) 1.1mm (B) 0.5° (C) 0.2mm and (D) 1.4°.

## 2.4 Discussion

The objectives of this chapter were to describe the SVIB technique for analyzing shoulder kinematics and compare the differences between the single vertebra coordinate system to the ISB thorax coordinate system in addition to assessing the repeatability of the SVIB technique. Results from this study indicate that, as expected, there are discrepancies between the coordinate systems, but these differences were found to be less than 11.6° on average (Figure 2–3), and show similar trends (Figure 2–4). Furthermore, when looking at entire ROM over the dynamic scans (Figure 2–6), no statistical differences were found for

any DoF (translation: anterior/posterior, superior/inferior, medial/lateral; rotation: protraction/retraction, upward/downward, anterior/posterior). It should be noted that the absence of a difference is not necessarily indicative of equivalence. However, given that the p-values were relatively high (0.53 to 0.99), the probability of a difference is low. Thus, ROM values can be accurately compared to other studies that have used an ISB thorax coordinate system. Overall, it has been demonstrated that it is sufficient to treat the vertebra and thorax systems as comparable in the scapula JCS.

The Bland-Altman analysis revealed systematic biases between the vertebra and thorax coordinate systems, particularly in the translational DoF (Figure 2–5). Notably, using the vertebra consistently produced higher values for X and Z translations compared to the thorax method, with mean differences of 14.2mm and 7.2mm, respectively. This discrepancy increased with higher translation values, as indicated by the positive regression slopes, ranging from 11mm to 17mm for the X axis, and 1mm to 13mm for the Z axis. For Y translation, a small bias (-1.1mm) was observed, although the negative regression slope ranged from 8mm to -13mm. In terms of rotational DoF, the mean differences were generally smaller, and with flatter regression lines. The vertebra method showed slightly higher measurements for Y and X rotations ( $3.2^\circ$  and  $1.0^\circ$ , respectively), with respective regression lines ranging from  $0^\circ$  to  $6^\circ$  and  $3^\circ$  to  $0^\circ$ . The mean difference for Z rotation was minimal ( $0.1^\circ$ ), but the positive trend in the regression line ranging from  $-3^\circ$  to  $3^\circ$  suggests a potential increase in bias at higher rotation values. These findings indicate that the vertebra and thorax methods are not perfectly interchangeable, as the observed biases may affect the interpretation of scapula kinematics, particularly the translational DoF, depending on the chosen reference coordinate system. However, quantifying these biases allows for approximate conversion factors between the coordinate systems, improving comparability between studies using the different approaches.

A restriction of CT-based imaging is that certain movement types, such as a full abduction, are not possible due to the scanner's narrow bore (75cm diameter). The internal rotation to the back motion is one that can be comfortably performed in the scanner. Additionally, because it is a non-planar motion that requires all DoF to perform, it is challenging to examine with other imaging techniques, but showcases the full potential of the SVIB

technique. Furthermore, internal rotation behind the back is uncommonly studied in the literature, but it is an important motion to study as it is essential in many activities of daily living (Langer et al., 2012; Rojas et al., 2020), restriction of this motion is also a common disadvantage of reverse shoulder arthroplasties (Rojas et al., 2020).

A study by Kolz et al. (2021) looked at static internal rotation poses in reference to a neutral pose. Their results showed less scapulothoracic ROM (10° medial rotation, 5° posterior tilt) than the values determined using the SVIB technique (13° protraction, 22° medial rotation, 19° posterior tilt); however, our results show that the maximum and minimum rotations are not necessarily at the endpoints of motion, which may partially contribute to the discrepancy. Additionally, the neutral position used by Kolz et al. for ROM reference had the humerus in an anatomically neutral pose, whereas our study had the humerus internally rotated such that the hand rested on the abdomen. When looking at Kolz et al. glenohumeral kinematics, the ROM results more closely aligned with ours apart from internal rotation (80° vs 60°), however, the differences in starting positions could again account for the discrepancy.

The ISB thorax coordinate system landmarks require a large field of view to capture, and others have proposed alternative thorax coordinate systems to address the issue. Baumer et al. (2016) conducted a study where they created thorax coordinate systems using various rib pairs. The rib3:rib4 pair had the lowest error compared to ISB thorax, with an RMSE of 4.4°, while the highest had an RMSE of 26.1° (Baumer et al., 2016). One limitation of a rib-based coordinate system is the relative motion of ribs during breathing which may introduce errors when measuring dynamic motion. The largest error for the rib coordinate system was internal/external rotation (Baumer et al., 2016), while the vertebra coordinate system had the largest error with anterior/posterior rotation. This relative anterior tilting of the T1 vertebra compared to the thorax is expected based on the natural kyphotic curvature of the thoracic vertebrae, this presents as the vertebral body, and subsequently the coordinate system, to appear anteriorly tipped. The advantages of using the T1 vertebra are that it is a distinguishable landmark that is easily identifiable in scans and convenient to include in a narrow field of view as it is aligned at a similar level to the glenohumeral joint.

The results of this study also indicate that the SVIB technique is repeatable. The largest difference when looking at kinematics was scapulothoracic translation in the inferior/superior direction (Figure 2–7). This direction closely aligns with the axial CT direction, which only has a slice thickness of 2.5mm. This value is comparable in magnitude to the total translational RMSE of 2.6mm. Thus, a single slice difference could contribute to most of the error. Glenohumeral translational RMSE was much smaller at only 0.3mm, and both JCS had rotational RMSE of about 1°. This suggests that the largest source of error is the T1 vertebra models, as scapula or humerus model differences would result in larger glenohumeral discrepancies. When looking at ROM values (Figure 2–8), the errors are similar to the RMSE apart from scapulothoracic translations in which the mean error was only 1.8mm. Overall, the error is reasonably small, but it is important to know the limitations of this technique. Regarding landmark selection, the errors were relatively small. The selected points on average had a standard deviation of only 0.25mm; the impact on coordinate system creation was also minimal, with translational deviations less than 0.3mm and rotational deviations less than 0.7°. It is also important to mention that the assessment of multi-operator reproducibility, which could have offered further insights into the technique's overall reliability and applicability, was not able to be conducted. Although this study did account for repeatability, it was constrained to a single operator's involvement because of resource limitations, specifically the availability of adequately trained personnel and time restrictions.

This study only included the male sex and because the scans had to include landmarks for the ISB thorax coordinate system, this resulted in participants that had short torsos. This is a limitation as there is evidence that a participant's sex and anthropometry can influence the calculation of shoulder kinematics (Lavaiil et al., 2022). Additionally, there was variability in how participants performed the motion as it was unconstrained, and the final arm position was dictated by each participant's individual maximum range.

One major limitation of this technique is the time to conduct the analysis. The most time-consuming step is bone model reconstruction for every frame of motion; additionally, the skill to properly make bone models needs to be learned. The consequences of this are smaller study sample sizes and interpolation of kinematics, which in this study meant only

every other frame was analyzed. Development of a neural network to assist with scan segmentation and model creation will not only reduce the time necessary to calculate kinematics, addressing the time limitation, but artificial intelligence-based segmentation may also reduce human errors which would subsequently improve the reliability of the bone models.

The SVIB approach described in this chapter can effectively assess dynamic motion, all the necessary landmarks are easy to include in a reduced field of view, and there is no skin motion artifact. When looking at the repeatability of the SVIB technique, the associated errors are for the whole analysis, including model making, registration, and landmark selection. Each step can introduce errors, so given the relatively small errors over the whole analysis, the SVIB technique is a reliable approach to measure kinematics.

## Chapter 3

### 3 Automating Bone Model Creation from Computed Tomography Scans Using Neural Networks

#### OVERVIEW

*This chapter describes the development of a neural network for automated segmentation of the humerus and scapula. The network architecture, training parameters, and performance are detailed. Lastly, this chapter describes the integration of the neural network into 3DSlicer.*

## 3.1 Introduction

The time-consuming process of manually creating three-dimensional (3D) bone models from computed tomography (CT) scans is a major limiting factor in the number of participants that can be analyzed within a given timeframe. Automating the creation of bone models would greatly reduce the time spent on each participant, accelerating the entire analysis pipeline, thus allowing for more participants to be included in research studies. Given the intricacies involved in image segmentation, the use of machine learning, particularly neural networks, is an optimal approach. Additionally, neural networks have the advantage of deterministic performance, eliminating the bias and variability of manual approaches. Therefore, the objective of this project is to develop specialized neural networks capable of accurately segmenting the scapula and humerus from CT scans, effectively automating a labour-intensive process.

## 3.2 Methods

### 3.2.1 Network Architecture

The general architecture of the network that was used follows the U-Net structure, first described by Ronneberger and colleagues (Ronneberger et al., 2015). This type of network is a convolutional neural network commonly used for image segmentation tasks since the output is a label assigned to each pixel. The network diagram for the architecture used, adapted from the original U-Net design (Ronneberger et al., 2015), is shown in Figure 3–1. The architecture of a U-Net is distinctive for its U-shaped structure, consisting of a contracting path (left side) and an expansive path (right side). This innovative design enables the network to capture both local features through the contracting path and context information through the expansive path.



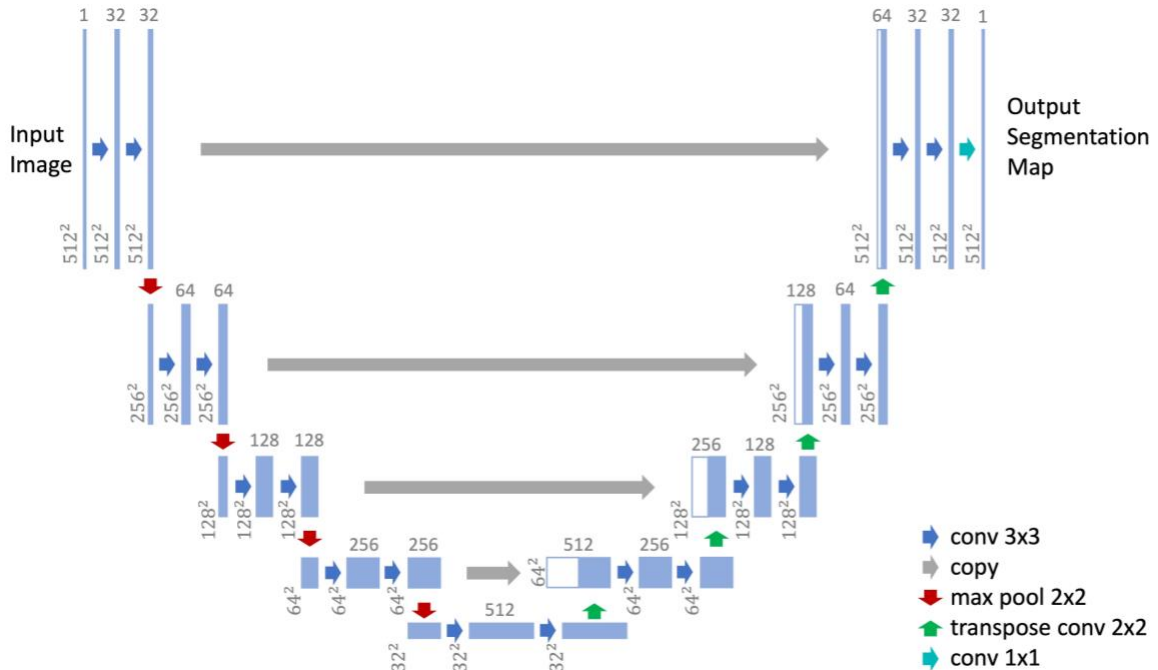


**Figure 3–1: Modified U-Net architecture.**

*Diagram depicting the adapted U-Net architecture utilized in the project. Each blue box represents a multi-channel feature map, with the number of channels indicated at the top, and the x-y size provided at the lower left corner of each box. White boxes signify copied feature maps, while arrows indicate the various operations performed.*

The contracting path consists of repeated blocks of convolutional layers followed by a downsampling operation. For this design, each block includes two 3x3 convolutions with a rectified linear unit activation, each consecutive block doubling the number of feature maps. Padding was applied to each convolution in order to preserve image dimensions which allows the final output to have the same dimensions as the input. Downsampling was achieved by applying 2x2 max-pooling with a stride of 2, reducing the spatial dimensions of the feature maps by half for each block. The expansive path is the mirror image of the contracting path, consisting of repeated blocks of upsampling followed by convolutional layers. The purpose of the expansive path is to gradually recover the spatial resolution lost during the contracting path and refine the segmentation output. The upsampling operation used was 2x2 transposed convolution to double the spatial

dimensions of the feature maps. Each block in the expansive path consists of two 3x3 convolutions, similar to the contracting path, except each consecutive block halves the number of feature maps.

One of the key features of the U-Net is the skip connections that directly connect corresponding layers between the contracting and expansive paths. These skip connections concatenate feature maps from the contracting path to the corresponding upsampling layers in the expansive path. These connections help in preserving finer details and spatial information. To reduce overfitting, a dropout layer was applied where a certain proportion of neurons are randomly selected to be ignored during the forward and backward passes of training. The original U-Net specified a dropout layer at the end of the contracting path (Ronneberger et al., 2015) although that is not entirely clear. Therefore, dropout layers were tested both at the beginning and end of the bottleneck layer and while both similar in performance, a dropout after the final max pooling layer produced the best results. While 50% is a common dropout value, a dropout of only 30% was used as higher dropouts prevented the network from properly converging. The final layer of the U-Net consists of a 1x1 convolutional layer with a sigmoid activation function since the output is binary, either bone or background. This layer produces the final segmentation mask, where each pixel of the image is assigned a probability value indicating the likelihood of belonging to the target segment. During reconstruction, any pixel with a probability exceeding 50% was considered to be bone, while any below this threshold were classified as background.

### 3.2.2 Training

The CT scans used for training were obtained from the participant pool of Chapter 4. A total of 16 scans, comprising of both static CT and dynamic four-dimensional CT (4DCT), for a total of 14,000 individual images were used for training, although a random 20% (2,800) were reserved for validation. The data from the CT scans is a sequence of 3D images stored as DICOM files; however, the network is designed to segment two-dimensional (2D) images. To get the data into the proper format, each individual slice of the scans was converted into PNG format. Manual segmentations of the scans were created using 3DSlicer ([www.slicer.org](http://www.slicer.org), Version 4.11) and transformed into binary masks. Separate masks were generated for the humerus and the scapula where a pixel value of 255

represented bone and 0 denoted the background. Subsequently, two distinct networks were trained utilizing the same architecture and parameters, one dedicated to segmenting the humerus and one for segmenting the scapula. The project was programmed in Python 3.8 utilizing Keras, a deep learning application programming interface (API) for Python, with TensorFlow as the backend, an open-source software library specializing in machine learning. The computational resources required for training the networks were accessed through Compute Canada (Digital Research Alliance of Canada), which is a national organization that provides computing resources to researchers across Canada.

Various data augmentations were implemented, including width and height shifting up to  $\pm 20\%$ , rotations up to  $\pm 50^\circ$ , and zooms up to  $\pm 20\%$  to artificially increase the training data and increase robustness of the network. Horizontal and vertical flipping were specifically not implemented as the scanning procedure, including the general positioning of the participant, is consistent. In the few instances where a left shoulder is scanned rather than the right side, then the scan is mirrored regardless in order to keep the kinematic coordinate systems consistent.

The loss function used for training was dice coefficient loss, which measures the discrepancy between the predicted segmentation mask and the ground truth mask. Dice loss was chosen rather than binary-cross entropy as it performs better when the dataset is not balanced (Jadon, 2020). Given that many of the training images are primarily background, it is therefore appropriate for this task. The network implemented mini-batch gradient descent which provides a good balance between computational intensity and rate of convergence. A batch size of 32 was used as larger batch sizes may lead to overfitting and reduce the generalizability of a network (Keskar et al., 2016). The network used a learning rate of 0.0001 with the Adam optimizer, which is an adaptive stochastic gradient descent method that converges quicker than regular stochastic gradient descent. The humerus network converged within 50 epochs while the scapula network required 70. However, throughout training, a checkpoint callback saved the weights producing the best results on the validation data.

### 3.2.3 Reconstruction

To streamline the entire process of utilizing the networks, a custom module was developed within 3DSlicer. For greater usability and flexibility, this module was designed with a robust framework for future expandability. Users can configure various additional settings through a graphical interface (Figure 3–2), a more user-friendly alternative to a command line interface. First, the user selects the input volume to be processed. Optionally, a region of interest can be defined, isolating a specific region within the volume, which is particularly useful for optimizing runtime by excluding non-relevant areas. Users may also specify an output volume for the resulting segmentation map; as a default, if no selection is made, a new volume is automatically created. Finally, the user chooses the target segment, either humerus or scapula. Upon program execution (“Apply” button) the input volume is separated into individual slices, which are resized as necessary, before undergoing segmentation via the chosen network. The output images are reconstructed into the output volume with identical dimensions to the input volume. A notification is displayed in 3DSlicer’s built-in Python interactor, indicating the completion of segmentation on the target segment and providing the processing runtime. The final step for the user involves obtaining 3D bone models from the output volume, a step easily performed in 3DSlicer’s Segment Editor module with the threshold operator. This allows for subsequent manual adjustments to the segmentations, if required, before exporting the models as 3D objects.

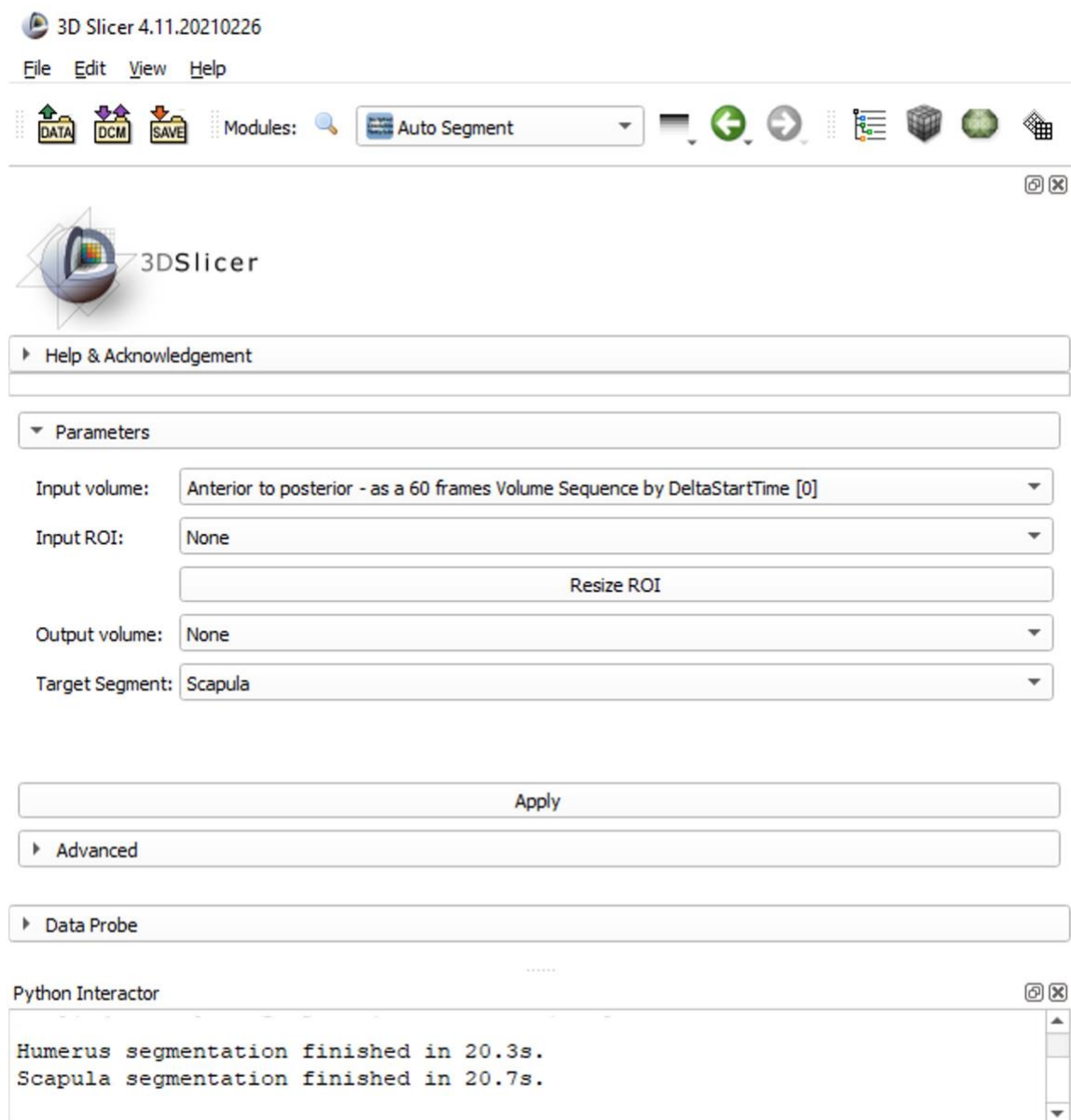


**Figure 3–2: Graphical interface of custom 3DSlicer module.**

### 3.2.4 Validation

The neural networks operate in 2D, however, the resultant models are used in a 3D application. To further validate the performance of the networks, and to quantify the effects on model registration, entire 3D models were used for analysis. A total of 15 frames were used for this validation. Five participants were randomly selected from the participant pool of Chapter 4, excluding those used for training, and three frames were taken from each

4DCT scan: the start, middle, and end of the motion. Ground truth models of the humerus and scapula were manually created in 3D slicer, and corresponding models were generated using the neural networks without any manual adjustments made to the segmentations. The neural network generated models were then registered to the ground truth models using a surface-based iterative closest point registration, generating a transformation matrix representing the positional difference between the models. These transformation matrices were subsequently decomposed into three translations and three rotations for analysis.

### 3.3 Results

For assessing accuracy, the dice metric was used as it provides a more proportionate representation of similarity compared to the standard accuracy metric, especially on datasets with significant class imbalances. Since the majority of each image consists of background, the accuracy metric could still yield high values despite the network predicting everything as background. The dice metric avoids this issue by specifically analyzing the intersection between the predicted and ground truth masks. In terms of performance, the humerus network achieved a final dice metric of 0.96 on both the testing and validation data sets, whereas the scapula network attained a final dice metric of 0.93 on testing data and 0.92 on validation data. An example of the network performance is shown in Figure 3–3. For the validation using model registration, the mean translations and rotations for both neural networks are detailed in Table 3–1.

**Table 3–1: Mean positional differences of neural network generated models relative to manual ground truth models.**

	Humerus	Scapula
Translation (signed)	0.43mm	0.14mm
Translation (absolute)	1.65mm	0.35mm
Rotation (signed)	0.14°	0.01°
Rotation (absolute)	0.78°	0.23°

When running the model on a central processing unit (CPU), the network is capable of segmenting a 512x512x64 pixel volume in roughly 20 seconds, for a total runtime of 40 seconds if implementing both the humerus and scapula networks. However, utilizing a graphics processing unit (GPU) significantly reduces the runtime to only 0.5 seconds per network.

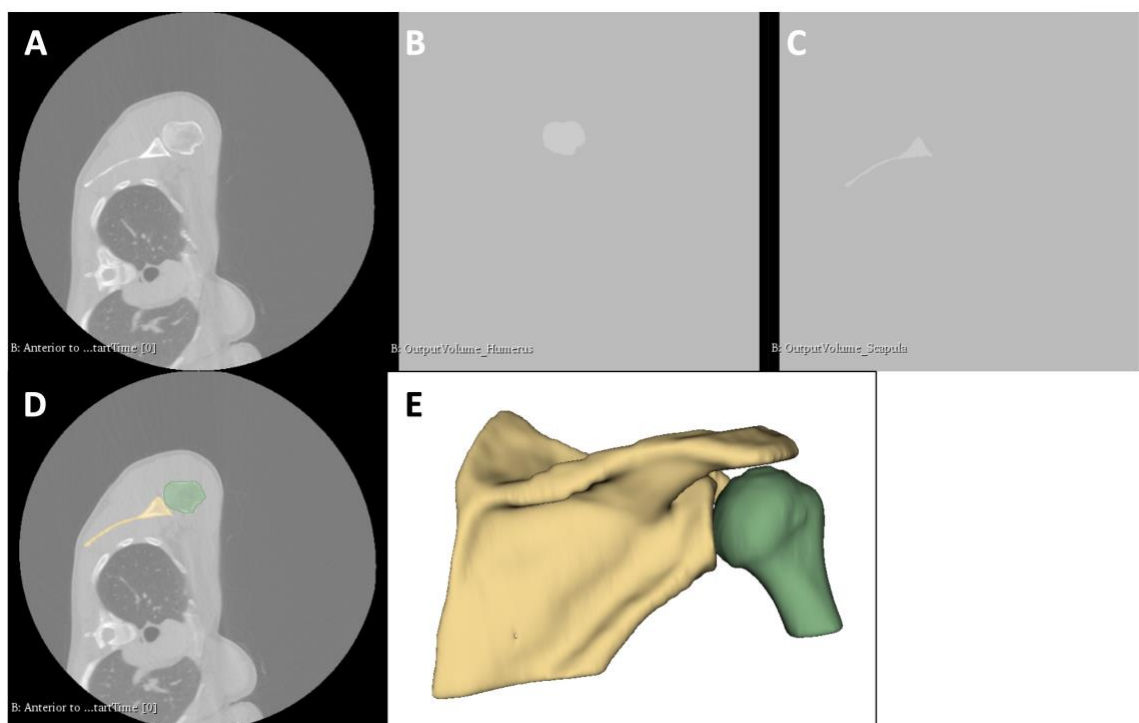


**Figure 3–3: Example performance of the networks.**

*This figure shows the (A) CT scan as input (B) segmentation map of humerus network (C) segmentation map of scapula network (D) segmentations overlaid on input (E) reconstructed bone models.*

### 3.4 Discussion

The development of specialized neural networks for the segmentation of the scapula and humerus from CT scans is a significant advancement that demonstrates the potential for machine learning to streamline a traditionally labour-intensive process. With this tool now available, it should significantly increase the efficiency and scalability of research.

Both networks achieved dice scores above 0.90, indicating a high level of accuracy. This performance shows the effectiveness of the neural networks in accurately segmenting complex anatomical structures. The scapula network had a lower dice score compared to the humerus network, but the overall model demonstrated greater accuracy in terms of model registration. The lower dice score for the scapula is likely a consequence of its more complex shape compared to the simpler humerus. However, the high registration accuracy is likely because the scapula models have a large surface area, making any imperfections in the model less impactful overall. In contrast, the humerus, with less surface area, especially when the model is cut off near the humeral neck, is more affected by imperfections. Notably, this testing did not involve any manual corrections to the neural network segmentations, so any obvious imperfections remained. In practice, these visible imperfections can be addressed by manually altering the models by filling gaps (false negatives) or removing erroneous regions (false positives). This combination of automated segmentation and targeted manual refinement is likely to further improve the accuracy of the models.

Beyond the scapula and humerus, the methods developed in this project could be applied to other joints and bones, such as the knee, hip, or wrist. These regions, like the shoulder, contain complex anatomical structures that may require precise segmentation. Automating the segmentation process for these areas would provide similar benefits, reducing the time needed for model creation and increasing the number of participants that can be included in studies.

Future work should focus on refining these networks to improve segmentation accuracy and reducing the need for post-processing to correct residual imperfections. Increasing the amount of training data would be particularly beneficial, as it would expose the networks to a wider variety of scans and anatomical variations. Additionally, since the networks are currently tuned to specific scanning parameters, incorporating training data with diverse energy and contrast levels would increase the generalizability across different imaging conditions. Finally, future work could involve transitioning from a strictly 2D approach, analyzing one CT slice at a time, to a 3D approach that considers the entire scan volume or sub-volumes within the scan. Implementing a 3D U-Net would allow the network to



capture spatial relationships between slices, leading to more accurate and consistent segmentations. While the current networks show promising results, further enhancements in accuracy and generalizability would increase the utility of automated image segmentation.

In conclusion, the neural networks developed in this project successfully automate the segmentation of the scapula and humerus, reducing the time and effort required for 3D model creation. This advancement has significant implications for research involving large datasets, as it enables the inclusion of more participants while providing more consistent and unbiased results.

## Chapter 4

### 4 Age-Related Differences in Healthy Shoulder Kinematics

#### OVERVIEW

*This chapter explores age-related differences in shoulder motion, focusing on the glenohumeral and scapulothoracic joints. It examines how these joints move during the motions of forward elevation and internal rotation to the back, in addition to analyzing the neutral positioning of the scapula and humerus. Age-related changes in kinematics and neutral position are characterized and discussed.*

## 4.1 Introduction

The human shoulder complex is intricate and versatile, capable of a wide range of motions important for performing daily activities, functional tasks, and sporting maneuvers. However, as individuals advance in age, the shoulder undergoes many physiological changes that can impact functional abilities (Murgia et al., 2018). Characterizing and understanding these natural age-related alterations in shoulder motion is important, as it has implications for maintaining independence, understanding disease progression, and informing rehabilitation strategies. Moreover, existing research disproportionately focuses on the glenohumeral joint, with scapulothoracic mechanics primarily explored in select planar motions such as abduction or flexion (Daher et al., 2023; Krishnan et al., 2019). This study aims to address these gaps by employing four-dimensional computed tomography (4DCT) to investigate all 6 degrees-of-freedom (DoF) in both shoulder joints during dynamic continuous motion, encompassing both a planar and a more intricate non-planar motion commonly encountered in daily activities.

The first objective of this study was to determine if there are statistically significant differences in 6 DoF kinematics and range of motion (ROM) between individuals <45 and >45 years of age during the motions of active forward elevation and internal rotation. The second objective of this study was to determine if there are age-related differences in the neutral positioning of the scapula and humerus. The last objective of this study was to determine if there are age-related differences in the scapulohumeral rhythm during these motions. It was hypothesized that both glenohumeral and scapulothoracic kinematics will demonstrate distinct age-related patterns throughout the motions. Specifically, that the older adults (aged >45) will exhibit less humeral motion, subsequently leading to a lower scapulohumeral rhythm compared to their younger counterparts (aged <45).

## 4.2 Methods

### 4.2.1 Participants

A convenience sample of 31 male participants were recruited for this study through local advertisement in the newspaper. The inclusion criteria were males 18 years of age or older

with no history of dominant shoulder injury. After obtaining informed consent, participants were checked to ensure they had a healthy, pain-free ROM in their dominant shoulder, this was defined as participants being able to reach behind their back, up to at least their lower thoracic vertebrae, and able to raise their arm from their side to vertical. A shoulder surgeon reviewed imaging for signs of pathology and any participants with abnormalities were excluded. Participants were divided by age into two cohorts: younger (<45 years) and older (>45 years).

#### 4.2.2 Motions

Two motions were examined in this study: active forward elevation (FE) and active internal rotation to the back (IR). The FE motion has participants lie obliquely on their back in the computed tomography (CT) scanner, with a foam wedge used to slightly elevate the shoulder and avoid impeding scapula motion. With their upper arm by their side and elbow flexed enough to fit in the CT scanner, the arm is then moved forward in the sagittal plane until the participant is reaching above their head as far as possible (and their elbow is fully extended), while keeping both shoulders level, and then returned to the starting position (Figure 4–1B). The IR motion has participants lie on their non-dominant side in the CT scanner with their dominant hand palm-down on their abdomen, the hand is then moved around the torso and up the back as far as possible, while keeping the elbow flexed, then returned to the start position (Figure 4–1C). For both motions, participants were also instructed to minimize torso movement. The IR motion was selected because the movement is important for activities of daily living (Langer et al., 2012; Rojas et al., 2020), yet it is uncommonly studied in the literature. Conversely, the FE motion is a basic motion that has been used in many other studies (Barnes et al., 2001; Doriot & Wang, 2006; Macedo & Magee, 2009; Pike et al., 2022), and serves as a basis for comparison and further analysis.

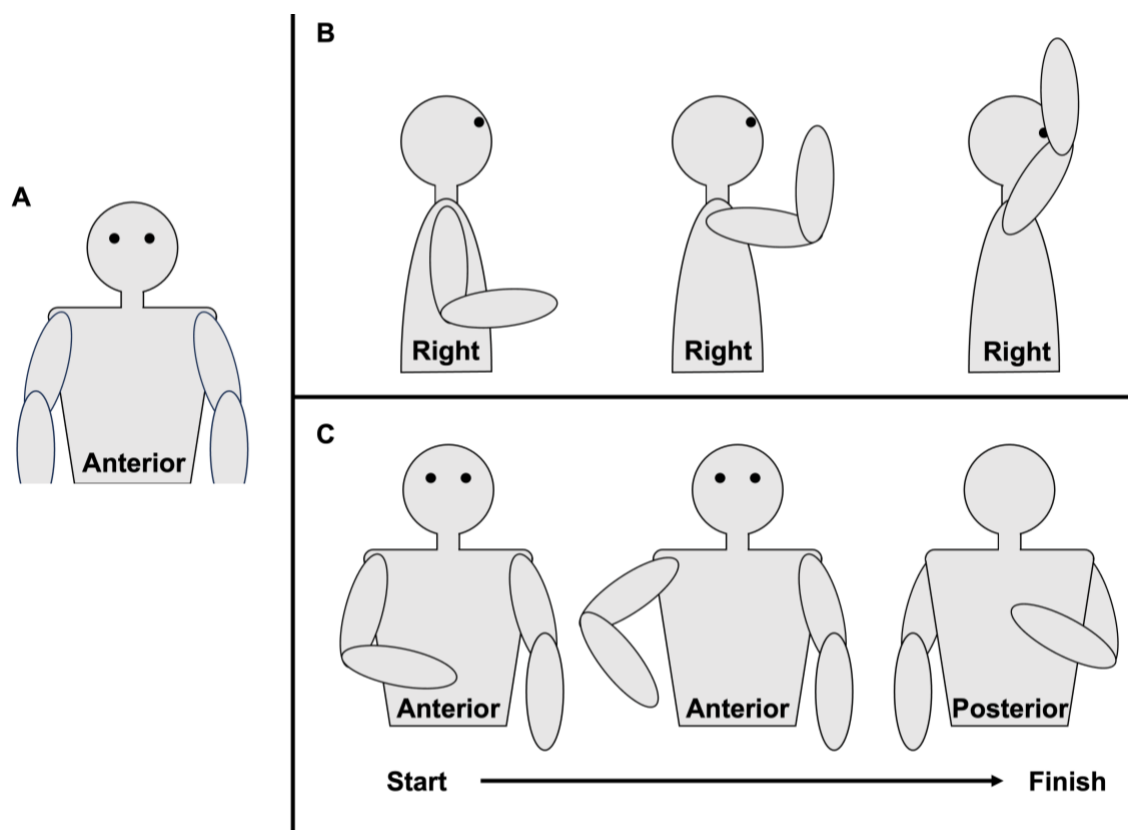


**Figure 4–1: Static position and examined motions.**

*Diagram of (A) neutral position, (B) forward elevation, and (C) internal rotation to the back motion.*

#### 4.2.3 Data Acquisition and Analysis

A Revolution CT Scanner (GE Healthcare, Waukesha, Wisconsin, USA) was used for all imaging. The entire procedure included a static scan and two dynamic 4DCT scans, each preceded by a localizer scan to determine the proper field of view. The static scan followed a standard static imaging protocol (120kV, 211mA, 1.0s rotation time, 512x512 matrix, axial) and produced 192 1.25mm thick slices for a volume of size 250x250x240mm<sup>3</sup>. For the static scan, the participant was positioned supine with their head and back supported (with padded foam) to ensure that the scapula was not pressed against the CT gantry table. Their arm was resting by their side keeping the shoulder in a neutral position (Figure 4–1A). The dynamic 4DCT scans followed a standard dynamic imaging protocol (80kV, 65mA, 0.35s rotation time, 512x512 matrix, axial) producing 64 2.50mm thick slices with

each volume of size  $450 \times 450 \times 160 \text{mm}^3$ . The IR dynamic scan lasted for 21 seconds generating 60 volumes and the FE scan lasted for 18 seconds generating 50 volumes. To ensure the motions were properly performed, demonstrations were given beforehand, and participants had the opportunity to practice; additionally, a CT technologist remained in the scanner room during the scans and counted throughout to ensure the motion was performed at the correct speed such that the motion was fully completed within the scan time. Each localizer scan has a dose length product (DLP) of  $8 \text{ mGy} \cdot \text{cm}$ , the static scan has a DLP of  $281 \text{ mGy} \cdot \text{cm}$ , the IR dynamic scan has a DLP of  $428 \text{ mGy} \cdot \text{cm}$ , and the FE dynamic scan has a DLP of  $357 \text{ mGy} \cdot \text{cm}$ . Therefore, using the effective dose conversion factor for a typical chest CT ( $0.014 \text{ mSv} \cdot \text{mGy}^{-1} \cdot \text{cm}^{-1}$ ) (American Association of Physicists in Medicine, 2008), the effective dose of the entire procedure is estimated at  $15.3 \text{ mSv}$ .

For the purposes of this study, only the first 20 – 35 frames were used based on the endpoint of motion. Kinematic analysis followed the single-vertebra image-based (SVIB) process described in Chapter 2 (Hunter et al., 2023). The three-dimensional (3D) bone models of the humerus, scapula, and first thoracic (T1) vertebra were created in 3DSlicer ([www.slicer.org](http://www.slicer.org), Version 4.11) for the static scan and every even numbered frame of the dynamic scans using the neural networks developed in Chapter 3. The static models were registered to each dynamic model using an iterative closest point algorithm (Besl & McKay, 1992), which overall describes the position of each dynamic model relative to the static models. Landmarks on the static models were used to create coordinate systems, which are related to each other such that the humerus is described relative to the scapular coordinate system and the scapula is relative to the T1 coordinate system, respectively representing the glenohumeral and scapulothoracic joints. The transformation at each frame of motion is decomposed into translations and rotations. For the glenohumeral joint a X-Z'-Y'' rotation sequence is used (Phadke et al., 2011), which corresponds to adduction (X), flexion (Z') and internal rotation (Y'') (Figure 1–5). For the scapulothoracic joint, a Y-X'-Z'' rotation sequence is used (Wu et al., 2005), which corresponds to protraction (Y), medial rotation (X'), and posterior tilting (Z'') (Figure 1–6). Additionally, the glenoid width of each participant was measured to normalize glenohumeral translation as a percentage of glenoid width. Data from each participant was upscaled to 20 data points to keep the length of each dataset consistent.

Neutral positioning was measured by decomposing the coordinate transforms describing the scapula relative to the vertebra coordinate system, and the humerus relative to the scapula coordinate system from the static scan bone models. These values were also used to offset the kinematics so that each DoF is relative to an individual's static position. Kinematic pathways were determined for each DoF throughout each motion. Since the start and end values are not necessarily the extreme values, ROM was calculated by taking the difference between maximum and minimum values for each DoF. To measure scapulohumeral rhythm, the ROM as Euler angles were converted into an axis-angle representation, which is a widely used method for representing rotations in 3D space. It expresses any rotation as a single axis and an angle of rotation about that axis. Having a single rotation value quantifying the magnitude of the rotation allows for convenient comparisons of 3D rotations. For the purpose of measuring scapulohumeral rhythm, only the rotation values ( $\theta$ ) of the axis-angle representation were used as follows:

$$\text{Scapulohumeral Rhythm} = \frac{\theta_{\text{Humerus}}}{\theta_{\text{Scapula}}}$$

#### 4.2.4 Statistical Analysis

All statistics were performed in SPSS (Version 29). To assess differences in kinematic pathways, a two-way mixed analysis of variance (ANOVA) was used for each DoF. Maximum ROM, neutral positioning, and scapulohumeral rhythm were all compared using two-tailed independent t-tests. Statistical significance was set as  $p \leq 0.05$ .

### 4.3 Results

#### 4.3.1 Participants

The participant data for each age cohort is summarized in Table 4–1. One participant was excluded from the IR motion and six were excluded from the FE motion due to either motion blurring or bones moving out of the CT scanner's field of view.

**Table 4–1: Participant demographics, categorized by age cohort and motion. The table includes sample sizes, the average age with standard deviation, and the age range for each subgroup.**

	Forward Elevation	Internal Rotation
Young (<45 years)	n = 12 26 ± 6 (18-37)	n = 15 26 ± 6 (18-37)
Old (>45 years)	n = 13 62 ± 12 (45-84)	n = 15 63 ± 12 (45-86)

### 4.3.2 Pathways

For the FE motion, no significant differences were measured between the cohorts for any DoF throughout the motion (Table 4–2). For the IR motion, the only significant difference between the cohorts was lateral translation (Z) of the scapula. However, both humeral and scapular translations and rotations varied significantly with respect to % cycle (time) (Table 4–2). The graphical representations (Figure 4–2, Figure 4–3) are included here to present the observed trends and values within the datasets. The data depicted in the graphs provide a visual understanding of the relationships between the various DoF throughout the investigated motions.



**Table 4–2: P-values for the kinematic pathways categorized by factor and degree of freedom. Bold values indicate significance ( $p \leq 0.05$ ).**

Degree of Freedom		Age (FE)	Age (IR)	% Cycle (FE)	% Cycle (IR)
Humerus Translations	X	0.075	0.342	<b>&lt;0.001</b>	0.178
	Y	0.634	0.964	0.241	<b>&lt;0.001</b>
	Z	0.468	0.716	<b>&lt;0.001</b>	<b>&lt;0.001</b>
Humerus Rotations	X	0.349	0.517	<b>&lt;0.001</b>	0.368
	Z	0.206	0.128	<b>&lt;0.001</b>	<b>&lt;0.001</b>
	Y	0.839	0.322	<b>&lt;0.001</b>	<b>&lt;0.001</b>
Scapula Translation	X	0.947	0.209	<b>&lt;0.001</b>	<b>0.002</b>
	Y	0.806	0.357	<b>0.004</b>	<b>0.014</b>
	Z	0.466	<b>0.024</b>	<b>&lt;0.001</b>	<b>&lt;0.001</b>
Scapula Rotations	Y	0.448	0.741	<b>&lt;0.001</b>	<b>0.014</b>
	X	0.961	0.585	<b>&lt;0.001</b>	<b>&lt;0.001</b>
	Z	0.71	0.639	<b>&lt;0.001</b>	<b>&lt;0.001</b>

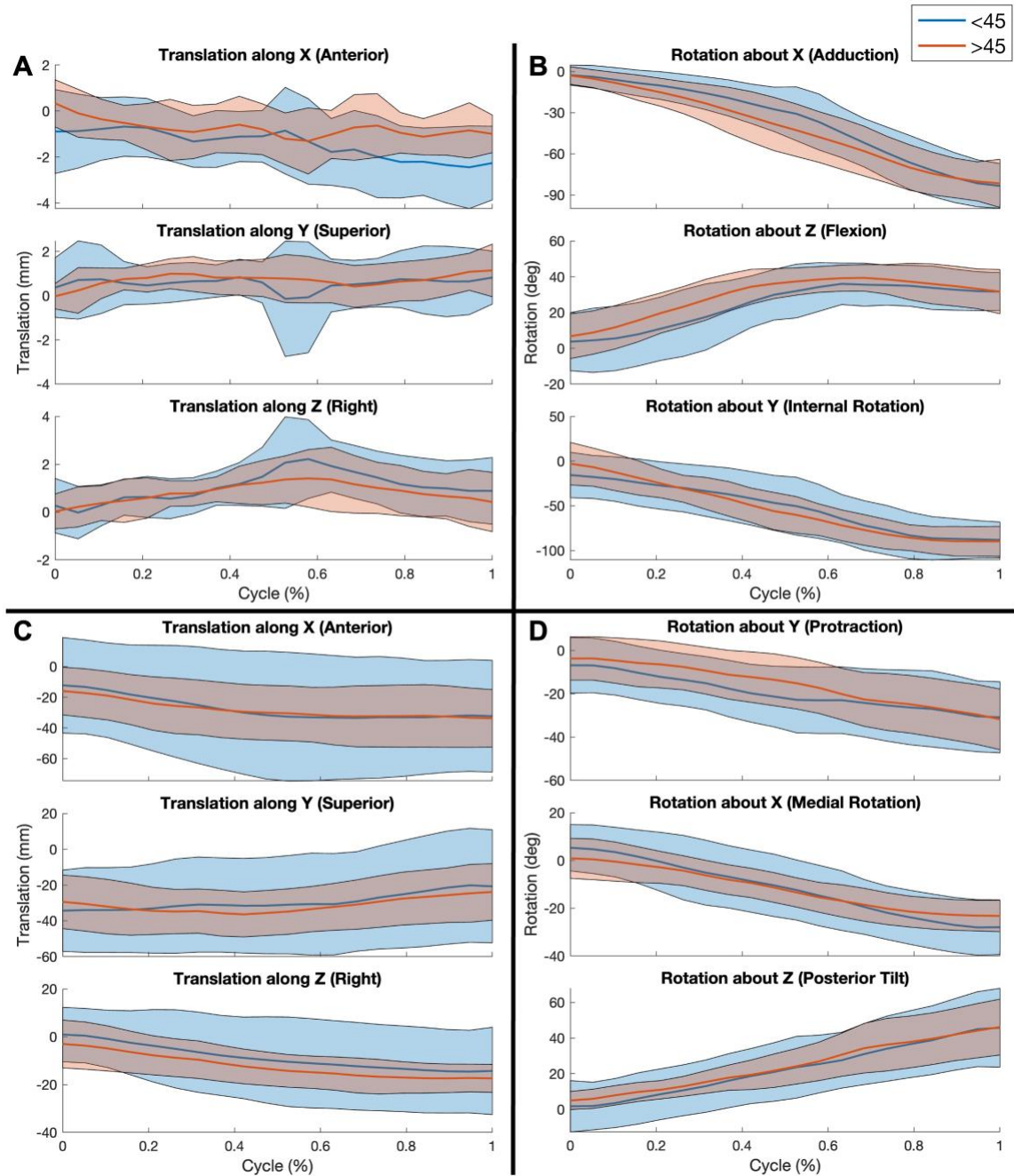


**Figure 4–2: Forward elevation kinematic pathways.**

*Kinematic pathways for the (A) humeral translation, (B) humeral rotation, (C) scapular translation, and (D) scapular rotation degrees of freedom for each cohort (blue for younger, red for older). Solid lines represent the mean value at each time point and the shaded regions represent the standard deviation at each time point.*

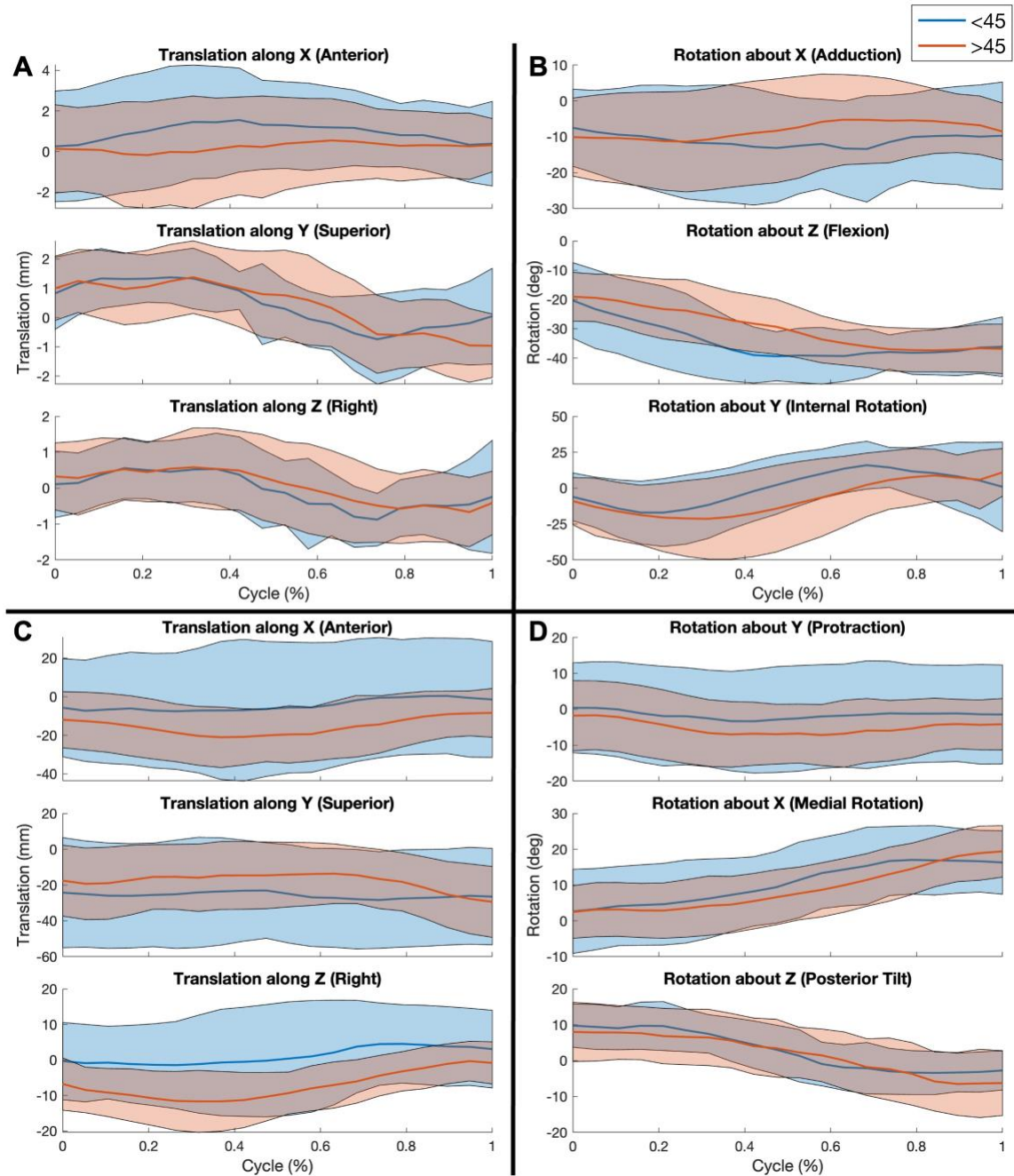


**Figure 4-3: Internal rotation kinematic pathways.**

*Kinematic pathways for the (A) humeral translation, (B) humeral rotation, (C) scapular translation, and (D) scapular rotation degrees of freedom for each cohort (blue for younger, red for older). Solid lines represent the mean value at each time point and the shaded regions represent the standard deviation at each time point.*

### 4.3.3 Maximum Range of Motion

During the FE motion, no significant differences were observed for humeral translation, while axial rotation (Y) of the humerus was significantly greater ( $13.3^\circ$ ,  $p=0.033$ ) in the older cohort (Figure 4–4). Conversely, the scapula displayed significantly increased anterior axis translation (X) ( $9.3\text{mm}$ ,  $p=0.022$ ) and medial rotation (X) ( $8.9^\circ$ ,  $p=0.021$ ) in the younger cohort (Figure 4–4). Regarding the IR motion, the younger cohort exhibited significantly more humeral translation in the anterior (X) direction ( $0.8\text{mm}$ ,  $p=0.05$ ) (Figure 4–5). No differences were detected for humeral rotations. The older cohort displayed significantly more superior axis (Y) translation ( $8.0\text{mm}$ ,  $p=0.006$ ) of the scapula (Figure 4–5). Lastly, when measuring humeral translation as a percentage of glenoid width rather than absolute translation, it was observed that the older cohort exhibited significantly less ROM across all DoF during both motions (Figure 4–6). Specifically, during the FE motion, the older cohort had 6% ( $p<0.001$ ), 5% ( $p=0.036$ ), and 5% ( $p=0.009$ ) less translation in the respective anterior, superior, and lateral DoF. Similarly, during the IR motion, the older cohort had 6% ( $p<0.001$ ), 6% ( $p<0.001$ ), and 4% ( $p<0.001$ ) less translation in the respective anterior, superior, and lateral DoF.

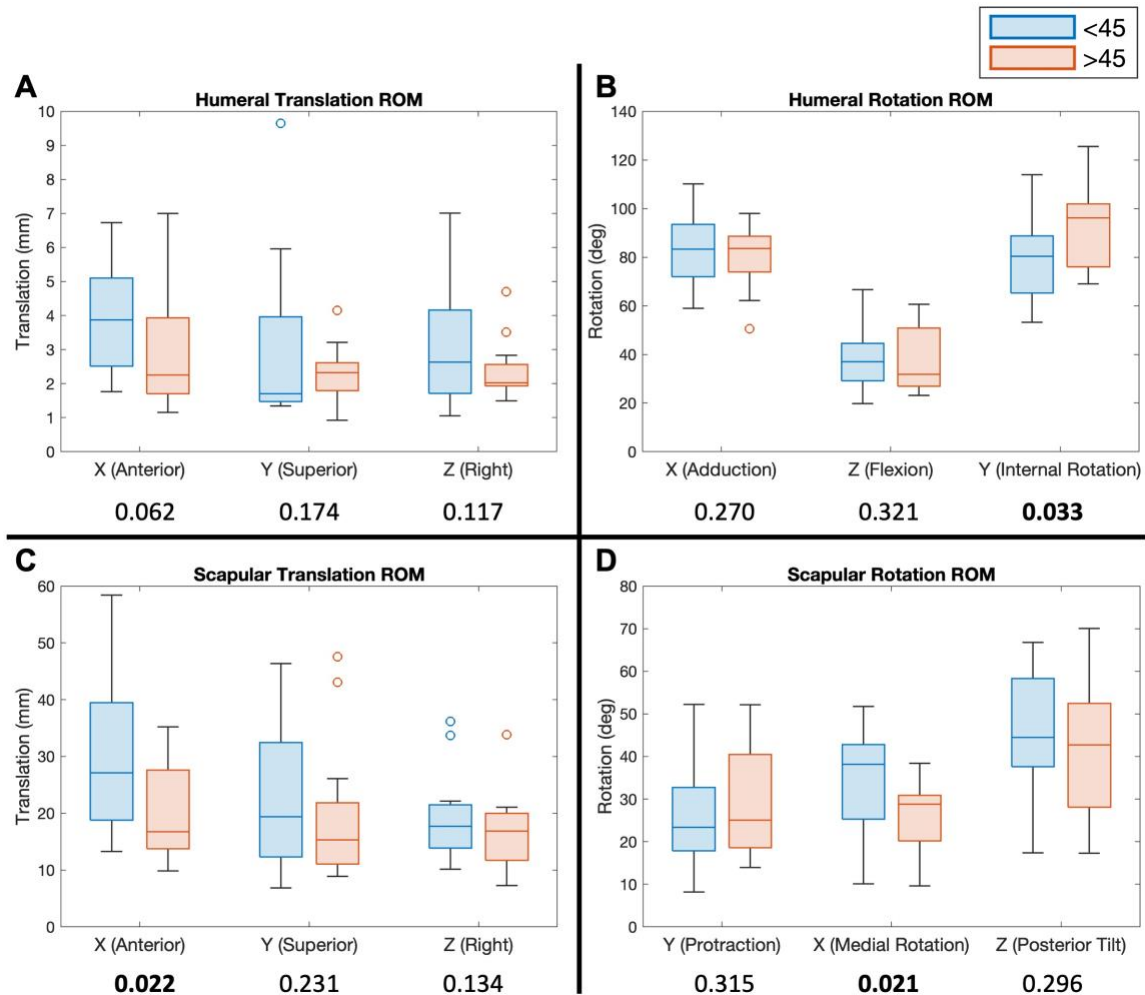


**Figure 4-4: Forward elevation range of motion.**

Boxplots comparing range of motion of the (A) humeral translation, (B) humeral rotation, (C) scapular translation, and (D) scapular rotation degrees of freedom for each cohort (blue for younger, red for older). The bottom and top of a box represent quartile 1 and 3 respectively and define the interquartile range, the line within each box represents the median. Whiskers show the range of non-outlier values and solitary circles indicate outliers (defined as values with a difference from the box greater than the interquartile range). The p-value is provided for each age-related comparison where **bold** values indicate significance ( $p \leq 0.05$ ). Note that each degree of freedom is labelled following the positive axis/rotation convention although the direction is not considered.

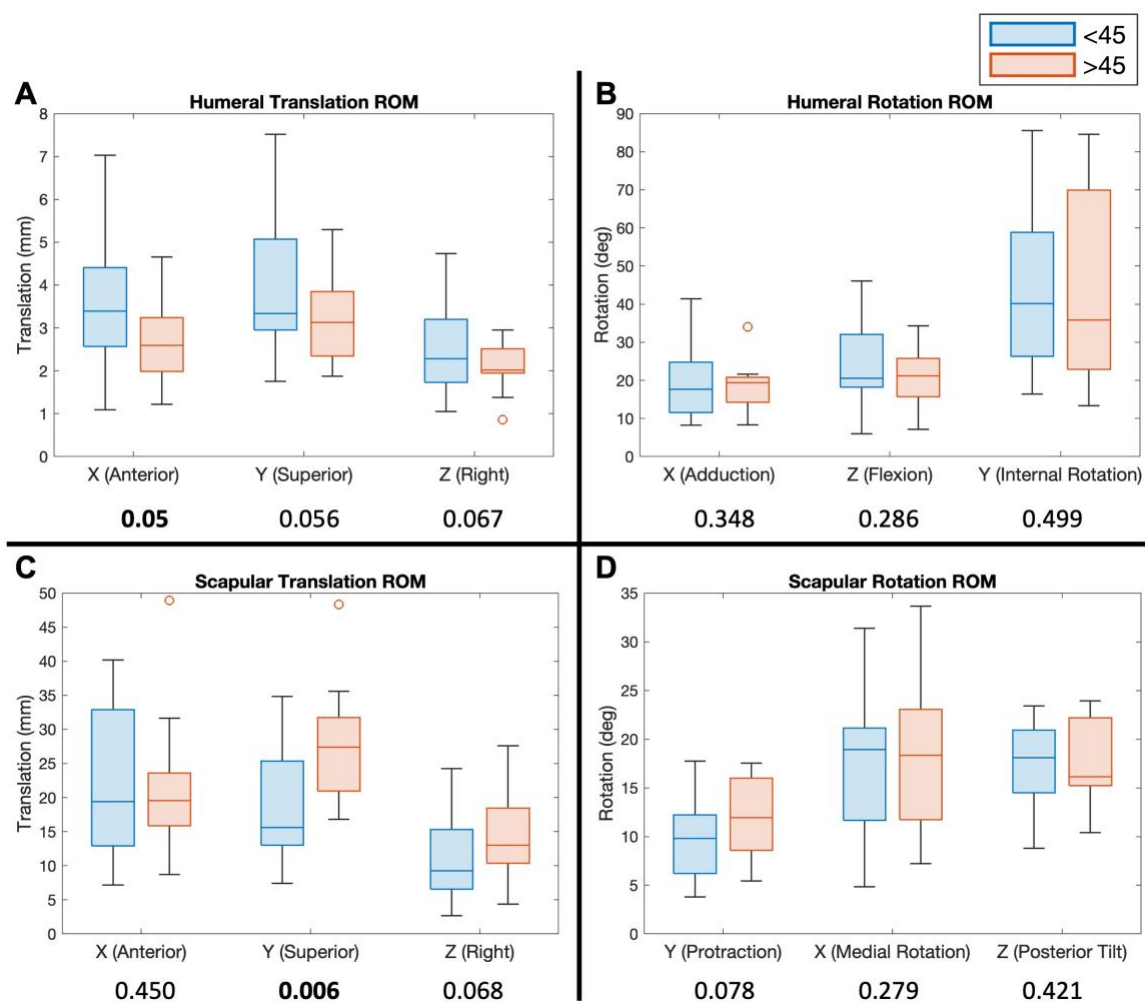


**Figure 4-5: Internal rotation range of motion.**

Boxplots comparing range of motion of the (A) humeral translation, (B) humeral rotation, (C) scapular translation, and (D) scapular rotation degrees of freedom for each cohort (blue for younger, red for older). The bottom and top of a box represent quartile 1 and 3 respectively and define the interquartile range, the line within each box represents the median. Whiskers show the range of non-outlier values and solitary circles indicate outliers (defined as values with a difference from the box greater than the interquartile range). The p-value is provided for each age-related comparison where **bold** values indicate significance ( $p \leq 0.05$ ). Note that each degree of freedom is labelled following the positive axis/rotation convention although the direction is not considered.

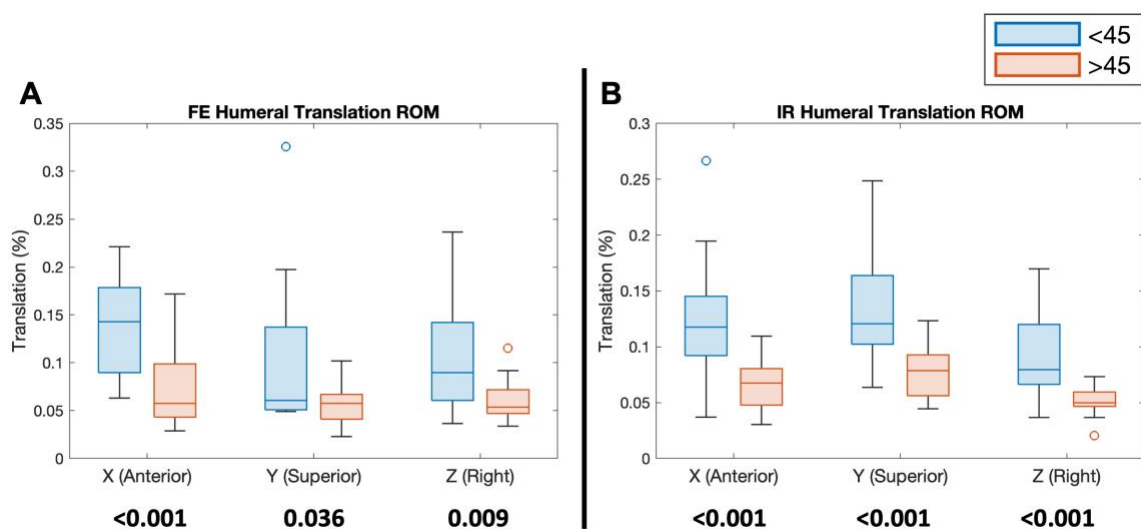


**Figure 4–6: Humeral translation as a percentage of glenoid width.**

Boxplots comparing humeral translation range of motion as a percentage of glenoid width for the (A) forward elevation and (B) internal rotation motion for each cohort (blue for younger, red for older). The bottom and top of a box represent quartile 1 and 3 respectively and define the interquartile range, the line within each box represents the median. Whiskers show the range of non-outlier values and solitary circles indicate outliers (defined as values with a difference from the box greater than the interquartile range). The p-value is provided for each age-related comparison where **bold** values indicate significance ( $p \leq 0.05$ ). Note that each degree of freedom is labelled following the positive axis/rotation convention although the direction is not considered.

#### 4.3.4 Neutral Positioning

Compared to the younger cohort, the older cohort had a neutral position with significantly more superior translation (Y) (17mm,  $p=0.05$ ), lateral rotation (-X) ( $8^\circ$ ,  $p=0.009$ ), and posterior tilting (Z) ( $10^\circ$ ,  $p<0.001$ ) of the scapula, and a more anteriorly positioned humerus (X) (2 mm,  $p=0.007$ ) (Table 4–3). Neutral positioning differences of humeral rotations were not measured because the humerus coordinate system was created with an orientation aligned to the scapula coordinate system (Hunter et al., 2023), therefore the difference was always  $0^\circ$  for each DoF. The combination of lateral rotation and posterior tilting culminates as a rotational movement in the scapular plane (Figure 4–7). The significant differences



between the cohorts indicate that the older cohort scapula is characterized by increased upward rotation in the scapular plane, also commonly referred to as scapular plane elevation. Additionally, the increased superior translation indicates that the rotation point of the scapular plane elevation is not at the origin (glenoid) of the scapula.

**Table 4–3: Average neutral positioning with standard deviation of each cohort for each degree of freedom. The p-value is provided for each age-related comparison where bold values indicate significance ( $p \leq 0.05$ ).**

Degree of Freedom		Younger	Older	p-value
Scapula Translations (mm)	X	10.3 ± 25.5	19.0 ± 17.8	0.145
	Y	-5.4 ± 30.2	12.0 ± 26.6	<b>0.050</b>
	Z	137.0 ± 80.2	154.7 ± 10.9	0.203
Scapula Rotations (deg)	Y	16.2 ± 46.8	25.2 ± 9.1	0.236
	X	-23.9 ± 7.9	-31.6 ± 8.7	<b>0.009</b>
	Z	6.2 ± 7.6	16.4 ± 8.5	<b>&lt;0.001</b>
Humerus Translations (mm)	X	4.8 ± 2.6	6.9 ± 1.7	<b>0.007</b>
	Y	-3.0 ± 2.0	-2.3 ± 2.1	0.179
	Z	27.0 ± 1.4	28.0 ± 2.0	0.056



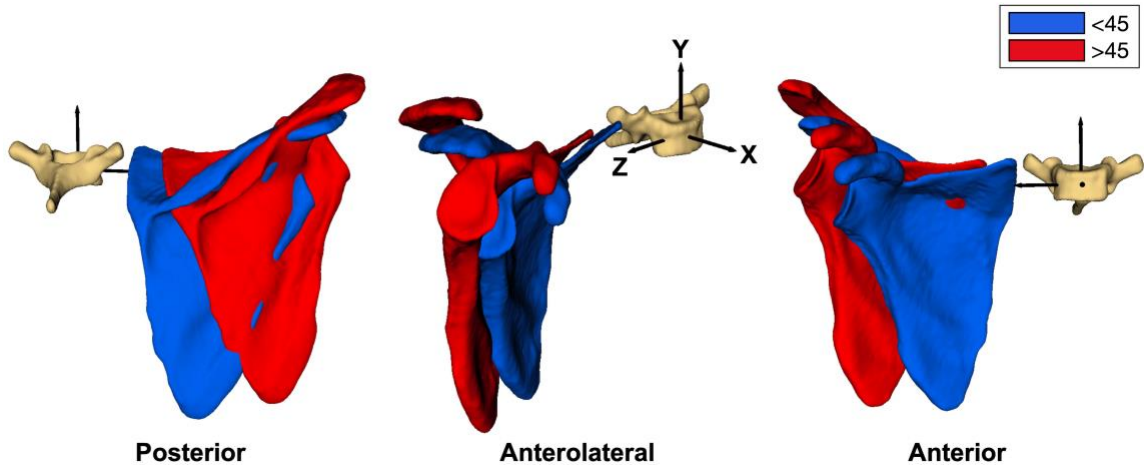


**Figure 4–7: Comparison of neutral scapula pose.**

*Diagram comparing the average scapula pose in the younger cohort (blue) and the older cohort (red) to illustrate the differences in neutral positioning between the cohorts.*

#### 4.3.5 Scapulohumeral Rhythm

There were no significant differences in the scapulohumeral rhythm between the two cohorts (Table 4–4).

**Table 4–4: Average scapulohumeral rhythm with standard deviation of each cohort for each motion. The p-value is provided for each age-related comparison.**

	Younger	Older	p-value
Internal Rotation	$2.3 \pm 0.9$	$1.9 \pm 0.9$	0.143
Forward Elevation	$2.1 \pm 0.8$	$2.6 \pm 1.3$	0.098

## 4.4 Discussion

This study found no significant age-related differences in scapulothoracic and glenohumeral translations and rotations during active FE and active IR motions. However, this study did find that there were significant differences in scapulothoracic and glenohumeral translations and rotations throughout the full range of motion, i.e., values

were not constant during motion. Additionally, this study did find age-related differences in the maximum ROM of the scapula and humerus during the FE and IR motions for certain DoF. Furthermore, this study found additional age-related differences in the neutral positioning of the scapula and humerus. No age-related differences were found regarding scapulohumeral rhythm, but this paper did report ratios for both the FE and IR motions that consider all three rotational DoF.

The significant differences observed in all DoF over time (Table 4–2) demonstrates that all six DoF are required for fully describing shoulder kinematics. This is evident for both a complex non-linear movement (IR) as well as a simple planar motion (FE). Consequently, this indicates that single-angle two-dimensional and rotation-only 3D measurements do not capture the intricacies of shoulder motion. Therefore, it is recommended for future shoulder studies to incorporate full six DoF assessments, as we did, for a more comprehensive understanding of shoulder kinematics.

For the active IR motion, the results showed that for all significant differences in humeral DoF, the younger cohort had the larger values (Figure 4–5, Figure 4–6) indicating an overall greater humeral contribution to the motion. In contrast, the scapula DoF demonstrated greater values within the older cohort (Figure 4–5). These results align with the scapulohumeral rhythm calculations, which revealed a larger ratio for the younger cohort denoting more humeral contribution while the older cohort is more reliant on the scapular contribution (Table 4–4). This suggests that as individuals age, they rely more on the scapulothoracic joint to maintain overall motion as the glenohumeral joint becomes less mobile. As for the FE motion, all DoF with significant differences favored the younger cohort, displaying a greater ROM across various DoF, with the exception of internal rotation of the humerus (Figure 4–4, Figure 4–6). This suggests that for FE, overall ROM decreases with age, which is consistent with other studies (Barnes et al., 2001; Doriot & Wang, 2006; Macedo & Magee, 2009; Pike et al., 2022).

It is postulated that some of the apparent differences in ROM between the cohorts can be attributed to differences in neutral positioning. For the ROM calculations the direction is not considered, but by analyzing the kinematic pathways the direction can be determined.

For the IR motion, the older cohort had greater inferior scapula translation (-Y) (Figure 4–3, Figure 4–5) in conjunction with a naturally more superiorly (Y) positioned scapula (Table 4–3). Therefore, the increased inferior translation of the scapula exhibited by the older cohort may be a direct consequence of a naturally more superior positioned scapula. Similarly for the FE motion, the younger cohort showed a significantly higher ROM for lateral rotation (-X) of the scapula (Figure 4–2, Figure 4–4). The younger cohort also has a scapula that is naturally positioned with more medial rotation (X) (Table 4–3). Therefore, younger individuals will have to rotate the scapula laterally more during the motion in order to reach a similar final position as the older individuals. This suggests that as the scapula position changes with age, scapular motion is altered as a compensatory response. Additionally, for both motions the younger cohort exhibited more anterior translation (X) of the humerus (Figure 4–6) while having a humerus positioned more posteriorly (-X) compared to the older cohort (Table 4–3). Finally, for the FE motion, the older cohort exhibited significantly more external rotation of the humerus (-Y) compared to the younger cohort (Figure 4–2, Figure 4–4). This study was not able to examine differences in neutral rotation of the humerus, but Kolz et al. (2021) showed that the neutral humerothoracic orientation of older adults (age >45) is more internally rotated. Therefore, it is expected for older adults to require more external rotation than the young cohort to perform the same motion.

The observation of consistently reduced glenohumeral translation among older individuals (Figure 4–6) is an important finding, although it does not explain the underlying mechanisms contributing to this phenomenon. Several factors may contribute to this, including alterations within the joint, or in the surrounding soft tissues and muscles. Firstly, age-related joint degeneration, such as cartilage thinning or osteophyte formation, may increase friction within the joint thus impeding motion. Additionally, alterations in the surrounding soft tissues, such as decreased ligamentous elasticity and increased joint capsule tightness, could restrict humeral translation. Concurrently, age-related deterioration and weakening of the rotator cuff muscles may lead to a reduction in the forces applied to the humerus, consequently decreasing motion. Older individuals having a scapula with naturally more scapular plane elevation (Figure 4–7) can also be explained by multiple mechanisms. One possibility is that age-related muscle deterioration leads to

less support for the scapula. Specifically, if there is a decrease in medial scapular support it would explain the apparent increased rotation. Alternatively, this change may be a compensatory mechanism for the humerus. If the rotator cuff muscles are not providing adequate stabilization, the altered angle of the scapula would provide additional support and overall help with shoulder function.

The hypothesis was that the older cohort would have less humeral motion but relatively unchanged scapula motion. The rationale behind this was that the glenohumeral joint is a typical synovial joint (Culham & Peat, 1993) which is known to deteriorate with age (Freemont & Hoyland, 2007). The scapulothoracic joint on the other hand is a fictitious joint that is entirely stabilized by muscles, and therefore the common effects of aging would be less apparent as ligaments, articular cartilage, and synovial fluids are not involved (Culham & Peat, 1993). Along this line, many studies have reported a decrease in ROM with age; however, these studies are limiting measurements to a single angle using a goniometer (Barnes et al., 2001; Macedo & Magee, 2009; Pike et al., 2022; Stathokostas et al., 2013), which is in effect only measuring the humerothoracic joint, ignoring the intricate glenohumeral-scapulothoracic relationship. In contrast, the results of this study suggest that older individuals do not necessarily have less overall ROM than their younger counterparts, but there are differences in resting neutral pose, which agrees with a study by Kolz et al. showing similar results. Specifically, Kolz et al. (2021) showed that the scapula of the older cohort (>45) tended to have more protraction, posterior tilt, and lateral rotation in a neutral position. These results are consistent with the results of this study and the differences are comparable in magnitude, approximately  $10^\circ$  for each DoF (Table 4–3). During scapular plane elevation, similar to the FE motion of this study, the older cohort had significantly more internal rotation of the humerus with no other differences regarding glenohumeral rotations (Kolz et al., 2021), again aligning with the results of this study (Figure 4–4).

The observed variability in motion pathways during both the FE and IR motions, even with guidance, highlights the complexity of upper arm motion. While the scapula and humerus work synchronously, overall arm positioning is accomplished through a coordination of the torso as well as the sternoclavicular, acromioclavicular, scapulothoracic, glenohumeral,

and elbow joints (Krishnan et al., 2019). These findings suggest that these other joints may play a significant role in achieving the necessary ROM, as the general goal of arm movement is to place the hand in a specific position rather than the individual joints, potentially explaining compensation mechanisms often observed in various shoulder disorders and injuries. This study also reported values for scapulohumeral rhythm in less studied motions, and while no significant differences were apparent, variations with age and motion were revealed and this should be investigated further within the context of compensatory movements.

A limitation of this study is the cutoff ages used to group the cohorts, which were chosen to be similar to other studies (Doriot & Wang, 2006; Kolz et al., 2021; Murgia et al., 2018), however, kinematics do not change suddenly, rather the physiology changes gradually over an individual's lifetime. Furthermore, another study suggests that change does not occur at a steady rate and ROM reduction is accelerated after the age of 71 (Stathokostas et al., 2013). While participants were given instructions on how to perform the motions, they were still unconstrained and there are individual differences in how the motion is performed. Lastly, lying down while performing these motions is uncommon during activities of daily living. Consequently, gravitational force is applied in a different direction compared to an upright position and while avoided as much as reasonably possible the scapula may contact the table, both which could affect the movement.

This study has significant implications for the treatment and management of shoulder injuries and diseases. The IR motion is especially important in the context of shoulder arthroplasties as this motion is often limited post-surgery and full restoration often does not occur (Rojas et al., 2020; Triplet et al., 2015). A deficiency in this motion is problematic for patients' functional ROM during everyday activities (Langer et al., 2012; Rojas et al., 2020; Triplet et al., 2015). The use of patient-specific preoperative planning programs has been shown to improve the outcomes of shoulder arthroplasties, however, they do not currently incorporate scapulothoracic motion into their preoperative plans (J. Iannotti et al., 2014; Walch et al., 2015). A key takeaway of this study is the crucial role of scapulothoracic motion in overall dynamic shoulder function, as it was shown that it contributes to approximately one-third of shoulder motion, both during a planar and

complex motion (Table 4–4). Additionally, this study identified humeral head translation during motion (approximately 3 to 5mm), which is not a movement inherently accommodated by current implant designs (Karduna et al., 1997; Muench et al., 2023). Recent studies have demonstrated that total shoulder arthroplasties with non-spherical humeral heads that allow for this glenohumeral translation can more accurately replicate native shoulder kinematics and ROM (Jun et al., 2013, 2016; Muench et al., 2022, 2023). The findings of joint translation indicate that overly constrained joint components may lead to deficiencies in motion, and increased implant stresses. As such, addressing these issues with implants that allow for normal glenohumeral translation could have positive implications on patient outcomes. This study was able to successfully characterize age-related differences but not the underlying processes causing these changes. Future research should assess age-related alterations in relevant soft tissues and musculature, providing insights into the physiological processes contributing to changes in ROM and pose. Lastly, age-related differences in the neutral positioning of the scapula and humerus could explain age-related differences in subluxation or other injury mechanisms, emphasizing the importance of tailored approaches to address these issues as individuals age. In summary, this study's results have important implications for improving the understanding and treatment of shoulder conditions and injuries.

## Chapter 5

### 5 Kinematic Analysis of Anatomic Total Shoulder Arthroplasty and the Effects of Patient Mobility and Implant Mismatch

#### OVERVIEW

*This chapter investigates the kinematics of patients following an anatomic total shoulder arthroplasty, focusing on the glenohumeral and scapulothoracic joints. Since motion recovery varies among patients, the effects of patient mobility are examined. Additionally, the study explores how implant mismatch influences kinematics. Finally, kinematics are compared to a non-implant control group to assess the overall impact of an implant on shoulder function.*

## 5.1 Introduction

With the technology and methods available for accurate six degree-of-freedom (DoF) kinematic assessments of the native glenohumeral and scapulothoracic joints, it is possible to extend these evaluations to shoulder implants. As described in Chapter 1, an anatomic total shoulder arthroplasty (aTSA) is a well-established surgical procedure for a variety of shoulder pathologies, generally yielding good outcomes. However, for some patients, restoration of motion, particularly internal rotation, is not achieved (Miller et al., 2003; Triplet et al., 2015, 2018). Studies have shown a strong correlation between preoperative and postoperative range of motion (ROM) (Friedman et al., 2019; Jacobs et al., 2016; Levy et al., 2016). Additionally, diminished mobility often correlates with issues in the subscapularis muscle (Liem et al., 2012; Miller et al., 2003). Nonetheless, it is unknown which specific DoF are affected as a result of the limited mobility. Furthermore, for patients with good mobility, it remains unclear if their motion is altered relative to individuals with natural joints. As defined in Chapter 1, mismatch is the difference in curvature between the glenoid and humeral components (Figure 1–9). While there is a consensus that a radial mismatch of 4 to 10mm is an acceptable range for both the mechanical properties of the implant and patient outcomes (Diop et al., 2006; Terrier et al., 2006), its impact on six DoF kinematics and ROM has not been quantified. Therefore, the objective of this study is to examine glenohumeral and scapulothoracic kinematics and ROM in aTSA patients, and to determine the influence of mismatch and mobility. It was hypothesized that glenohumeral and scapulothoracic kinematics will differ between mobility groups, as well as compared to a healthy control group. Specifically, it was anticipated that those with better mobility would exhibit kinematic patterns similar to the healthy controls, while the limited motion group would demonstrate less humeral translation and internal rotation of the humerus. Additionally, it was hypothesized that a higher mismatch would result in increased glenohumeral translation, potentially leading to further differences in shoulder kinematics.



## 5.2 Methods

### 5.2.1 Participants

For this retrospective study, male patients operated on by a single shoulder surgeon who had received an aTSA a minimum of two years ago were contacted and asked to volunteer in the study. Each participant had received either an AEQUALIS PERFORM or AEQUALIS PERFORM+ glenoid component, based on their respective type A or B erosion, and all participants were fitted with a SIMPLICITI humeral component. After obtaining informed consent, the participant's mobility was assessed by measuring the extent to which they could reach up behind their back. Participants capable of reaching above their belt line were categorized as having a full ROM while those restricted to or below their belt line were considered to have a limited ROM, hereafter referred to as the full motion and limited motion groups, respectively. Additionally, participants were categorized according to their level of mismatch, with a diametrical difference greater than 10mm classified as high mismatch, and less than 10mm categorized as low mismatch. Finally, glenohumeral and scapulothoracic kinematics and ROM of the older cohort from Chapter 4 were used as data from a non-implant control group.

### 5.2.2 Motions

The motion examined in this study was internal rotation to the back. This motion has participants lie on their non-implant side in the computed tomography (CT) scanner with their free hand palm-down on their abdomen, the hand is then moved around the torso and up the back as far as possible, while keeping the elbow flexed, then returned to the start position. Participants were also instructed to minimize torso movement as much as possible.

### 5.2.3 Data Acquisition and Analysis

A Revolution CT Scanner (GE Healthcare, Waukesha, Wisconsin, USA) was used for the imaging which included a single dynamic four-dimensional computed tomography (4DCT) scan preceded by a localizer scan to determine the proper field of view. The dynamic 4DCT scan followed a slightly modified dynamic imaging protocol with a higher voltage than

usual to account for the metallic implant (120kV, 60mA, 0.35s rotation time, 512x512 matrix, axial) producing 64 2.50mm thick slices with each volume of size 450x450x160mm<sup>3</sup>. The scan lasted for 17.5 seconds generating 50 volumes. To ensure the motion was properly performed, a demonstration was given beforehand, and participants had the opportunity to practice; additionally, a CT technologist remained in the scanner room during the scan and counted throughout to ensure the motion was performed at the correct speed such that the motion was fully completed within the scan time. The entire scanning procedure had a dose length product (DLP) of 1050 mGy\*cm. Therefore, using the effective dose conversion factor for a typical chest CT (0.014 mSv\*mGy<sup>-1</sup>\*cm<sup>-1</sup>) (American Association of Physicists in Medicine, 2008), the effective dose of the procedure is estimated at 14.8mSv.

For the purposes of this study, only the first 20 – 30 frames were used based on the endpoint of motion. Kinematic analysis was based on the single-vertebra image-based (SVIB) process from Chapter 2 (Hunter et al., 2023). The three-dimensional bone models of the humerus, scapula, and first thoracic (T1) vertebra were created in 3DSlicer (www.slicer.org, Version 4.11) for every even numbered frame of the dynamic scan. Modelling was assisted by the neural networks developed in Chapter 3; however, manual intervention was required for slices with metallic artifacts. Additionally, the preoperative static CT scans of the participants were obtained to create bone models of the entire scapula. The humerus and T1 models from the first frame of the dynamic scan and the scapula model from the preoperative scan were used as reference models. Landmarks were identified on the reference models to create coordinate systems, which are related to each other such that the humerus is described relative to the scapular coordinate system and the scapula is relative to the T1 coordinate system, respectively representing the glenohumeral and scapulothoracic joints. The reference models were registered to each dynamic model using an iterative closest point algorithm (Besl & McKay, 1992), which overall describes the position of each dynamic model relative to the reference models. The transformation at each frame of motion is decomposed into translations and rotations. For the glenohumeral joint a X-Z'-Y'' rotation sequence is used (Phadke et al., 2011), which corresponds to adduction (X), flexion (Z') and internal rotation (Y'') (Figure 1–5). For the scapulothoracic joint, a Y-X'-Z'' rotation sequence is used (Wu et al., 2005), which corresponds to

protraction (Y), medial rotation (X'), and posterior tilting (Z'') (Figure 1–6). Data from each participant was upscaled to 20 data points to keep the length of each dataset consistent. Kinematic pathways were determined for each DoF throughout the entire motion, additionally, the final half of the motion was analyzed separately to isolate the duration when the arm is behind the body. Additionally, total ROM for each DoF was calculated by taking the difference between maximum and minimum values.

### 5.2.4 Statistical Analysis

All statistics were performed in SPSS (Version 29). To assess differences in kinematic pathways, a two-way mixed analysis of variance (ANOVA) was used for each DoF. Maximum ROM was compared between groups using a one-way ANOVA. Tukey's post-hoc test was used for multiple comparisons. Statistical significance was set as  $p \leq 0.05$ .

## 5.3 Results

### 5.3.1 Participants

A total of 54 eligible participants were contacted and 24 participants (mean age  $70 \pm 7$  years) were included in the study. Reasons for refusal and exclusions are detailed in Figure 5–1. Four participants had type A (central) erosion and twenty had type B (posterior) erosion. Of the included participants, the mismatch and mobility groupings are summarized in Table 5–1.

**Table 5–1: Distribution of participants across mismatch and mobility groups.**

	Full Motion	Limited Motion	Total
High Mismatch	6	5	11
Low Mismatch	9	4	13
Total	15	9	24

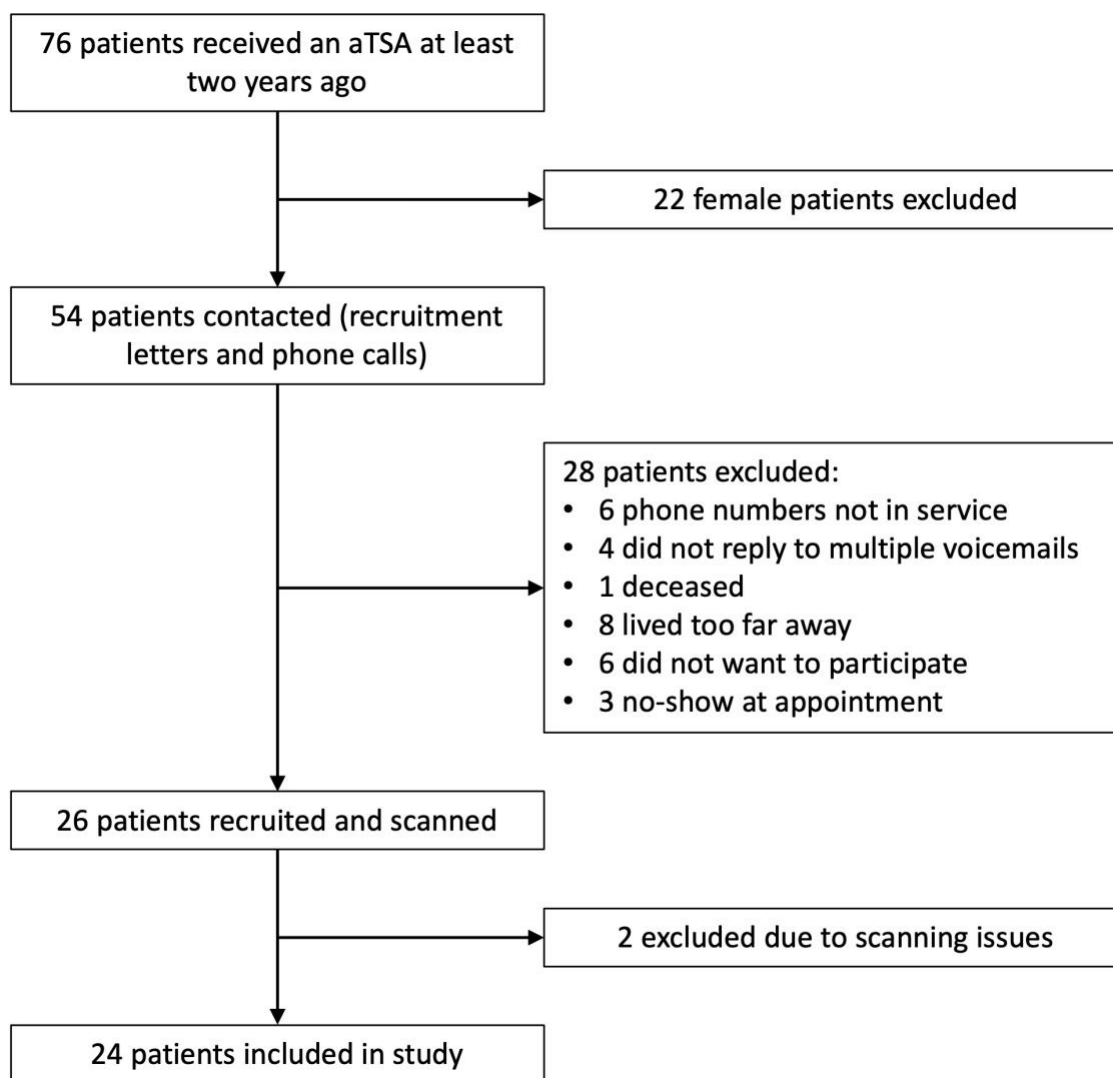


**Figure 5–1: Flowchart illustrating the recruitment and inclusion process.**

### 5.3.2 Mobility

No significant differences were measured between the full motion and limited motion groups for both ROM and kinematics pathways. However, several DoF showed differences when compared to the healthy participants. Specifically, for the full motion group there was greater humeral translation along the superior (Y) (1.4mm,  $p=0.029$ ) and lateral (Z) (1.1mm,  $p=0.016$ ) axes and increased (4.6°,  $p=0.05$ ) posterior tilting (Z) (Figure 5–2). Additionally, the full motion group exhibited increased (8.0°,  $p=0.025$ ) humeral rotation around the flexion (Z) axis, while rotation around the internal rotation (Y) axis was decreased (21.6°,  $p=0.014$ ) compared to the healthy participants (Figure 5–2). Similarly,

compared to healthy participants, those with limited mobility also demonstrated increased ( $9.2^\circ$ ,  $p=0.024$ ) humeral rotation around the flexion (Z) axis and decreased ( $21.8^\circ$ ,  $p=0.036$ ) rotation around the internal rotation (Y) axis (Figure 5–2). Overall, irrespective of motion level, all aTSA patients showed increased ROM of humeral flexion and decreased humeral internal rotation compared to the healthy control group. For the kinematic pathways, the limited motion group showed significant differences from the healthy cohort in humeral flexion (Z) ( $p=0.03$ ) and scapular protraction (Y) ( $p=0.042$ ) (Figure 5–3). Furthermore, both implant groups exhibited significant differences in humeral internal rotation (Y) ( $p=0.006$ ,  $p=0.002$ ) compared to the healthy cohort (Figure 5–3).

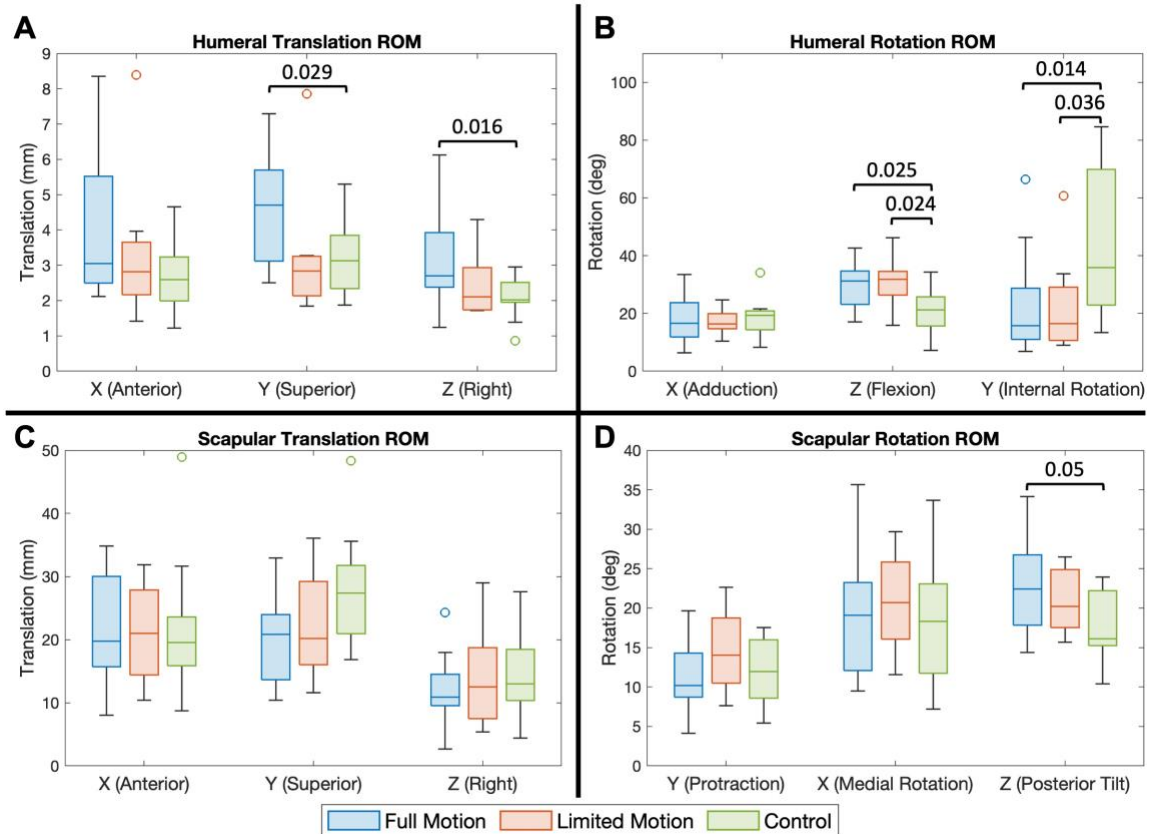


**Figure 5–2: Range of motion of the mobility groups.**

Boxplots comparing range of motion of the (A) humeral translation, (B) humeral rotation, (C) scapular translation, and (D) scapular rotation degrees of freedom for each mobility group (blue for full motion, red for limited motion, green for control). The bottom and top of a box represent quartile 1 and 3 respectively and define the interquartile range, the line within each box represents the median. Whiskers show the range of non-outlier values and solitary circles indicate outliers (defined as values with a difference from the box greater than the interquartile range). The p-value is provided for significant differences ( $p \leq 0.05$ ). Note that each degree of freedom is labelled following the positive axis/rotation convention although the direction is not considered.

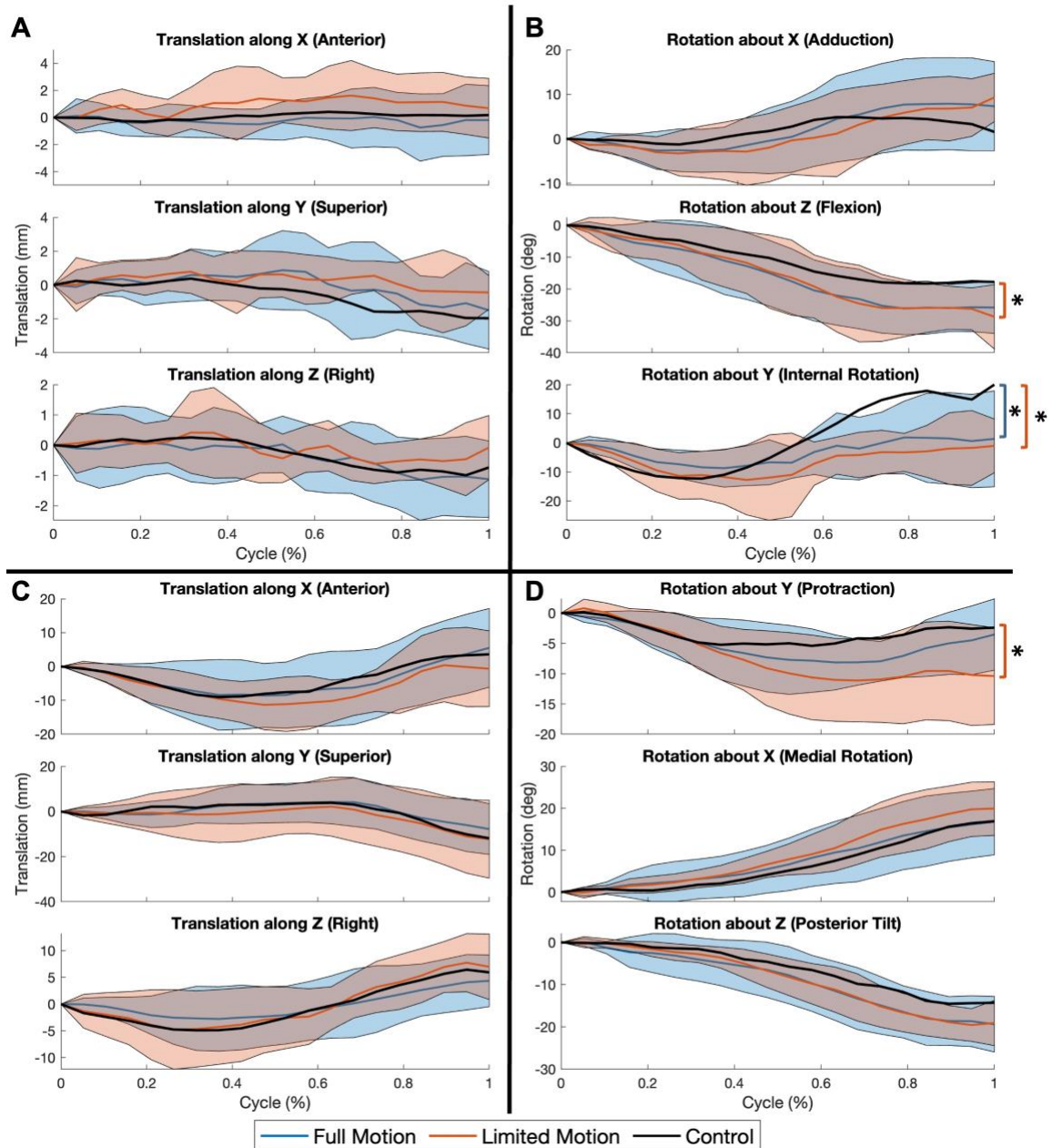


**Figure 5-3: Kinematic pathways of the mobility groups.**

*Kinematic pathways for the (A) humeral translation, (B) humeral rotation, (C) scapular translation, and (D) scapular rotation degrees of freedom for each mobility group (blue for full motion, red for limited motion, green for control). Solid lines represent the mean value at each time point and the shaded regions represent the standard deviation at each time point. A single asterisk (\*) represents a significant difference ( $p \leq 0.05$ ) in the final half of the motion.*

### 5.3.3 Mismatch

No significant differences were observed between the high and low mismatch groups. Compared to the healthy control, the low mismatch group demonstrated more ( $10.1^\circ$ ,  $p=0.005$ ) humeral rotation about the flexion (Z) axis and decreased ( $19.8^\circ$ ,  $p=0.033$ ) internal rotation (Y) (Figure 5–4). Additionally, the low mismatch group showed increased ( $5.8^\circ$ ,  $p=0.017$ ) posterior tilting (Z) of the scapula (Figure 5–4). The high mismatch group exhibited less ( $24.0^\circ$ ,  $p=0.012$ ) internal rotation (Y) of the humerus compared to the healthy control group (Figure 5–4). For the kinematic pathways, the low mismatch group showed significant differences from the healthy cohort in humeral flexion (Z) ( $p=0.05$ ) and scapular tilting (Z) ( $p=0.025$ ) (Figure 5–5). Furthermore, both mismatch groups exhibited significant differences in humeral internal rotation (Y) ( $p=0.002$ ,  $p=0.008$ ) compared to the healthy cohort (Figure 5–5). Finally, in the scatter plots depicting the relationship between mismatch and ROM, no significant correlation is evident for any DoF (Figure 5–6). This lack of correlation suggests that the degree of mismatch between the shoulder components does not have a meaningful influence on the ROM achieved by the participants.



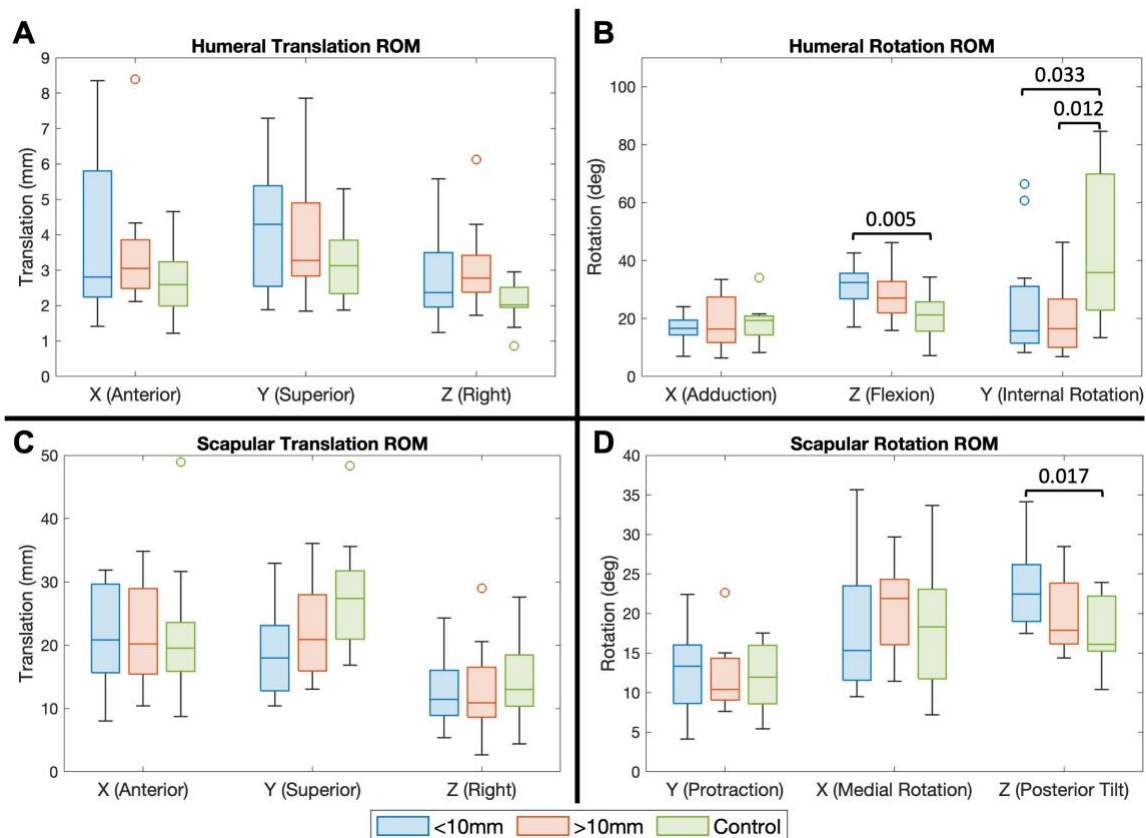


**Figure 5-4: Range of motion of the mismatch groups.**

Boxplots comparing range of motion of the (A) humeral translation, (B) humeral rotation, (C) scapular translation, and (D) scapular rotation degrees of freedom for each mismatch group (blue for low, red for high, green for control). The bottom and top of a box represent quartile 1 and 3 respectively and define the interquartile range, the line within each box represents the median. Whiskers show the range of non-outlier values and solitary circles indicate outliers (defined as values with a difference from the box greater than the interquartile range). The  $p$ -value is provided for significant differences ( $p \leq 0.05$ ). Note that each degree of freedom is labelled following the positive axis/rotation convention although the direction is not considered.

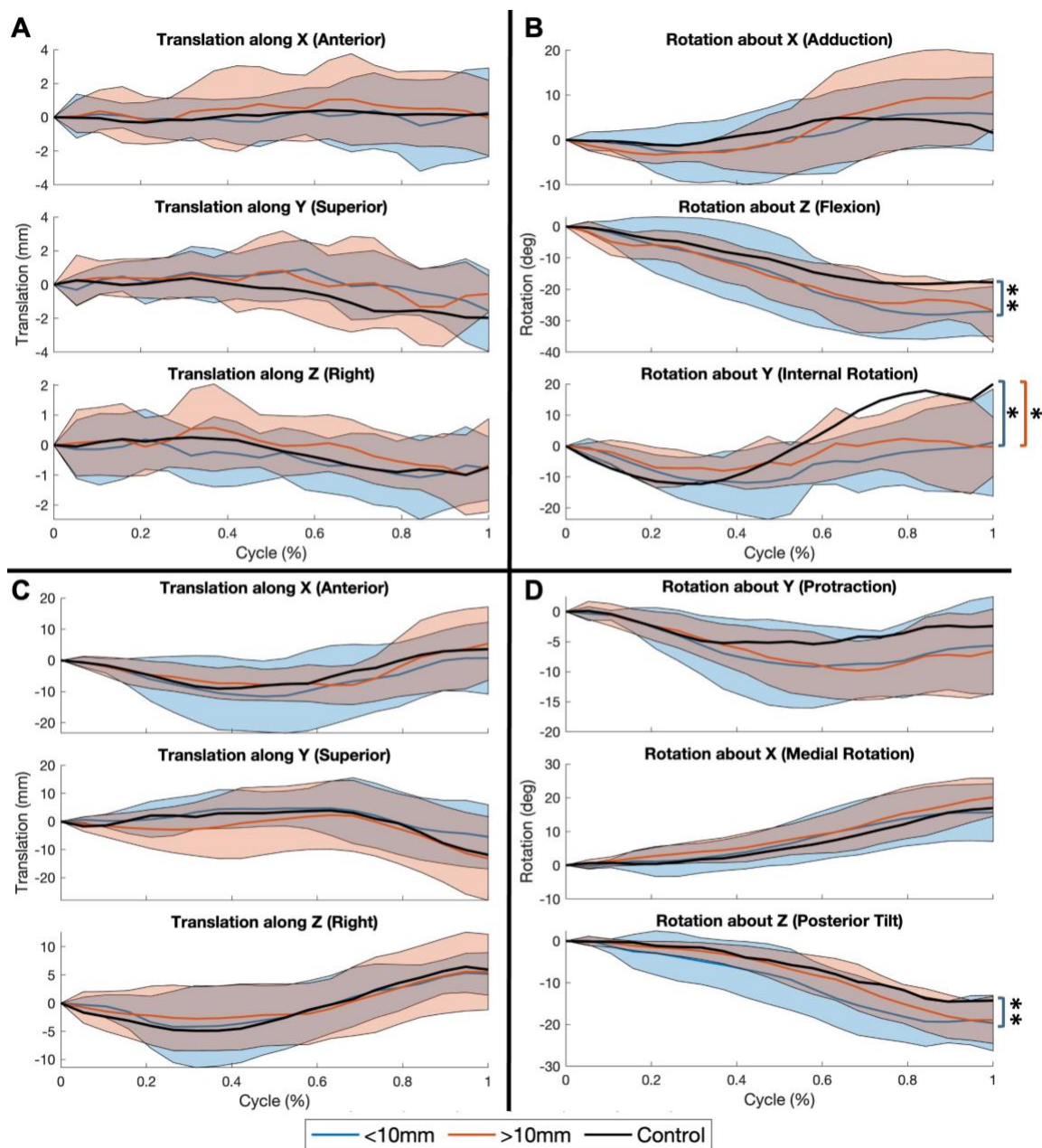


**Figure 5-5: Kinematic pathways of the mismatch groups.**

*Kinematic pathways for the (A) humeral translation, (B) humeral rotation, (C) scapular translation, and (D) scapular rotation degrees of freedom for each mismatch group (blue for low, red for high, green for control). Solid lines represent the mean value at each time point and the shaded regions represent the standard deviation at each time point. A single (\*) or double asterisk (\*\*) represents significant differences ( $p \leq 0.05$ ) in motion for the final half or throughout the entire motion, respectively.*

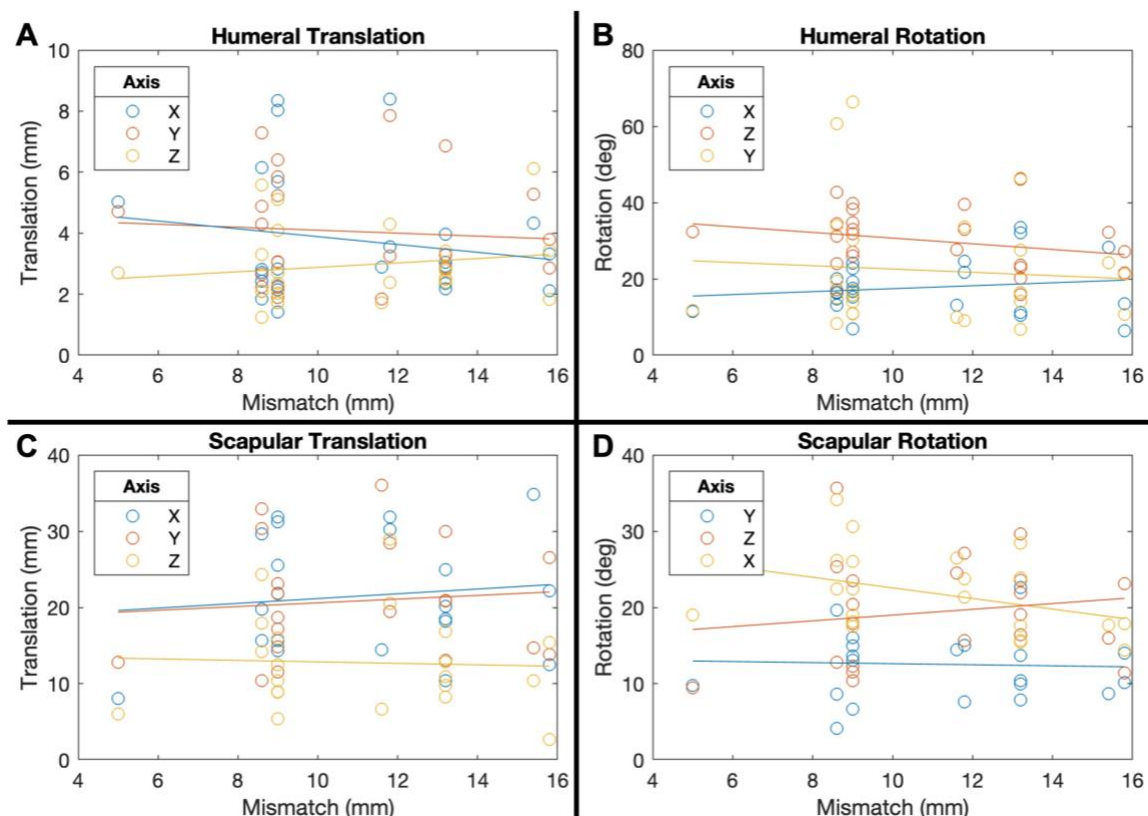


**Figure 5–6: Relationship between mismatch and range of motion.**

Scatter plots comparing diametrical mismatch to (A) humeral translation, (B) humeral rotation, (C) scapular translation, and (D) scapular rotation, range of motion. No strong correlations exist for any degree of freedom.

## 5.4 Discussion

This study did not find any significant differences between the various implant groups; however, there were notable differences when comparing to the healthy control group. When performing the internal rotation to the back motion, all participants with implants, regardless of motion ability, showed more rotation about the flexion (Z) axis and less about the internal rotation (Y) axis (Figure 5–2). The kinematic pathways show that the humerus extends (-Z) throughout the entire motion, and initially externally rotates (-Y) for about one-third of the motion before internally rotating (Y) for the remainder (Figure 5–3). Upon further analysis, it is logical to conclude that there is a dependent relationship between

these two DoF. Reduced internal rotation positions the lower arm more anteriorly, and as the body physically blocks this position, participants compensate by extending the arm farther behind their back. As a final position with the arm behind the back, the healthy population likely have their elbow pointing laterally, as that would be a position with high internal rotation but low extension. Conversely, the implant participants likely have their elbow pointing posterolaterally, as that would be a position with less internal rotation and greater extension of the humerus.

It has been established that those who struggle with internal rotation postoperatively have diminished subscapularis functionality (Liem et al., 2012; Miller et al., 2003). However, the results of this study suggest that even with good mobility, aTSA patients still exhibit altered kinematics, most notably about 22° less internal rotation (Figure 5–2). Given that internal rotation is the primary action of the subscapularis, it is likely that this muscle never fully recovers, and this persistent reduction in subscapularis capability is responsible for the reduced internal rotation. This insight highlights the need for targeted rehabilitation strategies and postoperative care that focus on improving subscapularis function. A stronger subscapularis would hopefully result in less compensatory motion and better replication of native kinematics, potentially leading to improved long-term outcomes and patient satisfaction following aTSA. Additionally, this knowledge could influence surgical techniques and implant design to better accommodate the limitations in subscapularis recovery.

The difference in the protraction pathway (Figure 5–3) is of particular interest because there was no corresponding difference in ROM. All groups begin the motion by retracting the scapula (-Y) as their arm moves towards their back. However, during the final third of the motion, where the arm is moved up the back, the full motion and healthy groups protract their scapula, whereas the limited motion group remains in the retracted position. Although it is important to note that statistical significance was only found between the pathways of the limited and healthy groups. It is unknown whether the limited group's inability to protract the scapula during this part of the motion is a result of their inability to perform the full motion or if it is a factor causing it. Given that an implant should ideally not affect scapular motion, reduced protraction is most likely a consequence of other factors.

It was expected that the full and limited groups would exhibit notable differences since they were performing the motion in different ways; however, the results do not support this hypothesis. Given the complexity of the motion, which involves contributions from both the glenohumeral and scapulothoracic joints, all DoF are constantly changing. This, combined with individual variations in performing the motion, results in large standard deviations. The portion of the motion that differs between mobility groups (the final slide up the back) is a relatively small movement involving multiple DoF concurrently. These small changes relative to the large variance result in no single DoF showing significant differences.

No significant differences or correlations were found between level of mismatch and ROM. Additionally, there was no large overlap between participant groups (Table 5–1), indicating that the ability to perform the motion is not strongly related to mismatch level. This result is likely due to the participants not having extreme levels of mismatch. The diametrical mismatch of the participants ranged from 8.6 to 15.8mm, with one outlier at 5mm. This is equivalent to a radial mismatch range of 4.3 to 7.9mm, which is a range not at an increased risk of complications (Schoch et al., 2019; Terrier et al., 2006; Walch et al., 2002). Given that mismatch within this range does not appear to correlate with ROM, optimal patient mismatch should be based on other factors that minimize the risk of failure, such as reducing implant stresses and micromotion.

Chapter 4 showed that humeral translation decreases with age. This study showed that for patients where motion is restored (full motion group), humeral translation along the superior and lateral axes is greater than their healthy counterparts (Figure 5–2). Therefore, some age-related changes can in part be reversed by an aTSA. Given that the implant modifies the glenohumeral joint, it can be concluded that decreased glenohumeral translation with age is primarily due to increased joint friction rather than alterations in the surrounding soft tissues. If ligamentous or muscular changes were primarily responsible for the altered kinematics, an implant would not have a significant impact. However, changes to and within the joint capsule – such as reduced articular cartilage, reduced synovial fluid, osteophyte formation, and joint capsule tightening – are removed with the

introduction of the implant. Thus, glenohumeral translation is restored because the deteriorating synovial environment is replaced by a low friction metal-plastic interface.

The scope of this study was limited to only one motion due to the metallic components requiring the scan to have a higher voltage and subsequent dosage. The internal rotation motion was chosen due to the established issues with recovery of this motion (Miller et al., 2003; Rojas et al., 2020; Triplet et al., 2015, 2018), however other movements may reveal differences between mobility groups or mismatch that were not found during this study. Preoperative conditions such as ROM, level of pain, and surgery wait-time were unknown, consequently, the impact of these factors on the resultant kinematics was not able to be assessed. Given that preoperative ROM has shown to be correlated with postoperative ROM (Friedman et al., 2019; Jacobs et al., 2016; Levy et al., 2016), it is likely that many participants categorized as limited motion had poor motion preoperatively as well.

A significant finding of this study was the diminished internal rotation observed across all aTSA patients. With this deficiency identified, future work should further explore whether the implants are physically preventing this movement or if subscapularis insufficiency is responsible. If the latter proves to be the primary factor, then the development of new surgical techniques and/or rehabilitation strategies should be a focus of future research. However, designing implants that better replicate normal glenohumeral motion may be more important for improving patient outcomes. Implant mismatch was not found to affect kinematics or ROM; however, mismatch is known to influence implant stress and micromotion (Diop et al., 2006; Terrier et al., 2006). As such, research optimizing mismatch should focus on mechanical factors and failure modes as the primary dependent factors. Overall, this study has important implications for improving functionality and rehabilitation following shoulder arthroplasties.

## Chapter 6

### 6 General Discussion and Conclusions

#### OVERVIEW

*This concluding chapter summarizes the objectives and hypotheses, along with the work performed to satisfy these objectives. The strengths and limitations of the work are discussed, and future research directions are proposed.*

## 6.1 Summary and Conclusions

Dynamic kinematics of the shoulder remain not fully understood, particularly the interplay between the glenohumeral and scapulothoracic joints, and how this relationship may change with age. Existing research often focuses on simple motions, overlooking more complex movements needed for activities of daily living, such as internal rotation. Post-total shoulder arthroplasty (TSA) surgery, many patients struggle with internal rotation, which is important for tasks such as dressing and bathing, with recovery influenced by factors such as muscle restoration, rehabilitation, and surgical techniques. However, the exact causes and effects on shoulder kinematics and range of motion (ROM) post-surgery remain unclear. This dissertation used four-dimensional computed tomography (4DCT) to provide precise assessments of shoulder kinematics, both pre- and post-implant, to improve the understanding of shoulder biomechanics and TSA outcomes.

The first objective of this thesis was to develop a process of measuring glenohumeral and scapulothoracic kinematics through bone motion obtained via 4DCT, and then to assess the repeatability of this process. This objective was achieved in Chapter 2, which described and validated the single-vertebra image-based (SVIB) process. Using a single vertebra in place of the entire torso as a reference for scapulothoracic motion was an important concept for the viability of using 4DCT to measure shoulder kinematics. Furthermore, the repeatability of the necessary steps was shown to be acceptable.

Chapter 3 had the objective of improving the feasibility of using 4DCT by automating the most time-consuming step, segmenting the scans to create bone models. To complete this task, a unique convolutional neural network designed for image segmentation was developed. Two networks, one for the humerus and one for the scapula, were trained on thousands of individual computed tomography (CT) slices and were able to segment bones with accuracy comparable to a trained human. Additionally, these networks can be implemented directly within 3DSlicer, allowing an entire frame of segmentations to be completed in less than a minute, fulfilling the objective.

The main objective of Chapter 4 was to quantify healthy shoulder kinematics and investigate the influence of age. The first hypothesis was that humeral translation is



necessary for proper shoulder motion. This was shown to be true as all participants exhibited some degree of humeral translation, approximately 2 – 5mm on average. It was also hypothesized that older participants would exhibit less humeral motion and unchanged scapular motion, subsequently resulting in a lower scapulohumeral rhythm. The basis of this hypothesis was that the effects of aging would be more pronounced in a synovial joint. The results of this chapter only partially supported this hypothesis, as humeral ROM was lower for the translational degrees-of-freedom (DoF), but no significant differences in scapulohumeral rhythm were apparent. Given that scapulohumeral rhythm only accounts for rotational DoF, it is logical that this metric did not reflect the major translational differences observed. Unexpectedly, the older cohort showed increased humeral internal/external rotation ROM during the forward elevation motion. Also contrary to the hypothesis was that the scapula did display ROM changes with age, specifically less posterior translation and medial rotation during forward elevation and greater inferior translation during internal rotation. However, the reduced medial rotation and inferior translation ROM of the scapula appear to be correlated to increased medial rotation and superior translation of the neutral scapula pose. These results also answer the final objective of this chapter which was to determine if the natural position of the bones change with age. In addition to the increased medial rotation and superior translation of the scapula, the scapula is also more posteriorly tilted, and the humerus is positioned more anterior in older participants.

The main objective of Chapter 5 was to compare the kinematics between natural and aTSA shoulders, in addition to exploring the effects of mobility and mismatch. The first hypothesis was that patients with good mobility would have similar kinematics and ROM as non-implant participants. However, the results did not support this hypothesis, on the contrary, the full motion group had more significant differences than the limited motion group when compared to the healthy control group. The second hypothesis was that patients with poor mobility would exhibit less humeral translation and humeral internal rotation. However, it was found that regardless of mobility, an aTSA limits internal rotation of the humerus, which for the internal rotation behind the back motion is compensated for with increased extension of the humerus. In terms of humeral translation, no differences were found between mobility groups, but the full motion group did show increased ROM

in comparison to the healthy participants. The final objective was to explore the effects of mismatch with the hypothesis that greater mismatch would correlate with greater humeral translation. The results did not support this hypothesis and no correlation between mismatch and ROM was found for any DoF.

## 6.2 Strengths and Limitations

The motions examined throughout the studies of this dissertation were all unconstrained, individuals were allowed to move naturally without forced or guided actions. This approach results in data that is representative of genuine, real-world movements, providing a realistic understanding of shoulder kinematics. However, this approach also introduces a major limitation, the natural variation in how individuals perform upper limb movements leads to high variability in the data (Rau et al., 2000). Consequently, this increased variation can make it more difficult to identify significant differences between groups. Furthermore, differences in starting position could further compound this variability. Since participants were not rigorously constrained to a standardized initial posture, subtle discrepancies could influence the observed kinematic pathways and ROM.

Another limitation of the studies in this dissertation is the discrete grouping of participants. The established groups were based on age, mobility, and implant mismatch; however, these factors represent continuous variables rather than distinct categories. As a result, the boundaries between groups are somewhat arbitrary, potentially leading to overlap that could obscure meaningful differences. Moreover, each analysis focused on a single variable at a time, without considering potential confounding factors. Metrics such as BMI, height, profession, or activity level, all of which could influence shoulder kinematics, were not accounted for.

To maintain sample homogeneity, the studies exclusively focused on the male sex. This choice acknowledges that shoulder kinematics may be different between sexes due to physiological differences. Furthermore, aging effects on shoulder kinematics may manifest differently in women, notably due to the significant biological and hormonal changes associated with menopause. While this focus on a single sex provides more consistent

results, it also limits the generalizability of the findings and is a consideration for future work.

New generations of CT machines have 4DCT capability, and as this technology becomes more widespread, its prevalence in research is likely to increase. Future studies intending to use 4DCT for analyzing shoulder kinematics can emulate the methodology developed in this thesis. The details of the SVIB process are meticulously described in Chapter 2, ensuring others can follow this protocol and allowing for consistency in future research. Moreover, the use of 3DSlicer, a free open-source program, is a notable strength. This software's accessibility enables other researchers to easily replicate and build upon the methodology of this thesis.

### 6.3 Future Directions

This dissertation has achieved the specific objectives outlined in Chapter 1; however, there are still various opportunities for further investigating shoulder biomechanics and TSA implants.

With the SVIB process now established, additional motions should be examined to further characterize shoulder kinematics across more possible movements. Collecting additional data, such as video recordings or motion capture, while participants perform the motions, would be beneficial for understanding how the various DoF relate to the execution of these motions, considering the variability in movement. Likewise, using guides or constraints to reduce participant variability may be beneficial for isolating differences between participant groups. One such factor that should be investigated is the impact of bone morphology on kinematics, ROM, and motion variability. The size and shape of the various bones likely affects the location and line of action of muscles, thereby affecting movement. Future studies should also explore sex-specific considerations, examining the natural differences between sexes as well as the impact of aging. Physiological differences and hormonal transitions could cause the effects of aging to present differently in males and females.

Radiation exposure is a limiting factor in the number and duration of scans that can be safely performed, increasing the risk for participants and constraining the scope of studies. Therefore, it would be valuable to explore strategies to reduce the radiation dose while maintaining adequate image quality. One potential approach is to conduct a cadaveric study, where various imaging parameters – such as tube current, voltage, slice thickness, and scan frequency and duration – are systematically adjusted. A similar approach by Lalone et al. (2011) successfully reduced the effective dose to the shoulder 88.9% compared to standard clinical CT images. Applying this method to 4DCT could help identify an optimal balance that minimizes patient dose without compromising the subsequent kinematic analysis. Additionally, advancements in image reconstruction algorithms, particularly with the use of artificial intelligence, could further enhance image quality at lower doses, making 4DCT safer for research applications.

This thesis was limited to analyzing bones and consequently only resultant motion; however, the surrounding soft tissues are important for enabling motion. Future work should integrate imaging modalities capable of capturing muscles and ligaments, investigating how differences in kinematics may be correlated to variations in musculature and the surrounding passive soft tissues. Studying age-related alterations in these tissues and musculature would provide insights into the physiological processes contributing to the changes in ROM and pose observed in Chapter 4.

The work done in Chapter 5 provided insights into implants, but further investigation is needed. Other motions and functional tasks should be analyzed, as different movements may reveal correlations between mobility or mismatch not identified in Chapter 5. Furthermore, investigating the effects of preoperative conditions on postoperative kinematics would likely be beneficial as many possible factors may influence patient outcomes. The most common type of glenoid erosion (type B) results in a posteriorly subluxated humerus, and 4DCT can be used to investigate the influence of subluxation on kinematics and ROM. This could further include determining how the effectiveness of correcting the subluxation postoperatively, and any long-term subluxation changes, influences kinematics. A significant finding in Chapter 5 was the diminished internal rotation observed across all aTSA patients. Future work should try to determine the

underlying mechanism, whether it is due to implant impingement preventing internal rotation, or if subscapularis deficiency is responsible. Lastly, similar methodologies to those used in Chapter 5 should be employed to investigate the effects of a reverse TSA on shoulder kinematics and ROM.

## References

- Alta, T. D., Bell, S. N., Troupis, J. M., Coghlan, J. A., & Miller, D. (2012). The New 4-Dimensional Computed Tomographic Scanner Allows Dynamic Visualization and Measurement of Normal Acromioclavicular Joint Motion in an Unloaded and Loaded Condition. *Journal of Computer Assisted Tomography*, 36(6), 749–754. <https://doi.org/10.1097/RCT.0b013e31826dbc50>
- American Association of Physicists in Medicine. (2008). *The measurement, reporting, and management of radiation dose in CT: AAPM report no. 96*.
- Barnes, C. J., Van Steyn, S. J., & Fischer, R. A. (2001). The effects of age, sex, and shoulder dominance on range of motion of the shoulder. *Journal of Shoulder and Elbow Surgery*, 10(3), 242–246. <https://doi.org/10.1067/mse.2001.115270>
- Baumer, T. G., Giles, J. W., Drake, A., Zael, R., & Bey, M. J. (2016). Measuring Three-Dimensional Thorax Motion Via Biplane Radiographic Imaging: Technique and Preliminary Results. *Journal of Biomechanical Engineering*, 138(1), 1–5. <https://doi.org/10.1115/1.4032058>
- Bell, S. N., Troupis, J. M., Miller, D., Alta, T. D., Coghlan, J. A., & Wijeratna, M. D. (2015). Four-dimensional computed tomography scans facilitate preoperative planning in snapping scapula syndrome. *Journal of Shoulder and Elbow Surgery*, 24(4), e83–e90. <https://doi.org/10.1016/j.jse.2014.09.020>
- Bercik, M. J., Kruse, K., Yalozis, M., Gauci, M.-O., Chaoui, J., & Walch, G. (2016). A modification to the Walch classification of the glenoid in primary glenohumeral osteoarthritis using three-dimensional imaging. *Journal of Shoulder and Elbow Surgery*, 25(10), 1601–1606. <https://doi.org/10.1016/j.jse.2016.03.010>
- Besl, P. J., & McKay, N. D. (1992). A method for registration of 3-D shapes. *IEEE Transactions on Pattern Analysis and Machine Intelligence*, 14(2), 239–256. <https://doi.org/10.1109/34.121791>
- Bey, M. J., Kline, S. K., Zael, R., Lock, T. R., & Kolowich, P. A. (2008). Measuring dynamic in-vivo glenohumeral joint kinematics: Technique and preliminary results. *Journal of Biomechanics*, 41(3), 711–714. <https://doi.org/10.1016/J.JBIOMECH.2007.09.029>
- Bey, M. J., Zael, R., Brock, S. K., & Tashman, S. (2006). Validation of a new model-based tracking technique for measuring three-dimensional, in vivo glenohumeral joint kinematics. *Journal of Biomechanical Engineering*, 128(4), 604–609. <https://doi.org/10.1115/1.2206199>
- Bourne, D. A., Choo, A. M., Regan, W. D., MacIntyre, D. L., & Oxland, T. R. (2011). The Placement of Skin Surface Markers for Non-Invasive Measurement of Scapular Kinematics Affects Accuracy and Reliability. *Annals of Biomedical Engineering*,

39(2), 777–785. <https://doi.org/10.1007/s10439-010-0185-1>

- Charbonnier, C., Chagué, S., Kolo, F. C., Chow, J. C. K., & Lädermann, A. (2014). A patient-specific measurement technique to model shoulder joint kinematics. *Orthopaedics and Traumatology: Surgery and Research*, 100(7), 715–719. <https://doi.org/10.1016/j.otsr.2014.06.015>
- Chillemi, C., & Franceschini, V. (2013). Shoulder Osteoarthritis. *Arthritis*, 2013, 1–7. <https://doi.org/10.1155/2013/370231>
- Churchill, R. S., & Athwal, G. S. (2016). Stemless shoulder arthroplasty—current results and designs. *Current Reviews in Musculoskeletal Medicine*, 9(1), 10–16. <https://doi.org/10.1007/s12178-016-9320-4>
- Culham, E., & Peat, M. (1993). Functional Anatomy of the Shoulder Complex. *Journal of Orthopaedic & Sports Physical Therapy*, 18(1), 342–350. <https://doi.org/10.2519/jospt.1993.18.1.342>
- Daher, B., Hunter, J., Athwal, G. S., & Lalone, E. A. (2023). How does computed tomography inform our understanding of shoulder kinematics? A structured review. *Medical & Biological Engineering & Computing*. <https://doi.org/10.1007/s11517-022-02755-1>
- Diop, A., Maurel, N., Grimberg, J., & Gagey, O. (2006). Influence of glenohumeral mismatch on bone strains and implant displacements in implanted glenoids. An in vitro experimental study on cadaveric scapulae. *Journal of Biomechanics*, 39(16), 3026–3035. <https://doi.org/10.1016/j.jbiomech.2005.10.015>
- Doriot, N., & Wang, X. (2006). Effects of age and gender on maximum voluntary range of motion of the upper body joints. *Ergonomics*, 49(3), 269–281. <https://doi.org/10.1080/00140130500489873>
- Farley, K. X., Wilson, J. M., Kumar, A., Gottschalk, M. B., Daly, C., Sanchez-Sotelo, J., & Wagner, E. R. (2021). Prevalence of Shoulder Arthroplasty in the United States and the Increasing Burden of Revision Shoulder Arthroplasty. *JBJS Open Access*, 6(3). <https://doi.org/10.2106/JBJS.OA.20.00156>
- Freemont, A., & Hoyland, J. (2007). Morphology, mechanisms and pathology of musculoskeletal ageing. *The Journal of Pathology*, 211(2), 252–259. <https://doi.org/10.1002/path.2097>
- Friedman, R. J., Eichinger, J., Schoch, B., Wright, T., Zuckerman, J., Flurin, P.-H., Bolch, C., & Roche, C. (2019). Preoperative parameters that predict postoperative patient-reported outcome measures and range of motion with anatomic and reverse total shoulder arthroplasty. *JSES Open Access*, 3(4), 266–272. <https://doi.org/10.1016/j.jses.2019.09.010>
- Gill, T. K., Shanahan, E. M., Tucker, G. R., Buchbinder, R., & Hill, C. L. (2020).

- Shoulder range of movement in the general population: age and gender stratified normative data using a community-based cohort. *BMC Musculoskeletal Disorders*, 21(1), 676. <https://doi.org/10.1186/s12891-020-03665-9>
- Giphart, J. E., Brunkhorst, J. P., Horn, N. H., Shelburne, K. B., Torry, M. R., & Millett, P. J. (2013). Effect of Plane of Arm Elevation on Glenohumeral Kinematics. *Journal of Bone and Joint Surgery*, 95(3), 238–245. <https://doi.org/10.2106/JBJS.J.01875>
- Hajizadeh, M., Michaud, B., & Begon, M. (2019). The effect of intracortical bone pin on shoulder kinematics during dynamic activities. *International Biomechanics*, 6(1), 47–53. <https://doi.org/10.1080/23335432.2019.1633958>
- Hansen, M. L., & Routman, H. (2019). The biomechanics of current reverse shoulder replacement options. *Annals of Joint*, 4, 17–17. <https://doi.org/10.21037/aoj.2019.01.06>
- Hsiao, E. M., Rybicki, F. J., & Steigner, M. (2010). CT Coronary Angiography: 256-Slice and 320-Detector Row Scanners. *Current Cardiology Reports*, 12(1), 68–75. <https://doi.org/10.1007/s11886-009-0075-z>
- Hunter, J., Lee, T.-Y., Athwal, G. S., & Lalone, E. A. (2023). Development of a single-vertebra image-based technique to quantify shoulder kinematics using four-dimensional computed tomography. *Computer Methods in Biomechanics and Biomedical Engineering: Imaging & Visualization*, 1–9. <https://doi.org/10.1080/21681163.2023.2282074>
- Iannotti, J., Baker, J., Rodriguez, E., Brems, J., Ricchetti, E., Mesiha, M., & Bryan, J. (2014). Three-Dimensional Preoperative Planning Software and a Novel Information Transfer Technology Improve Glenoid Component Positioning. *Journal of Bone and Joint Surgery*, 96(9), e71. <https://doi.org/10.2106/JBJS.L.01346>
- Iannotti, J. P., Gabriel, J. P., Schneck, S. L., Evans, B. G., & Misra, S. (1992). The normal glenohumeral relationships. An anatomical study of one hundred and forty shoulders. *The Journal of Bone and Joint Surgery. American Volume*, 74(4), 491–500. <http://www.ncbi.nlm.nih.gov/pubmed/1583043>
- Ibounig, T., Simons, T., Launonen, A., & Paavola, M. (2021). Glenohumeral osteoarthritis: an overview of etiology and diagnostics. *Scandinavian Journal of Surgery*, 110(3), 441–451. <https://doi.org/10.1177/1457496920935018>
- Jackson, M., Michaud, B., Tétrault, P., & Begon, M. (2012). Improvements in measuring shoulder joint kinematics. *Journal of Biomechanics*, 45(12), 2180–2183. <https://doi.org/10.1016/J.JBIOMECH.2012.05.042>
- Jacobs, C. A., Morris, B. J., Sciascia, A. D., & Edwards, T. B. (2016). Comparison of satisfied and dissatisfied patients 2 to 5 years after anatomic total shoulder arthroplasty. *Journal of Shoulder and Elbow Surgery*, 25(7), 1128–1132. <https://doi.org/10.1016/j.jse.2015.12.001>



- Jadon, S. (2020). *A survey of loss functions for semantic segmentation*.  
<https://doi.org/10.1109/CIBCB48159.2020.9277638>
- Jun, B. J., Iannotti, J. P., McGarry, M. H., Yoo, J. C., Quigley, R. J., & Lee, T. Q. (2013). The effects of prosthetic humeral head shape on glenohumeral joint kinematics: a comparison of non-spherical and spherical prosthetic heads to the native humeral head. *Journal of Shoulder and Elbow Surgery*, 22(10), 1423–1432.  
<https://doi.org/10.1016/j.jse.2013.01.002>
- Jun, B. J., Lee, T. Q., McGarry, M. H., Quigley, R. J., Shin, S. J., & Iannotti, J. P. (2016). The effects of prosthetic humeral head shape on glenohumeral joint kinematics during humeral axial rotation in total shoulder arthroplasty. *Journal of Shoulder and Elbow Surgery*, 25(7), 1084–1093. <https://doi.org/10.1016/j.jse.2015.11.058>
- Karduna, A. R., Williams, G. R., Williams, J. L., & Iannotti, J. P. (1997). Glenohumeral Joint Translations before and after Total Shoulder Arthroplasty. A Study in Cadavera\*. *The Journal of Bone & Joint Surgery*, 79(8), 1166–1174.  
<https://doi.org/10.2106/00004623-199708000-00008>
- Keskar, N. S., Mudigere, D., Nocedal, J., Smelyanskiy, M., & Tang, P. T. P. (2016). *On Large-Batch Training for Deep Learning: Generalization Gap and Sharp Minima*.  
<http://arxiv.org/abs/1609.04836>
- Kijima, T., Matsuki, K., Ochiai, N., Yamaguchi, T., Sasaki, Y., Hashimoto, E., Sasaki, Y., Yamazaki, H., Kenmoku, T., Yamaguchi, S., Masuda, Y., Umekita, H., Banks, S. A., & Takahashi, K. (2015). In vivo 3-dimensional analysis of scapular and glenohumeral kinematics: comparison of symptomatic or asymptomatic shoulders with rotator cuff tears and healthy shoulders. *Journal of Shoulder and Elbow Surgery*, 24(11), 1817–1826. <https://doi.org/10.1016/j.jse.2015.06.003>
- Klotz, M. C. M., Kost, L., Braatz, F., Ewerbeck, V., Heitzmann, D., Gantz, S., Dreher, T., & Wolf, S. I. (2013). Motion capture of the upper extremity during activities of daily living in patients with spastic hemiplegic cerebral palsy. *Gait & Posture*, 38(1), 148–152. <https://doi.org/10.1016/J.GAITPOST.2012.11.005>
- Kolz, C. W., Sulkar, H. J., Aliaj, K., Tashjian, R. Z., Chalmers, P. N., Qiu, Y., Zhang, Y., Bo Foreman, K., Anderson, A. E., & Henninger, H. B. (2021). Age-related differences in humerothoracic, scapulothoracic, and glenohumeral kinematics during elevation and rotation motions. *Journal of Biomechanics*, 117, 110266.  
<https://doi.org/10.1016/j.jbiomech.2021.110266>
- Kon, Y., Nishinaka, N., Gamada, K., Tsutsui, H., & Banks, S. A. (2008). The influence of handheld weight on the scapulohumeral rhythm. *Journal of Shoulder and Elbow Surgery*, 17(6), 943–946. <https://doi.org/10.1016/j.jse.2008.05.047>
- Krishnan, R., Björzell, N., Gutierrez-Farewik, E. M., & Smith, C. (2019). A survey of human shoulder functional kinematic representations. *Medical & Biological Engineering & Computing*, 57(2), 339–367. <https://doi.org/10.1007/s11517-018->

1903-3

- Lalone, E. A., Fox, A.-M. V., Kedgley, A. E., Jenkyn, T. R., King, G. J. W., Athwal, G. S., Johnson, J. A., & Peters, T. M. (2011). The effect of CT dose on glenohumeral joint congruency measurements using 3D reconstructed patient-specific bone models. *Physics in Medicine and Biology*, *56*(20), 6615–6624. <https://doi.org/10.1088/0031-9155/56/20/006>
- Langer, J. S., Sueoka, S. S., & Wang, A. A. (2012). The Importance of Shoulder External Rotation in Activities of Daily Living: Improving Outcomes in Traumatic Brachial Plexus Palsy. *The Journal of Hand Surgery*, *37*(7), 1430–1436. <https://doi.org/10.1016/J.JHSA.2012.04.011>
- Lau, H., & Weerakkody, Y. (2016, March 4). *Shoulder bursae*. Radiopaedia.Org; Radiopaedia.org. <https://doi.org/10.53347/rid-43309>
- Lavaill, M., Martelli, S., Gilliland, L., Gupta, A., Kerr, G., & Pivonka, P. (2022). The effects of anatomical errors on shoulder kinematics computed using multi-body models. *Biomechanics and Modeling in Mechanobiology*, *21*(5), 1561–1572. <https://doi.org/10.1007/s10237-022-01606-0>
- Levasseur, A., Tétreault, P., de Guise, J., Nuño, N., & Hagemester, N. (2007). The effect of axis alignment on shoulder joint kinematics analysis during arm abduction. *Clinical Biomechanics*, *22*(7), 758–766. <https://doi.org/10.1016/J.CLINBIOMECH.2007.04.009>
- Levy, J. C., Ashukem, M. T., & Formaini, N. T. (2016). Factors predicting postoperative range of motion for anatomic total shoulder arthroplasty. *Journal of Shoulder and Elbow Surgery*, *25*(1), 55–60. <https://doi.org/10.1016/j.jse.2015.06.026>
- Liem, D., Kleeschulte, K., Dedy, N., Schulte, T. L., Steinbeck, J., & Marquardt, B. (2012). Subscapularis function after transosseous repair in shoulder arthroplasty: transosseous subscapularis repair in shoulder arthroplasty. *Journal of Shoulder and Elbow Surgery*, *21*(10), 1322–1327. <https://doi.org/10.1016/j.jse.2011.09.022>
- Loeser, R. F. (2011). Aging and osteoarthritis. *Current Opinion in Rheumatology*, *23*(5), 492–496. <https://doi.org/10.1097/BOR.0b013e3283494005>
- Macedo, L. G., & Magee, D. J. (2009). Effects of age on passive range of motion of selected peripheral joints in healthy adult females. *Physiotherapy Theory and Practice*, *25*(2), 145–164. <https://doi.org/10.1080/09593980802686870>
- Massimini, D. F., Boyer, P. J., Papannagari, R., Gill, T. J., Warner, J. P., & Li, G. (2012). In-vivo glenohumeral translation and ligament elongation during abduction and abduction with internal and external rotation. *Journal of Orthopaedic Surgery and Research*, *7*, 29. <https://doi.org/10.1186/1749-799X-7-29>
- Matsuki, K., Matsuki, K. O., Mu, S., Yamaguchi, S., Ochiai, N., Sasho, T., Sugaya, H.,

- Toyone, T., Wada, Y., Takahashi, K., & Banks, S. A. (2011). In vivo 3-dimensional analysis of scapular kinematics: comparison of dominant and nondominant shoulders. *Journal of Shoulder and Elbow Surgery*, *20*(4), 659–665. <https://doi.org/10.1016/j.jse.2010.09.012>
- Matsumura, N., Oki, S., Fukasawa, N., Matsumoto, M., Nakamura, M., Nagura, T., Yamada, Y., & Jinzaki, M. (2019). Glenohumeral translation during active external rotation with the shoulder abducted in cases with glenohumeral instability: a 4-dimensional computed tomography analysis. *Journal of Shoulder and Elbow Surgery*, *28*(10), 1903–1910. <https://doi.org/10.1016/j.jse.2019.03.008>
- McClure, P. W., Michener, L. A., Sennett, B. J., & Karduna, A. R. (2001). Direct 3-dimensional measurement of scapular kinematics during dynamic movements in vivo. *Journal of Shoulder and Elbow Surgery*, *10*(3), 269–277. <https://doi.org/10.1067/mse.2001.112954>
- Miller, S. L., Hazrati, Y., Klepps, S., Chiang, A., & Flatow, E. L. (2003). Loss of subscapularis function after total shoulder replacement: A seldom recognized problem. *Journal of Shoulder and Elbow Surgery*, *12*(1), 29–34. <https://doi.org/10.1067/mse.2003.128195>
- Muench, L. N., Murphey, M., Oei, B., Kia, C., Obopilwe, E., Cote, M. P., Mazzocca, A. D., & Berthold, D. P. (2023). Elliptical and spherical heads show similar obligate glenohumeral translation during axial rotation in total shoulder arthroplasty. *BMC Musculoskeletal Disorders*, *24*(1), 171. <https://doi.org/10.1186/s12891-023-06273-5>
- Muench, L. N., Otto, A., Kia, C., Obopilwe, E., Cote, M. P., Imhoff, A. B., Beitzel, K., Mazzocca, A. D., & Mehl, J. (2022). Rotational range of motion of elliptical and spherical heads in shoulder arthroplasty: a dynamic biomechanical evaluation. *Archives of Orthopaedic and Trauma Surgery*, *142*(1), 67–76. <https://doi.org/10.1007/s00402-020-03587-0>
- Mulieri, P. J., Holcomb, J. O., Dunning, P., Pliner, M., Bogle, R. K., Pupello, D., & Frankle, M. A. (2010). Is a formal physical therapy program necessary after total shoulder arthroplasty for osteoarthritis? *Journal of Shoulder and Elbow Surgery*, *19*(4), 570–579. <https://doi.org/10.1016/j.jse.2009.07.012>
- Murgia, A., Hortobágyi, T., Wijnen, A., Bruin, L., Diercks, R., & Dekker, R. (2018). Effects of age and sex on shoulder biomechanics and relative effort during functional tasks. *Journal of Biomechanics*, *81*, 132–139. <https://doi.org/10.1016/j.jbiomech.2018.10.001>
- Nishinaka, N., Tsutsui, H., Mihara, K., Suzuki, K., Makiuchi, D., Kon, Y., Wright, T. W., Moser, M. W., Gamada, K., Sugimoto, H., & Banks, S. A. (2008). Determination of in vivo glenohumeral translation using fluoroscopy and shape-matching techniques. *Journal of Shoulder and Elbow Surgery*, *17*(2), 319–322. <https://doi.org/10.1016/j.jse.2007.05.018>

- Phadke, V., Braman, J. P., LaPrade, R. F., & Ludewig, P. M. (2011). Comparison of glenohumeral motion using different rotation sequences. *Journal of Biomechanics*, 44(4), 700–705. <https://doi.org/10.1016/j.jbiomech.2010.10.042>
- Pike, J. M., Singh, S. K., Barfield, W. R., Schoch, B., Friedman, R. J., & Eichinger, J. K. (2022). Impact of age on shoulder range of motion and strength. *JSES International*, 6(6), 1029–1033. <https://doi.org/10.1016/j.jseint.2022.08.016>
- Rau, G., Disselhorst-Klug, C., & Schmidt, R. (2000). Movement biomechanics goes upwards: from the leg to the arm. *Journal of Biomechanics*, 33(10), 1207–1216. [https://doi.org/10.1016/S0021-9290\(00\)00062-2](https://doi.org/10.1016/S0021-9290(00)00062-2)
- Richards, R. R., An, K.-N., Bigliani, L. U., Friedman, R. J., Gartsman, G. M., Gristina, A. G., Iannotti, J. P., Mow, V. C., Sidles, J. A., & Zuckerman, J. D. (1994). A standardized method for the assessment of shoulder function. *Journal of Shoulder and Elbow Surgery*, 3(6), 347–352. [https://doi.org/10.1016/S1058-2746\(09\)80019-0](https://doi.org/10.1016/S1058-2746(09)80019-0)
- Rojas, J., Joseph, J., Srikumaran, U., & McFarland, E. G. (2020). How internal rotation is measured in reverse total shoulder arthroplasty: a systematic review of the literature. *JSES International*, 4(1), 182–188. <https://doi.org/10.1016/j.jses.2019.10.109>
- Ronneberger, O., Fischer, P., & Brox, T. (2015). *U-Net: Convolutional Networks for Biomedical Image Segmentation*. <http://arxiv.org/abs/1505.04597>
- Sabesan, V. J., Ackerman, J., Sharma, V., Baker, K. C., Kurdziel, M. D., & Wiater, J. M. (2015). Glenohumeral mismatch affects micromotion of cemented glenoid components in total shoulder arthroplasty. *Journal of Shoulder and Elbow Surgery*, 24(5), 814–822. <https://doi.org/10.1016/j.jse.2014.10.004>
- Sanchez-Sotelo, J. (2011). Total Shoulder Arthroplasty. *The Open Orthopaedics Journal*, 5(1), 106–114. <https://doi.org/10.2174/1874325001105010106>
- Schick, S., Dombrowsky, A., Egbaria, J., Paul, K. D., Brabston, E., Momaya, A., & Ponce, B. (2023). Variability in physical therapy protocols following total shoulder arthroplasty. *Clinics in Shoulder and Elbow*, 26(3), 267–275. <https://doi.org/10.5397/cise.2023.00115>
- Schoch, B. S., Wright, T. W., Zuckerman, J. D., Flurin, P.-H., Bolch, C., Roche, C. P., & King, J. J. (2019). The effect of radial mismatch on radiographic glenoid loosening. *JSES Open Access*, 3(4), 287–291. <https://doi.org/10.1016/j.jses.2019.09.007>
- Scibek, J. S. (2012). Assessment of scapulohumeral rhythm for scapular plane shoulder elevation using a modified digital inclinometer. *World Journal of Orthopedics*, 3(6), 87. <https://doi.org/10.5312/wjo.v3.i6.87>
- Šenk, M., & Chèze, L. (2006). Rotation sequence as an important factor in shoulder kinematics. *Clinical Biomechanics*, 21, S3–S8. <https://doi.org/10.1016/j.clinbiomech.2005.09.007>

- Singh, J. A., Sperling, J. W., & Cofield, R. H. (2011). Revision surgery following total shoulder arthroplasty. *The Journal of Bone and Joint Surgery. British Volume*, *93-B*(11), 1513–1517. <https://doi.org/10.1302/0301-620X.93B11.26938>
- Stathokostas, L., McDonald, M. W., Little, R. M. D., & Paterson, D. H. (2013). Flexibility of Older Adults Aged 55–86 Years and the Influence of Physical Activity. *Journal of Aging Research*, *2013*, 1–8. <https://doi.org/10.1155/2013/743843>
- Strauss, E. J., Roche, C., Flurin, P.-H., Wright, T., & Zuckerman, J. D. (2009). The glenoid in shoulder arthroplasty. *Journal of Shoulder and Elbow Surgery*, *18*(5), 819–833. <https://doi.org/10.1016/j.jse.2009.05.008>
- Terrier, A., Büchler, P., & Farron, A. (2006). Influence of glenohumeral conformity on glenoid stresses after total shoulder arthroplasty. *Journal of Shoulder and Elbow Surgery*, *15*(4), 515–520. <https://doi.org/10.1016/j.jse.2005.09.021>
- Triplet, J. J., Everding, N. G., Levy, J. C., & Moor, M. A. (2015). Functional internal rotation after shoulder arthroplasty: a comparison of anatomic and reverse shoulder arthroplasty. *Journal of Shoulder and Elbow Surgery*, *24*(6), 867–874. <https://doi.org/10.1016/j.jse.2014.10.002>
- Triplet, J. J., Kurowicki, J., Berglund, D. D., Rosas, S., Horn, B. J., & Levy, J. C. (2018). Loss of Functional Internal Rotation Following Various Combinations of Bilateral Shoulder Arthroplasty. *Surgical Technology International*, *33*, 326–331. <http://www.ncbi.nlm.nih.gov/pubmed/30029285>
- UNSCEAR. (2008). *Sources and effects of ionizing radiation*. [https://www.unscear.org/unscear/en/publications/2008\\_1.html](https://www.unscear.org/unscear/en/publications/2008_1.html)
- Walch, G., Badet, R., Boulahia, A., & Khoury, A. (1999). Morphologic study of the Glenoid in primary glenohumeral osteoarthritis. *The Journal of Arthroplasty*, *14*(6), 756–760. [https://doi.org/10.1016/S0883-5403\(99\)90232-2](https://doi.org/10.1016/S0883-5403(99)90232-2)
- Walch, G., Edwards, T. B., Boulahia, A., Boileau, P., Molé, D., & Adeleine, P. (2002). The influence of glenohumeral prosthetic mismatch on glenoid radiolucent lines: Results of a multicenter study. *Journal of Bone and Joint Surgery*, *84*(12), 2186–2191. <https://doi.org/10.2106/00004623-200212000-00010>
- Walch, G., Vezeridis, P. S., Boileau, P., Deransart, P., & Chaoui, J. (2015). Three-dimensional planning and use of patient-specific guides improve glenoid component position: an in vitro study. *Journal of Shoulder and Elbow Surgery*, *24*(2), 302–309. <https://doi.org/10.1016/j.jse.2014.05.029>
- Wong, M. T., Wiens, C., Kuczynski, M., Manske, S., & Schneider, P. S. (2022). Four-dimensional computed tomography: musculoskeletal applications. *Canadian Journal of Surgery*, *65*(3), E388–E393. <https://doi.org/10.1503/cjs.023420>

- Wright Medical Group. (2016). *AEQUALIS Perform Glenoid Surgical Technique*.
- Wu, G., Siegler, S., Allard, P., Kirtley, C., Leardini, A., Rosenbaum, D., Whittle, M., D’Lima, D. D., Cristofolini, L., Witte, H., Schmid, O., & Stokes, I. (2002). ISB recommendation on definitions of joint coordinate system of various joints for the reporting of human joint motion—part I: ankle, hip, and spine. *Journal of Biomechanics*, 35(4), 543–548. [https://doi.org/10.1016/S0021-9290\(01\)00222-6](https://doi.org/10.1016/S0021-9290(01)00222-6)
- Wu, G., van der Helm, F. C. T., (DirkJan) Veeger, H. E. J., Makhsous, M., Van Roy, P., Anglin, C., Nagels, J., Karduna, A. R., McQuade, K., Wang, X., Werner, F. W., & Buchholz, B. (2005). ISB recommendation on definitions of joint coordinate systems of various joints for the reporting of human joint motion—Part II: shoulder, elbow, wrist and hand. *Journal of Biomechanics*, 38(5), 981–992. <https://doi.org/10.1016/j.jbiomech.2004.05.042>

## **Appendix A: The Impact of Voxel Resolution and Scan Orientation on CT-Based Bone Models**

There is inherent error in creating models from CT scans due to the finite resolution of the voxels. Additionally, if the voxel size is anisotropic, orientation may further affect the error. A CT scanner uses XYZ coordinates, where Z represents the rotational axis. For the static scans, the voxel size is (0.49mm, 0.49mm, 1.25mm), whereas the 4DCT scan voxel size is (0.88mm, 0.88mm, 2.50mm). To quantify the error in model making and the impact of orientation, a single cadaveric shoulder was scanned in three different positions with a static scan used as the ground truth. The static scanning procedure involved positioning the shoulder as a participant would be, aligning the superior axis with the Z axis. The first 4DCT scan copied the orientation of the static scan. In the second scan the shoulder was rotated 90° to align the medial axis with the Z axis. The third scan positioned the shoulder obliquely, aligning the Z axis between the medial and superior axes.

Bone models were created of the humerus and scapula from both the static scan and the initial three frames of each 4DCT scan. Coordinate systems were created on the static scan models which were registered to the 4DCT models. This quantifies the spatial relationship between the humerus and the scapula in the 4DCT scans. This position was then compared to the static position. Since the cadaveric shoulder was frozen, any relative motion between the scapula and humerus was indicative of error. This error was measured in terms of both translations and rotations. The mean translational errors were 0.09mm, 0.20mm, and 0.13mm for the first, second, and third scans, respectively. For rotational errors, the means were 0.24°, 0.31°, and 0.31° for the first, second, and third scans, respectively. Overall, the error was lowest when the shoulder was orientated identical to the static scan, and greatest when positioned orthogonally relative to the static scan.

## Curriculum Vitae

<b>Name:</b>	James Hunter
<b>Post-secondary Education and Degrees:</b>	<p>University of Guelph Guelph, Ontario, Canada 2016-2020 B.Eng</p> <p>Western University London, Ontario, Canada 2020-2024 Ph.D.</p>
<b>Honours and Awards:</b>	<p>Western Graduate Research Scholarship 2020-2024</p> <p>University of Guelph Dean's Honours List 2016-2020 (8 consecutive semesters)</p>
<b>Related Work Experience:</b>	<p>Teaching Assistant Western University 2020-2024</p> <ul style="list-style-type: none"> <li>• Foundations of Engineering Practice (ES1050)</li> <li>• Programming Fundamentals for Engineers (ES1036)</li> <li>• Robotics and Manufacturing Automation (MME4452)</li> </ul> <p>Computer Vision Consultant Wosler Diagnostics 2022</p> <ul style="list-style-type: none"> <li>• Developed a neural network to identify deep vein thrombosis from ultrasound</li> <li>• Developed a program to identify a target location from depth sensor camera data</li> </ul> <p>Undergraduate Research Assistant University of Guelph 2019</p> <ul style="list-style-type: none"> <li>• Created 3D models of mammalian hearts from MRI scans</li> <li>• Applied finite element analysis and fluid simulation</li> </ul>



### **Publications:**

**Hunter, J.,** Lee, T. Y., Athwal, G. S., & Lalone, E. A. (2023). Development of a single-vertebra image-based technique to quantify shoulder kinematics using four-dimensional computed tomography. *Computer Methods in Biomechanics and Biomedical Engineering: Imaging & Visualization*, 12(1). <https://doi.org/10.1080/21681163.2023.2282074>

Daher, B., **Hunter, J.,** Athwal, G. S., & Lalone, E. A. (2023). How does computed tomography inform our understanding of shoulder kinematics? A structured review. *Medical & Biological Engineering & Computing*. <https://doi.org/10.1007/s11517-022-02755-1>

### **Presentations:**

Age-Related Differences in Healthy Shoulder Kinematics using Four-Dimensional Computed Tomography (Oral). Ontario Biomechanics Conference 2024, Toronto, Canada.

Glenohumeral And Scapulothoracic Kinematics During the Belly Press Test using Four-Dimensional Computed Tomography (Poster). Canadian Orthopedic Research Society 2023, Calgary, Canada.

Age-Related Differences in Healthy Shoulder Kinematics using Four-Dimensional Computed Tomography (Poster). Ontario Biomechanics Conference 2023, Waterloo, Canada.

Glenohumeral And Scapulothoracic Kinematics During the Belly Press Test using Four-Dimensional Computed Tomography (Poster). Orthopedic Research Society 2023, Dallas, United States of America.

Three-Dimensional Glenohumeral and Scapulothoracic Kinematics using Four-Dimensional Computed Tomography (Oral). Canadian Orthopedic Research Society 2022, Quebec City, Canada.

Three-Dimensional Glenohumeral and Scapulothoracic Kinematics using Four-Dimensional Computed Tomography (Oral). Orthopedic Research Society 2021, *Virtual*.